IEEE Access
Multidisciplinary | Rapid Review | Open Access Journal

Received May 25, 2021, accepted June 16, 2021, date of publication July 19, 2021, date of current version August 2, 2021.

Digital Object Identifier 10.1109/ACCESS.2021.3098061

ZnO Based Resistive Random Access Memory Device: A Prospective Multifunctional Next-Generation Memory

USMAN BATURE ISYAKU, (Student Member, IEEE), MOHD HARIS BIN MD KHIR, (Member, IEEE), I. MD NAWI, (Member, IEEE), M. A. ZAKARIYA, (Member, IEEE), AND FURQAN ZAHOOR, (Student Member, IEEE)

Department of Electrical and Electronic Engineering, Universiti Teknologi PETRONAS, Seri Iskandar 32610, Malaysia

Corresponding author: Mohd Haris Bin Md Khir (harisk@utp.edu.my)

This work was supported by the Graduate Assistantship (GA) Scheme Grant from the Universiti Teknologi PETRONAS, Malaysia.

ABSTRACT Numerous works that have demonstrated the study and enhancement of switching properties of ZnO-based RRAM devices are discussed. Several native point defects that have a direct or indirect effect on ZnO are discussed. The use of doping elements, multi-layered structures, suitable bottom and top electrodes, controlling the deposition materials, and the impact of hybrid structure for enhancing the switching dynamics are discussed. The potentials of ZnO-based RRAM for invisible and bendable devices are also covered. ZnO-based RRAM has the potential for possible application in bio-inspired cognitive computational systems. Thus, the synapse capability of ZnO is presented. The sneak-path current issue also besets ZnO-based RRAM crossbar array architecture. Hence, various attempts to subdue the bottleneck have been shown and discussed in this article. Interestingly, ZnO provides not only helpful memory features. However, it demonstrates the ability to be used in nonvolatile multifunctional memory devices. Also, this review covers various issues like the effect of electrodes, interfacial layers, proper switching layers, appropriate fabrication techniques, and proper annealing settings. These may offer a valuable understanding of the study and development of ZnO-based RRAM and should be an avenue for overcoming RRAM challenges.

INDEX TERMS Nonvolatile memory, RRAM, synapse device, flexible-transparent memory, ZnO, multifunctional device.

I. INTRODUCTION

Semiconductor memory is an essential element to numerous modern automated devices, ranging from devices used in computing podiums like handheld devices to supercomputers; all employ temporary or permanent memory systems for information and data storage [1], [2]. The demand increases with the growing popularity of consumer electronics, industrial/automotive, portable gadgets, and smartphones [3], [4], as shown in Fig. 1. Generally, memories are divide into two; volatile memory that lost its content when the control is switched off, and nonvolatile memory (NVM) that is proficient in regulating or limiting the flow of electrical current, maintaining its internal resistance, an applied voltage [5]. After power is turned off, it can retain its content, thus offering a new memory device's trend that acts as a bistable memory with non-destructive read-out features. Over some years, numerous NVM devices have emerged, such as the flash memory [6], and emerging memories like the magnetic RAM (MRAM) [7], phase-change memory (PCM) [8], Spin-transfer torque RAM (STT-RAM) [9], ferroelectric memory (FeRAM) [10] and resistive RAM (RRAM) [11], each having some technical limitations in reliability, scalability, endurance, power consumption, retention and operating speed. However, resistive switching (RS) memories possess better switching advantages, thus good candidates for future next-generation memories [12], [13].

Furthermore, emerging memories are faced with complex challenges like the low density, high operating power, and the foreseen scaling power to be up to or even

The associate editor coordinating the review of this manuscript and approving it for publication was Cristian Zambelli.

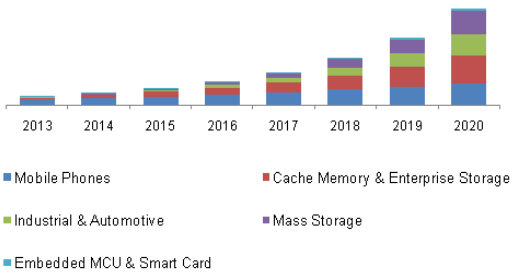

FIGURE 1. The NVM market trend from 2013 – 2020, as the demand increases in the adoption of PCM over flash memory in smartphones, and possible use of PCM, STT-RAM, and MRAM in smart cards and Microcontrollers, may further the market growth over the entire forecast period [4].

beyond 22nm. Since continued scaling functionality and dimension of CMOS are approaching their fundamental limits, new alternative approaches are now being discovered to endure the idea of further scaling cadence and reduction of function and cost into future years [14]. The evolution of extended CMOS was proposed; it aims to provide ceaseless alternative solutions, as shown in Fig. 2. And this would be accomplished by the following; the CMOS platform's functionality should be extended through the mixt structure of emerging technologies and encouraging new information processing projects [14]. The emergence of CMOS compatible RRAM oxide materials like the TiO_x, HfO_x, ZrO_x, TaO, and ZnO have proved promising due to their outstanding durability, good switching speed, and high density capability. Also, their simple cell structures, low power consumptions, and nonvolatile nature [15], [16]. Thus, it reassures that these new findings could help in achieving the CMOS evolution platform targets.

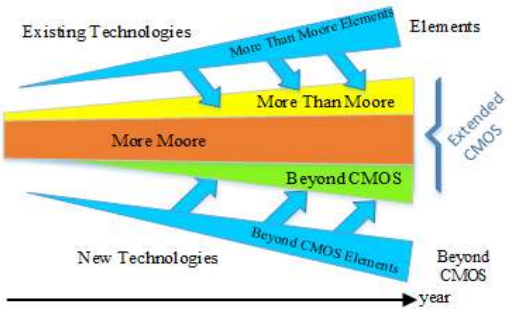

FIGURE 2. The Evolution of CMOS Platform. This extension of CMOS platform scaling via the dimension and function is called "More Moore." It can be further lengthened by the "More than Moore." The advancement in architecture and information processing devices is called "Beyond CMOS." The mixt structure of "More Moore," "More than Moore," and "Beyond CMOS" will lengthen the platform functionality to produce "Extended CMOS" [14].

In this review article, recent works and progress of ZnO-based RRAM technology are presented. Emerging memories and the evolution of the CMOS platform are shown in the ''Introduction'' section. The ''Historical Trend of the RRAM Device'' section presents the historical trend of RRAM that shows its evolution right from its discovery in the laboratory to realizing the practical RRAM device. The RRAM structure and details of the switching mechanism and switching modes are highlighted in the ''RRAM Structure and Operation'' section. Several native point defects associated with ZnO are discussed, and their effects and contributions are also shown in the ''ZnO Defects and their Contribution'' section. The ''ZnO for RRAM Application'' section highlights the significance of electrodes in the operation of ZnO-based RRAM, the effect of doping elements, and their contributions. The section also presents the importance of the multi-layered and embedded structure, the effect of deposition parameters, the hybrid layer, and its impact. Also, the section provides recent progress on ZnO-based transparent and flexible devices, the synapse potential of ZnO-based RRAM devices, and the sneak-path current issues. Finally, the section discussed the recent development of the multifunctional potential of ZnO-based RRAM.

A. HISTORICAL TREND OF THE RRAM DEVICE

In 1971, L. Chua discovered a two-terminal circuit element called memristor [17]. Though, as of then, the memristor's fabrication as a physical device with no internal power supply has not been realized. It was only recognized in the laboratory in 1962 [18] as a nonvolatile resistive switching device with sizeable current density, and negative differential resistance observed in ZrO_2, SiO, Al_2O_3, Ta_2O_5, and TiO_2 sandwiches. Similarly, N. M. Bashara, in 1963, illustrates in SiO thin film sandwich between gold (Au) electrodes [19]. In mid-1966, a team argues about the switching action of SiO_2 [20]. Moreover, after 30years, a multilayer thin-film material for sensors and memory devices was presented [21]. The summery of the brief historical trends is presented in Fig. 3.

However, RRAM research and fabrication's heat was fully kicked in the earliest 2000 research from the University of Houston on colossal Magnetoresistive (CMR) films [22]. After two years, a team from Sharp Laboratories fabricated CMR-based RRAM using the 1R1T 0.5 μm CMOS technology [15]. Therein the emergence of numerous bodies filling their patent applications claiming various device implementations [23], initially on a limited kilobytes capacity scale. In 2004, the reproducible capability of polycrystalline NiO film [24] was identified for the first time. In the same year, also for the first time, the integration of OxRRAM with 0.18 μm CMOS technology without the need for any other dedicated facility was presented [25]. The potential use of the multilevel stacking method was proposed [26] after a year. In 2007, the first 2-stack 1D1R array of 8×8 RRAM structure was successfully integrated [27]; this reaffirms the RRAM high-density stack's realism. Sony Corporation presents a 4-level RRAM array structure in 2007 [28]; due to discrepancies found in the characterization methods, a single characterization tool for metrology requirements was proposed [29], the heat of RRAM was further instigated by [1], proposed memristor for the neural network application. Thereon, so many successes were recorded from both the

FIGURE 3. RRAM Historical Trend from 1962 to 2020 [1], [15], [17]–[45]. The history trend provides the development trends of RRAM captured from 1962 to 2019, and it also shows some of the recent RRAM development.

academia and manufacturing section. In 2009, the possibility of RRAM for flexible NVM devices was reported [30], after a year, a 64 Mb NAND compatible memory [31] was fabricated. In 2011, the Sony LSI design team developed a 4 Mb RRAM [32]. After a year, Panasonic developed 8 Mb RRAM with 443 MB/s write throughput [33]. Unity Semiconductor was bought by Rambus in 2012 [34] to produce 1 Tb chip by 2014. Crossbar announced their 1Tb RRAM based chip in 2013 [35], HP planned the production of their 100 Tb SSDs RRAM based technology in 2018, and additional capacities of 1.5 Pb in 2020 [36]. Scandisk and Toshiba present 32 Gb RRAM [37], and Panasonic produces 0.18 μm RRAM microcomputer [38]. In 2014 a joint team from Micron and Sony developed 16 Gb RRAM [39]. After a year, low power 2 Mb RRAM was designed for IoT applications [40], CAS and SICAM centre presented a 3D high-density RRAM [41] in 2016. Panasonic developed 8Mbit low power 40 nm RRAM technology in 2019 [42], Fujitsu and Panasonic to produce 8Mbit RRAM named MB85AS8MT [43]. The 22nm ultra-low leakage process of embedded RRAM chips technology announced in 2017 by TSMC [44], expected to pass its IP reliability requirement in 2020, and their 40 nm ultra-low-power embedded RRAM already been completed IPs reliability 2019 [45], and the improved mismatch projected to be ready 2020.

B. RRAM STRUCTURE AND OPERATION

A typical RRAM cell comprises three layers that mimic a simple-capacitor-like structure, and it is poised with an insulating layer inserted between two conductors termed bottom electrode (BE) and top electrode (TE) as Metal–Insulator-Metal (MIM), as shown in Fig. 4. RRAM is termed a two-terminal cell, its property changes upon the application of voltage. It works based on oxidation and reduction reaction and toggles between the low resistance states (LRS) and the high resistance states (HRS).

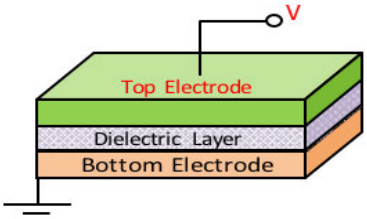

FIGURE 4. The structure of the RRAM cell. It shows the plan of the sandwich structure that shows the TE-Dielectric layer-BE arrangement, respectively.

In a digital memory storage scenario, there are two distinct binary states, logic "0" corresponds not to store data, and logic "1" represents data stored [46]. In RRAM, an electrical field applied across the structure forms a conductive bridge or filament across the two conducting sheets. Thus, due to redox reactions, a conductive bridge will be created, then the two electrodes will be electrically connected. Therefore, when a conductive filament (CF) is formed, the device will be at an LRS, corresponding to the state of logic "1". In contrast, the HRS is created once the filament ruptured. HRS corresponded to a state of logic "0," as shown in Fig. 5. The essential element of the memory in semiconductor-based RRAM is the insulating, resistive switch layer. RRAM stores/erases information with the resistance switching process under the electric field's influence [47]. Generally, RRAM operates within two switching processes. The SET process is the operation that modifies the device's resistance state from HRS to LRS in the influence of an electric stimulus (V_{top} or V_{set}). In contrast, the RESET process changes the resistance back to HRS under (V_{top} or V_{reset}) as presented in Fig. 5 [46].

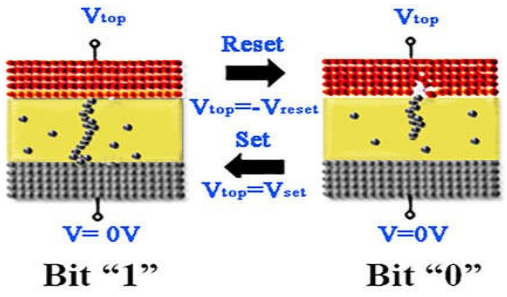

FIGURE 5. The resistive switching mechanism in the RRAM device, a bit "1" corresponds to the state when the filament is formed, while bit "0" corresponds to the state when the filament is destroyed [46].

Resistive switching processes of RRAM are roughly divided into unipolar and bipolar processes, as presented in Fig. 6. [48]. In unipolar switching mode, the process does not usually be influenced by the applied voltage's polarity; rather, it depends on its voltage amplitude. Thus, SET and RESET processes can be achieved using the same voltage polarity, and during reset state, CF is usually dissolved by the Joule heating effect. Some of its switching properties can be understood via the thermal dissolution model [49]. On the other hand, the bipolar switching mode usually takes place at some voltages. It usually depends on the voltage's applied polarity, and opposite voltage polarities are used to set or reset the device. Some of its switching properties can be known using the ion migration model [50]. During the SET transition, the current in bipolar and unipolar switching modes is usually narrow down in setting the compliance current (CC) to regulate CF's formation and evade permanent breakdown [13].

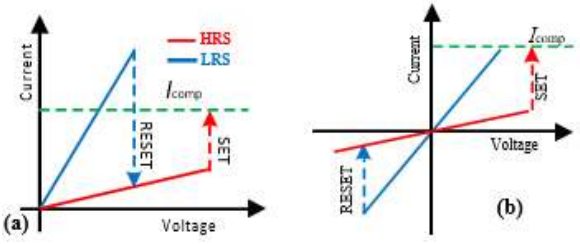

FIGURE 6. The resistive switching mechanism in the RRAM device, a bit "1" corresponds to the state when the filament is formed, while bit "0" corresponds to the state when the filament is destroyed.

Forming process in RRAM can be explained using a soft dielectric breakdown in a fresh dielectric material. The formation and breakup of the conductive layer in the RRAM system can be described using two processes: the valence change memory (VCM) for oxygen ions the CF-based on metal atoms for conductive-bridge RAM (CBRAM). It can also be described using a programmable metallization cell (PCM) or electrochemical metallization memory (ECM) [51]. ECM usually is formed by the tiny metal clusters across the resistive switching layer under the electric field's influence, normally associated with Ag, Ni, and Cu's active metals electrode, and electrodes of the inactive metals like Au Pt, Ir, and W [52].

VCM is usually triggered by anions migration like the oxygen anions (O^{2-}) which are usually defined by the vacancies' motion within the resistive layer [11]. Successive stoichiometry change results in the valance change and electronic conductivity change formed by a redox reaction in some transition metals. The amount of current flow during the set process or forming process typically determines the size of the CF formed across the resistive layer [16]. It is a robust reversible pathway and usually behaves as a conducting material with a current flowing through it [53]. It is worth noting that the electrode size does not usually influence the LRS due to the electrode area is usually more extensive than the filament size [54], [55].

VCM based RRAM requires a facilitating electrode called an oxygen scavenger, which will aid the anionic movement. Forming-free properties were observed in RRAM devices doped with Ge [56] or Ti [57] in their switching layer. They have oxygen deficiency due to metal doping, which lowers the formation energy of the oxygen vacancy. A forming-free process is also possible in an undoped RRAM device. Appropriate fabrication methods and proper annealing environments may form free behavior. It was shown that regulating the O_2 plasma time during the deposition of ZnO films resistive layer using an improved plasma atomic layer deposition method facilitates the anionic movement and produced forming free properties [58]. The confinement of CF in multilayer devices consisting of TiO_x prepared via Ti film oxidation [59] also demonstrates a free-forming process. Forming-free devices exhibit self-compliance, high uniformity, and low operation power [57]; their HRS is similar to their initial resistance state.

In ECM, ion flux could intensely affect the turn-on voltage, and ion flux is proportional to ion concentration and diffusion coefficient [60]. Thus, it reveals the possibility of realizing a low switching voltage in ECM-based RRAM because a large diffusion coefficient means a large ion flux. This is discussed in [61], with Ag shown to exhibits a large diffusion coefficient, also reveals a forming free operation with a low voltage in [62]. On the order hand, high forming voltage could be obtained in a device with a gold top electrode, and this could be attributed to its chemical inertness and hard to oxidize to ions [63]. Thus a high voltage is required for its activation. Though filamentary-based switching mechanism in RRAM is still not clear and a subject of debate.

The mechanism behind resistive switching (RS) operation in RRAM is stochastic [64]; thus, mathematical models describing this phenomenon are highly required. Therefore, many microscopic models were proposed [65]–[68]. These methods explain the RS mechanism phenomenon based on either field-induced or temperature-induced ions migration, such as the compact model, which is the process of characterizing an electron device for circuit simulation via some set of equations and some fitting parameters [69]. These models were still under investigation since new materials, device dimensions, and fabrication methods are continuously discovered day-by-day. However, a mere explanation of the insulator's microscopic origin suddenly changes to conductor under applied voltage is not enough. Still, in-depth findings on how conducting local regions were interconnected under an electric field [70], [71] are required. Therefore, it will significantly help address multilevel switching issues, sneak-path, and high resistance fluctuations.

Moreover, a comprehensive physical RS mechanism in oxides-based RRAM is still open for dynamic research [72], [73]. Generally, producing more resistive switching findings can significantly improve RS characteristics and open novel RRAM fabrication methods [74]–[76].

C. ZnO DEFECTS AND THEIR CONTRIBUTION

Zinc oxide (ZnO) is known as a white powder that is not soluble in water, environmentally friendly substances, non-poisonous listed by the US Food and Drug Administration (FDA) or GRAS known [77]. ZnO is considered to be a promising candidate in numerous areas; it is used as an additive in many materials like in anti-parasite [78], drugs [79], ointments [80], food conservation [81], and water treatment [82]. ZnO memory is considered a substitute for conventional charge-based flash memory and has proven to be a promising candidate for the RRAM device [83]. ZnO occurs naturally as the mineral zincite and can also be prepared synthetically [84], [85]. ZnO is a binary transition metal oxide with a high binding energy of about 60meV, a wide optical band gap of nearly 3.37eV, good RS performance, high carrier mobility, simple preparation techniques, and well-regulated oxygen vacancy (V_O) concentration [30], [86]–[88].

ZnO is undoubtedly a natural n-type semiconductor with an inherent, intrinsic defect of around 0.01-0.05eV under the conduction band. It can retain its hexagonal wurtzite structure and can be grown in polycrystalline and epitaxial nature [89], [90]. ZnO can be fabricated on a wide morphological setting [91]–[97], like in piezoelectrical transducers [94], [95]. The piezoelectric activity of ZnO, as well as other intriguing physical features, is owing to its unique crystal structure, which may be classified into three frameworks: rocksalt, zinc blende, and wurtzite. Furthermore, the coupling of ZnO piezoelectricity and semiconducting capabilities produced the so-called ''piezotronic effect.'' The charge carrier transport properties may be regulated and modified by the inner electric potential made in ZnO [95]. The idea

of combining ZnO's unique characteristics with various morphologies has piqued researchers' interest in the material. ZnO has large exciton binding energy and a wide bandgap that makes it suitable for photonic application [96], also used in chemical gas sensors [84]. ZnO can be doped with some metals and applied in areas like spintronic application [85]. ZnO is a biocompatible device, which makes it appropriate for biomedical uses [97], [98]. ZnO is a multifunctional material that attracted attention, but many of its potentials had not been explored yet.

ZnO is associated with several native point defects that may hinder its material properties, like the anti-sites, vacancies, substitution, and self-interstitials. ZnO native point defects directly or indirectly affect its physical properties like the luminescence efficiency, lifetime of the minority carrier, and doping concentration. Also, these native defects have an impact on the diffusion process during development or processing. As such, this may hinder the growth device's performance and subsequently drop into degradation [99]–[101]. In [102], it was presented that impurities and small point defects down to 10-14 cm^{-3} can affect some functional properties, such as ZnO's optical and electrical properties. Hence, controlling these defects' manipulation may influence the material's functional properties [103]. Therefore, comprehensive knowledge of the ZnO extrinsic and intrinsic point defects is vital for the potential material application in various morphological settings.

Zinc vacancies (V_{Zn}) are shown to have a probable effect on the ZnO green luminescence property [104]. They are deep acceptors and function as a compensating point in n-type ZnO material. The green emission observed in ZnO materials was reported to have originated from V_{Zn} due to electrons' transitions from the conduction band to a deep acceptor level [105]. It is good to know that defects like zinc interstitials and V_O are the geneses behind the ZnO n-type conductivity [106], making it challenging to reproduce reliable p-type doping obstructs its uses as a light-emitting device [107]. Doping in ZnO can be affected by these point defects as self-compensation may be formed. Consider doping in p-type material; the intentionally introduced dopants (acceptors) may be compensated by some native defects that act as donors in the material [104]. The photoluminescence effect was observed and reported in [108], [109]. The effect was significantly enhanced after introducing the acceptor Lithium (Li) dopant with green and yellow emissions at 526 nm and 574 nm, respectively. It was shown that the yellow emission observed could be substituted by green and red bands [109] through post-growth annealing and concluded that the emission could be modified after the desorption of the hydroxyl group. This emission is rare in ZnO was described to have resulted from oxygen interstitials transitions [110]. During zinc vacancy transitions [117], the orange-red emission and red emission are related to changes from zinc interstitials [111]. Therefore, this shows the role played by the native defect present in ZnO could be applied for lighting and display purposes. The V_{Zn} and V_O defects present in ZnO could be employed in enhancing the magnetic effects of diluted magnetic semiconductors [112], which reveals the significance of V_{Zn} in achieving ferromagnetic long-range order. At the same time, the Li-doped ZnO with V_O shows a nonmagnetic effect.

Nowadays, it is pertinent to enhance sensing devices' implementation due to increased environmental hazards for safety and control purposes [113]. However, its application is retarded by the complications faced during high-temperature operations [114], [115], like the explosive and flammable gas atmosphere. ZnO exhibits a gas sensing capability due to its large exciton binding energy (60meV), good thermal and chemical stability, photoelectric response, wide bandgap (3.37eV), and high electron mobility [116]–[119].

Moreover, this work aims to highlight these ZnO native point defects' significance for the optimization and comprehension of its basic physical properties. Despite numerous studies, the issue still needs further studies, and it is critical since several ZnO properties defend against these defects.

II. ZnO FOR RRAM APPLICATION

A. SIGNIFICANCE OF ELECTRODES IN ZnO BASED RRAM

The low resistance effect in ZnO is associated with V_{Zn} and Vo defects [104]. Hence, unsatisfactory switching characteristics may be experienced due to the excess volume of native point defects. Numerous attempts have been reported in the literature on ZnO's switching dynamics based on electrodes' effects to alleviate ZnO's defects for improving switching characteristics, such as ZnO's stacking with various metal electrodes [120]–[124]. In RRAM, electrodes serve as the transport path for charge carriers and affect the resistance switching behaviour. Hence, It was inveterate in [125] using four different electrodes of Pt, Ti, Au, and Al. It was noticed that resistive switching could be induced at a higher voltage in the Al top electrode than Pt and Au structures. Still, the use of a Ti top electrode a significant voltage dropped, but the NiO film's effective electric pulse could not induce resistance switching. Similarly, in [126], the difference in the HRS/LRS resistance ratio of Al 10^6 against the Pt 10^3 reaffirmed that electrodes could influence the resistance switch in the RRAM device.

Additionally, according to the electrochemical process, the electrodes' behavior shows that those electrodes from the oxidized, inert, and active metals are usually found to stack with the resistive layer or material. The oxidized metal electrode offers advantages of oxygen storage capabilities when used as an anode. Also, consider a TiN metal used as a top electrode (TE) in ZnO/Pt device produced a thin buffer layer that controls the oxygen outflow during SET operation [123]. Thus, it exhibits a fast switching speed, operation's low power, and good retention time. The formation of frail cell-area dependence illustrates this effect during LRS, indicating that the SET operation equals the mechanism of filamentary conduction [11]. It also shows that the density and the conducting filament's diameter in oxidized metal

depend on the effective cell area formed. Though several oxidized metals are available, the appropriate anode for better performance in ZnO still needs to be carefully selected. The use of electrochemically inert cathode electrodes like the Ru, W, Pt, Au, or Ag is shown to produce a high interface barrier. Their high work function is due to the ratio of ON/OFF resistance [127]. Their capacitance depends on the distributed charges usually found on the surfaces, and the behavior of their capacitance-voltage could be used to comprehend the charge distribution scenario [128]. On the other hand, when used as an anode, the inert high work function makes the oxygen reservoir capability limited [129] even with their excellent electrochemical behavior.

The mechanism of the resistive switching schematic of various metal TE on a structure of ZnO/Pt is shown in Fig. 7 [122], despite forming an Ag-bridge between the electrodes after the application of a low positive voltage (0 – 1) V, an amorphous V_O filament is observed. An oxygen reservoir layer is observed using Ti TE, the interfacial layer formed is reported to have dominated the switching properties in [130]. Thus, the Ti TE has an oxygen-gathering nature and sources of oxygen ions from the ZnO film. It was evident from the use of Pt TE that poor resistive switching (RS) is observed when TE and bottom electrochemically inert electrodes are used. The Pt's inability to source oxygen from the resistive layer makes it possible for the current in the forward bias form to be larger than the reverse bias.

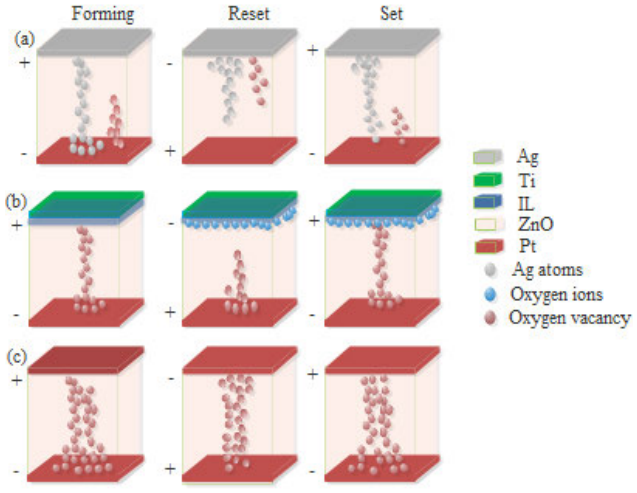

FIGURE 7. Schematic description of Ti, Ag, and Pt TE's effect in the switching behaviours of ZnO-based RRAM. RS layer thickness of the ZnO was maintained as 90nm, and the bottom electrode was Pt for all scenarios [122].

Furthermore, consider the asymmetrical current nature observed, and this must be due to some microscopical mechanism observed in Pt/ZnO/Pt configuration. Thus, it reveals the possibility of an energy barrier between the Pt BE and the ZnO dielectric layer that hinders the smooth flow of electrons through the layers. Therefore, this will also be better understood using Fig. 8, showing an XPS analysis on the Pt BE surface [131]. It illustrates Pt 4f signal displaying four peaks, the peak at 71.2 and 74.5eV corresponds to the metallic Pt while the peaks at 75.9 and 72.6 eV depict the Pt at oxidized state (PtO_x). Moreover, the figure's inset with a peak at 530.4 eV further suggests the Pt's oxidation. But both peaks are revealing the formation of the interfacial layer of PtO_x. It is worth noting that this layer leads to the asymmetrical current nature of the Pt/ZnO/Pt structure.

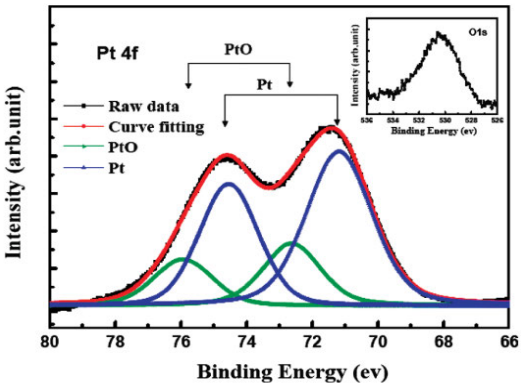

FIGURE 8. The bottom Pt electrode XPS spectra, showing the interfacial layer of PtO_x that is formed from the oxidation of Pt BE, spectra show the 4f signal of the Gaussian distribution form on the Pt BE. The inset of the O 1s spectrum shows the fusion of oxygen with the Pt to form PtO_x [131].

Interestingly, this rectifying effect could be applied in a cross-point array to alleviate misreading error [131]. The Pt's wettability would also significantly improve when a 2 nm Ge film is inserted between the Pt BE and the SiO_2 substrate [132]. Therefore, this would significantly resolved the array fabrication issue in obtaining high-quality thin film [133].

B. DOPING AND ITS SIGNIFICANCE IN ZnO BASED RRAM

The storage media is the insulating layer that functions as the critical component of the memory's resistance switching processes. The reliability and efficiency of a device are often the results of carrier-concentration in the storage layer. Therefore, numerous dielectric layer treatment and modification methods were reported to clarify the phenomenon and logic behind macroscopic modifications observed in various dielectric materials and control the resistive switching properties. Moreover, comprehension of charge carrier-concentration influence via native defects and structural modifications is vital to memristor material development and commercialization. However, several materials' modifications were proposed in the literature, like post-thermal material annealing or controlling the deposition parameters. These proved to be useful but not as effective as doping, as it carefully regulates and completely adjusts the native defects concentration [134], [135].

Nonetheless, doping is a process of improving material properties by the inducement of the microstructure and structural modifications for better performance and application in a particular scenario [136]. Numerous dopant elements were used to alleviate the native point defects typically found in

ZnO material, like Ti [134], [137], [138]. Ti has the capability of oxygen gathering effect. Ti has been reported to exhibit smooth structural incorporation within ZnO lattice due to its ionic-size (Ti^{4+}) is smaller than the Zn^{2+} [139], and its higher valence electrons may lessen the electrical resistivity and enhance electrical characteristics when dissipated into ZnO lattice [140]. The Fourier transform infrared spectroscopy (FTIR) of the Ti-doped ZnO is shown in Fig. 9. The FTIR image shows the chemical bonds and confirms the decomposition of TiO_2 after the dissolution of Ti^{4+} ions within the ZnO lattice by displacing the Zn^{2+} sites [141].

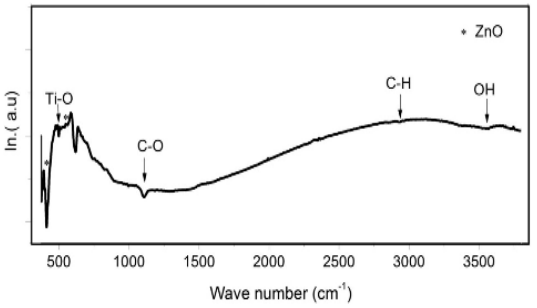

FIGURE 9. FTIR spectra showing Ti-doped ZnO nanostructure, the spectrum is measured within the region of the wave-number 370 to 4000 cm^{-1}, the shoulder observed at 500 cm^{-1} depicts the Ti-O bond, Reproduced from [141] with permission from Elsevier, 2017.

The exchange and correlation energies of the electrons in Ti-doped ZnO could be studies using local density approximation and computed based on density function theory [137]. The formation energies of V_O in numerous structures are usually calculated using (1). [142].

$$E^f[O^q] = E_{tot}[O^q] - E_{tot}[ZnO, bulk] - \sum_i n_i u_i + q[E_F + E_V + \Delta V]. \quad (1)$$

The over-all energy due to supercell with V_O in the cell is denoted by $E_{tot}O[^q]$, the over-all energy for the same supercell having the only ZnO is represented as $E_{tot}[ZnO, bulk]$. n_i Represents the number of atoms of type-i (either impurity or host atoms) that had been combined with $n_i > 0$ or detached from $n_i < 0$ supercell during the formation of the impurity. The equivalent chemical potential of atom i is giving as u_i, but the E_V, E_F are the Fermi level referenced to the bulk and the valence band maximum respectively. Finally, the ΔV represents correction-term. The term is used to align the reference potential found in doped supercell to the term found in pure-bulk ZnO.

Chromium (Cr) is known as a steel-grey metal, and it can increase alloy strength/corrosion resistance. Cr was demonstrated to increase the concentration of V_O when used doped with ZnO film (Cr-ZnO). Cr produces ferromagnetic property at room temperature in ZnO films. This is due to the radii differences of Zn^{2+} ion (0.74 A) and Cr^{2+} ion (0.62 A). Also, due to their similarities in electronegativity [143]. However, the real origin of this effect is still in contention [144].

Improved electrical performance decreases the dielectric values and increases the loss of tangents [145]. These were attributed to reducing the grain sizes due to the doped Cr in the host ZnO film. Interestingly, this form of the electrical resistivity reduction in (Cr:ZnO) may be applied in the ReRAM process and the microwave devices [145]. Also reported that Cr-doped ZnO function in dye contamination as impurity remover in water and enhance antibacterial activity was revealed by Cr^{3+} in ZnO nanoparticles [146], [147].

However, Cr doped ZnO film's effect may be best understood using Fig. 10 that shows the XPS-spectra of the Cr doped and undoped-ZnO films [148]. Fig. 10(a) illustrates the O 1s state showing binding energy of some (3) peaks at 529.8 eV, 531 eV, and 532.4 eV. Consider the plot shown at 532.4 eV peak, and it shows the state of the loosely bound O ions in the film. The peat at 531 eV shows the abundance of Vo in the film, while the peak at 529.8 eV shows the O_2 ions concentration in the crystal. In Fig. 10(b), the Cr-doped ZnO film peaks showing the Zn 2p3/2 and the 2p1/2 states show the film's oxygen insufficiency, which is due to the abundant V_O in the film [149]. In contrast, the undoped film shows a slightly higher Zn 2p state that indicates the abundance of oxygen in the film [131]. Fig. 10(c) shows the reduction in the states' size in the Cr 2p 3/2 and Cr 2p1/2 clearly shows the film's oxygen deficiency and confirms the substitution of some Cr^{2+} for Zn^{2+} sites [150].

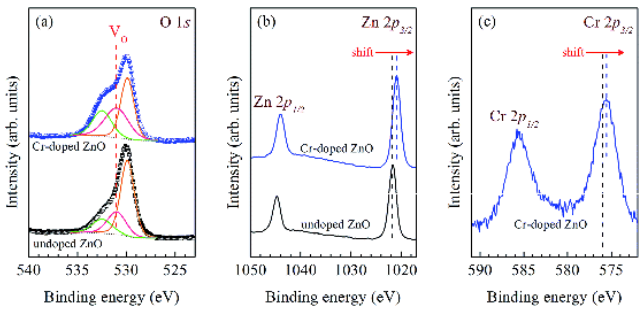

FIGURE 10. The XPS spectra are showing the binding energy states of the Cr-doped and undoped ZnO films. Interestingly, in (a), the peak at 529.8 eV of the Cr-doped ZnO film reveals a reduction in both the XPS signal area and the peak intensity, while the increase is witnessed in the 531 eV peak that depicts the abundance of V_O. In (b), the shift in the binding energy states between the bulk and doped ZnO films confirms the film's oxygen deficiency. In (c), the dotted shift in the lines shows the oxygen deficiency in the Cr-doped ZnO film. Reprinted with permission from [148]. Copyright 2019 Royal Society of Chemistry.

Furthermore, doping in ZnO thin film using Co was shown to enhance resistive switching performance, low operating voltage, forming-free switching, and set voltage stability [151]. But using 1%, Co has been proven to be more efficacious [135]. Interestingly, Co-doped ZnO film may reduce electrode materials' effect on the switching operation [152]. Additionally, controlling defect concentration alone is not enough to achieve better memory performance, but the orientation of the grain's growth of the RS layer also needs to be deliberated [151]. The grain size could be computed using Scherrer expression or the reviewed version of

the Scherrer constant [153] that gives additional broadening from small crystallites as shown in (2).

$$\epsilon = \lambda / b \cos\theta \tag{2}$$

where ϵ is the apparent crystallite size, b is the additional broadening in radians, the wavelength of the radiation is denoted by λ, θ denoted the Bragg angle. Also, the cube root of the crystallite volume is the 'true size' and defined by (3):

$$p = K\epsilon \tag{3}$$

The Scherrer constant K is a dimensionless number of the order of unity, where its real value relies on three things: the crystallite shape, the breadth definition, and finally, the crystallite size distribution [153].

Therefore, as presented in Fig. 11(a), the Co-doped ZnO film shows a forming-free process, while the undoped film, as presented in Fig. 11(b), requires an initially high forming of 4.02 V to set the device to LRS [152]. Low set voltage (V_{set} = 0.78 V) observed in Co-doped ZnO film is attributed to the Co nanoparticles [154] against the undoped ZnO V_{set} of 1.44 V. From Fig. 11(c). However, Co and Cu's TE materials show good operational characteristics due to their smaller ionic sizes. The low work function and their electronegativity [151], [155] makes them quickly diffused into the film layer, but they still show higher V_{set} voltages than the Co-doped ZnO film.

It is good to know that lower V_{set} voltages in Cu and Co are due to their active nature [122], unlike Pt TE [125]. Moreover, the V_{set} voltages observed in the Pt/ZnO-Co/TE devices are lower than those seen in the undoped ZnO cells due to the active electrodes and diffuse Co nanoparticles. Fig. 11(c) from [152], it also revealed that the dielectric layer's thickness also shows an essential role in influencing the device's characteristics [156].

Fig. 12(a) shows the Co-doped ZnO stable operation without forming progress, and this confirms the enhancement capability of Co nanoparticle when doped in ZnO film [135]. Fig. 12(b) indicates the possibility of non-reliance on TE material for better device performance. The LRS and HRS ratio shows a bright point for differentiating the storage of information [157].

However, doping ZnO film aims to decrease the native point defect concentration and stimulate compensator defects. Then, the displacement of Zn by Li in a Li doped ZnO film follows on with the Li_{Zn} transport that happens through the dissociative mechanism and required just small activation energy, especially in a Zn-rich material [158]. Interestingly, the Li_{Zn} diffusion is governed by the intrinsic defect concentrations. Also, some analysis showed that space-charge-limited-current laws and ohmic are behind the mechanism of conductivity in Li doped ZnO cells [159]. The substitution exchange between Li atoms at interstitial sites results in the replacement of Li by vacancy or Zn, and this effect can be best described using possibilities; the kick-out mechanism or Frank-Turnbull mechanism [158]:

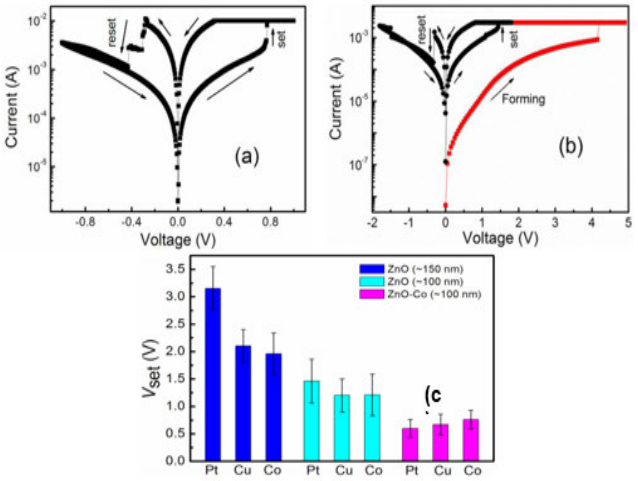

FIGURE 11. (a) The I-V curve for Co-doped ZnO film showing a forming-free process (b) The I-V curve for undoped ZnO film showing an initial requirement of high forming voltage to set the device for the first time. Both memory cells' sizes are fixed at approximately 100 nm, the first forming process (first cycle) is shown on the logarithmic scale in red dotted lines. (c) The set voltage values (V_{set})V using various top electrodes (Pt, Cu, and Co) on the structure of Pt/ZnO/TE and Pt/ZnO-Co/TE devices [152].

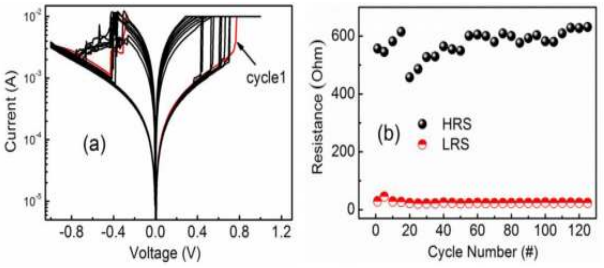

FIGURE 12. (a) I-V characteristics curve showing the sweeping directions for the Co-doped ZnO film (b) The semi-logarithmic scale. The endurance and reproducibility of the device [152].

Kickout mechanism shown in (4):

$$Li_{Zn} + Zn_i \rightarrow Li_i \tag{4}$$

While the Frank-Turnbull mechanism is in (5):

$$Li_{Zn} \rightarrow Li_i + V_{Zn} \tag{5}$$

Meanwhile, the Zn interstitial charge state is continually double-positive [104]. Therefore, in n-type, intrinsic, or Oxygen-rich materials, the kick-out reaction mechanism happens with no release or capture of free-charge carriers [158] as shown in (6).

$$Zn_i^{2+} + Li_{Zn}^{-} \rightarrow Li_i^{+} \tag{6}$$

But the exchange enthalpy proved to be independent of the Fermi level as depicted in (7).

$$\Delta H_{kick} = E_f(Li_i^{+}) - [E_f(Li_{Zn}^{-}) + E_f(Zn_i^{2+})] \tag{7}$$

The Li_{Zn}^{-} proven to be free Zn interstitials' sinks since the computation in (7) reveals the exoenthalpic nature of the reaction with the H_{kick} equals to −2.76 eV [158].

Consequently, the diffusion mechanism is usually resolved using the corresponding activation energies when the dominant is vacancy-mediated or interstitial-mediated. Hence, various doping elements were tabulated, and Table. 1 shows the summary of doping elements' influence on the ZnO-based RRAM device's operation.

Moreover, a controlled amount of doping reduces the bandgap of material and modulates its conductivity on either electrical, structural, or optical properties. But excessive doping may further weaken material conductivity and stability [137], [149], [151], [160]. Also, a well-textured c-axis structure is usually affected during doping. Hence deterioration often weakens this structure after excessive doping [151].

C. MULTI-LAYERED ZnO BASED RRAM

Significantly, the multi-layered and embedded structure is also considered a better alternative to doping because of the easy-tuning of the device's characteristics of the dielectric material. Switching behaviours like the set and reset currents could be easily modulated by manipulating the switching mechanism. A forming free device with operational voltages as low as 0.4 V ON state/-0.55V OFF state was reported [174]. A multi-layered structure device could be used to produce other forms of switching performance. It is significant to note that the RRAM device can exhibit both magneto-resistance and resistive switching characteristics when a bilayer of ZnO/ZnO-Co was employed [175]. A device with these properties can exhibit up to four resistance states via electrical and magnetic fields' proper modulation. Thus, this opens up a new trend towards achieving significant data densities in RRAM devices. Table. 2 illustrations various multi-layered and embedded ZnO-based RRAM found in some published literature.

Interestingly, Ga_2O_3 lacks V_O, while ZnO has abundant V_O. Li *et al.* [177] came up with an RS bilayer of Ga_2O_3/ZnO compound films using atomic layer deposition (ALD). The Zn and V_O content could be controlled within the dielectric layer by regulating the cycles during the ALD process. As such, enough V_O could be produced via the addition of Zn into the films of Ga_2O_3. A forming-free device could be achieved with 31% content of Zn in a sample having 14 sublayers of ZnO and 15 of Ga_2O_3 under 1 ALD cycles and 6 ALD cycles, respectively [177]. The current conduction mechanism (CCM), as shown in Fig. 13, follows the Space Charge Limited Conduction (SCLC) model, thus, controlled by the ohmic-conduction mechanism at LRS. Therefore, this shows a linear relationship due to the CF formation between the electrodes after the SET process. Usually, SCLC happens when the introduced charge-density surpasses the intrinsic free-carrier-density contained in the film. From Fig. 13(d) and (e), a multi-stacking structure of ZnO/Ga_2O_3 was formed due to a relatively thick layer of Ga_2O_3. But Fig. 13(f) shows no energy barriers in the GZIII films, and a substantial amount of V_O still occurs at HRS. The slop of 1.24 confirmed that this film's SCLC is a trap-assisted one, while those in GZI and GZII with a slope of 2.0 possess SCLC without tap-assistance. Due to the insignificant defects in the Ga_2O_3 layer at HRS.

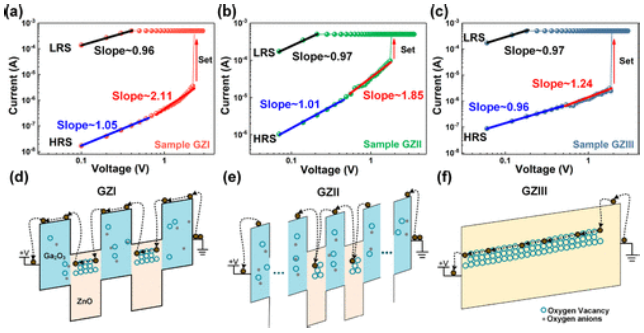

FIGURE 13. The double log scale showing Log of current (I) Vs log of voltage (V) at LRS and HRS, with energy-diagram at HRS for (a and d) of device GZI with an RS layer thickness of 14.2 nm, (b and e) for GZII with 11.8 nm and (c and f) for GZIII with a thickness of 10.5 nm. Reprinted with permission from [177]. Copyright 2020 American Chemical Society.

From Table. 2, nanostructured GZO/ZnO with Ag TE and Pt BE is shown to exhibits a low set voltage V_{set} of 0.4 V, and it required no electroforming process in the initial state. This device demonstrates low voltage than Ag/ZnO/Pt device developed without GZO nanoparticles [185]. The low voltage observed is due to the Ag TE and buffer layer of GZO films dispersed in the ZnO medium due to the Ag TE and buffer layer's positive influence. This mechanism originates conduction and reduces the operational power significantly [186].

The use of Ag TE's in the Ag/CuO/ZnO/Pt structure proved to be promising. The RS with the Ag TE is recognized by the process of migration of metal-cations and electrochemical metallization. Thus, it confirmed the notion that CF's operational nature affects several characteristics of the device's functional dynamics [184]. Fig. 14 shows the statistical analysis and current-voltage (IV) curves of Ag/CuO/ZnO/Pt (ACZP) and Pt/CuO/ZnO/Pt (PCZP) structures [184]. The IV curves of PCZP shown in Fig. 14(c) displays the dispersions of the V_{set} occur at 1.2 to 3 V while that of the V_{reset} occurs between -0.5 to -1 V. Unlike the dispersion of the ACZP that clearly shows a significant reduction in the V_{set} voltage, it happens at 0.6 to 0.8 V. Thus, the ACZP plots and curves indicate the effect of the Ag TE inflict on the switching-dynamics of the structure due to electrochemical metallization.

D. EFFECT OF DEPOSITION PARAMETERS

The thin-film deposition method significantly governs the control of material/layer thickness within a few tens of nanometers. Thin-film is a thin layer of material whose thickness ranges between numerous nanometers (nm) to a few nm. It's a layer of material deposited on a bulk substrate to change/imparting properties that are lacking/unattained by the base material. Therefore, thin films are regarded as the backbone of technology nowadays, used in various fields like telecommunications, energy storage devices, environmental,

TABLE 1. ZnO based RRAM with various doping elements.

TE	Oxide	Thickness (nm)	BE	Mode	V_{set} (V)	V_{reset} (V)	CC (mA)	V_f (V)	Retention (seconds)	Endurance (cycles)	ON/OFF ratio	Ref
Au	ZnO:Ti	NS	ITO	B	2.9	-2.7	-	FF	2×10^3/RT	100	14	[134]
Pt	Co:ZnO	90	Pt	B	∼1	∼-0.8	∼15	FF	NA	NA	NA	[135]
Pt	ZnO:Ti	50	n^+-Si	U	2 - 4	∼1	10	∼5.5	$>10^5$/RT	200	$>10^2$	[137]
Pt	ZnO:Cr	100	IZO	B	0.89	-0.86	1	∼2.5	10^5	10^5	9.12×10^2	[148]
ITO	$Zn_{1-x}Co_xO$	38	ITO	B	×1.2	×-1.5	5	∼3	NA	5000	15	[151]
Al	Cu:ZnO	50	ITO/glass	B	2.4	-1.8	1	∼4	10^4	NA	656	[155]
Al	ZnO:Li	NS	LaB_6	U	1.85	2.5	-	NS	NA	20	10-15	[159]
Pt	$Zn_{1-x}Cr_xO$	NS	Pt	B	∼3	∼-3.5	-	FF	36×10^3/RT	100	7×10^3	[149]
Pt	ZnLaO	∼200	p-Si	U	∼2.5	∼1	10	∼6	10^6	150	>10	[161]
Pt	$ZnO_{0.99}V_{0.01}O$	250	Pt	B	-1.5	2	0.1	FF	10^4	90	10^2/85°C	[160]
				U	∼-3.0	∼-0.8	∼10	∼-4		10^4	$>10^3$	
Pt	$Mn:ZnO_xS_{1-x}$	NS	Cu	U	1-3	∼0.5	NS	NS	10^4/RT	100	10^5-10^6	[162]
Ti	MZO	115	Pt	B	1.08	-0.76	-	NS	NA	300	3	[163]
Au/Cr	ZnO:N	40	TiN	B	∼0.75	∼-1	5	2.5	10^4/RT	100	∼1	[164]
Ti	$Mg_{0.1}ZnO_{0.9}$	NS	Pt	B	1.5	-1.5	1	FF	10^4	500	$>10_3$	[165]
Pt	$Zn_{0.99}Zr_{0.01}O$	∼200	Pt	B	∼-1.5	∼1	1	∼-2	NA	10^4	$\sim10_2$	[54]
				U	∼-2.34	∼-0.8	10	-	-	216	$>10_2$	
TiN	MgZnO/ZnO	25	Pt	B	∼-1.2	∼1.2	-	-	20×10^3	500	-	[166]
Ag	$Zn_{1-x}Pr_xO$	x≡4% of Pr	FTO	B	0.6	0.5	10	7.08	NA	NA	2.50	[167]
		x≡1% of Pr		B	1.2	0.8	10	8.0	NA	NA	2.35	
Ag	MgZnO	NS	Si	B	∼3.5	∼-3	-	FF	10^5	100	1000	[168]
Pt	Hf:ZnO	NS	TiN	B	0.75	-0.50	5	3.9	$10^4/85_oC$	100	100	[169]
Pt	$Mg_{0.2}Zn_{0.8}O$	350	Pt	U	∼1.0	∼0.65	-	30	NA	NA	50	[170]
Pt/Ag	ZnO:Li	46	Pt/T	B	0.18	-0.18	5.0	NS	-	-	$>10^2$	[171]
		92			0.33	-0.33	5.0	NS	10^4	$>10^2$	$>10^2$	
		223			0.53	-0.76	5.0	NS	-	-	$>10^2$	
Al	ZnO:Cu	100	Pt	U	∼2.0	∼0.5	10	NS	10^4	450	NA	[172]
Pt	Mn:ZnO	50	Si	B	-	-	NS	-	-	-	-	[120]
			Pt	U	∼6	∼1.2	-	-	>5000	-	2×10^2	
Pt	ZMO	NS	IZO	B	1.22	-1.01	10	FF	NA	$>10^5$	5.34×10^3	[173]

CC: compliance current, V_f: forming voltage, FF: forming free, B: bipolar, U: unipolar, NA: data not available and NS: not specified

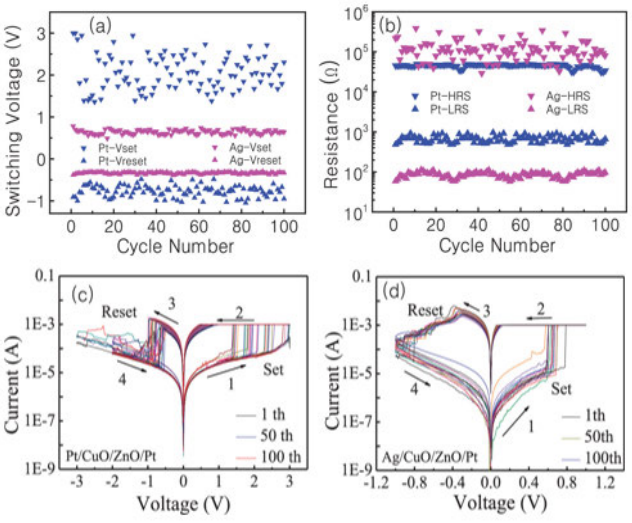

FIGURE 14. Statistical analysis and current-voltage (IV) curves of PCZP and ACZP structures, (a) V_{set} and V_{reset} voltages in the 100 sets/reset switching cycles [184]. (b) The R_{off} and R_{on} within the 100 reset/sets switching-cycles [184]. Blue triangles illustrate operation factors exhibits by PCZP film, and the magenta-triangles give the operation factors of the ACZP film. The semi-logarithmic scales are shown in (c) and (d), with the numbered arrows designate voltage sweeping orders [184].

medical devices, etc. [186]. Thin-film morphology and stability depend strongly on deposition techniques used. Hence, to obtain quality thin films for a particular application, there is a need to choose from the two main deposition methods; the chemical or the physical methods [186].

The sol-gel method is a wet chemical deposition method that involves some chronological steps. However, the technique is used for the preparation of metal oxides. Additionally, the sol-gel process is a low temperature and less expensive approach that permits fine control of material/thin film thickness. Ayana *et al.* [187] presented a sol-gel spin coating method employed during the preparation of 0.5 and 0.1 at.% undoped and Al-doped ZnO. They demonstrated that electronic charge carriers density of ZnO lattice are usually influenced/alters by the replacement of Zn^{2+} ions with cations of more significant oxidation states like the Al^{3+}. It is worth noting that adding Al^{3+} ions to Zn^{2+} solution enhances the nucleation-sites, hence producing an advanced density of the grain boundary and creating lesser grains that were predicted to improve switching characteristics of memristor [188]. Furthermore, the sol-gel route, curing conditions, and Al doping significantly influenced the homogenous ZnO thin-films morphological and structural grain-sizes. They were found to be promising for the development of dense/multi switching layers. Al-doped ZnO (AZO) possesses high transmittance in the visible wavelength range, hence a right candidate for optoelectronic devices. AZO is less expensive than Ga-doped ZnO (GZO) and a superior alternative to ITO. It is essential to note that increases in thickness in this AZO film decrease optical transmittance

TABLE 2. Multi-layered ZnO based RRAM.

TE	Oxide	Thickness (nm)	BE	Mode	V_{set} (V)	V_{reset} (V)	CC (mA)	V_f (V)	Retention (seconds)	Endurance (cycles)	ON/OFF ratio	Ref
Ag	GZO/ZnO	100/10	Pt	B	0.4	-0.55	10	FF	1.1×10^4	∼40	2×10^3	[174]
Pt	ZnO/ZnO-Co	80/(0.7:0.6)×50	Au	B	∼2.48	∼-1.08	∼15	FF	NA	NA	580@0.1V	[175]
Al	ZnO/ZnO_{1-x}	30/300	ZnOAl	B	∼1.4	∼-1.5	10	FF	NA	NA	4.8@1V	[176]
Pt	Ga_2O_3/ZnO	14.5	Pt	B	∼1.7	∼-1.4	NS	4	1×10^4	20	5×10^2	[177]
		11.6			∼1.8	∼-1.0		∼3.5		40	4×10^3	
		10.2			∼1.9	∼-1.0		∼3		100	6×10^3	
Au	ZnO-Co/SiO_2-Co	(0.7:0.60)× 50/(0.6:0.6)×60	Pt	B	∼0.7	∼-0.5	-	NS	NA	NA	NA	[178]
Pt	ZnO/CoO_x/ZnO	NS	Pt	B	1.5-2.9	0.8-1.8	10	FF	NA	200	$\sim10^2$	[179]
Pt	TiO_x/ZnO	50	n^+-Si	U	∼2	∼0.5	NS	∼2.8	NA	>50	$>10^2$	[180]
Pt	ZnO_{1-x}NRsTF	150/100	Pt	B	1.3	∼-0.7	∼10	∼2.8	10^4	90	40	[181]
Pt	ZnLaO/ZnO	200/20	Pt	U	2.3	∼1	10	∼3.5	10^4/65°C	100	$\sim10^4$	[182]
TiN	MgZnO/ZnO	NA	Pt	B	∼1	∼-2	10/20	∼6	3×10^4/RT	10^4	>50	[183]
Pt	$(ZnO/Ti/ZnO)_{1-4}$	NA	ITO	B	∼2	∼-2.5	NS	FF	$>10^6$	320	$\sim10^3$	[138]
Ag	CuO/ZnO	60/60	Pt	B	0.64 ± 0.15	- 0.35 ± 0.04	1	NS	NA	NA	10^3	[184]
Pt					2.1 ± 0.9	- 0.75 ± 0.25					10^2	

CC: compliance current, V_f: forming voltage, FF: forming free, B: bipolar, U: unipolar, NA: data not available and NS: not specified

and increase electrical conductivity. As such, the AZO film thickness needs to be higher than 895 nm to function as an excellent transparent conductance oxide, but care must be taken because of the difficulties in keeping the electric-oven temperature constant when developing the film [189]. A spin coating less expensive chemical technique was used in synthesizing the solution of Cu:ZnO. Thus, it reveals the potential of Cu as the electron trap in ZnO. It enhances resistivity and imparts ferroelectric properties [190]. The chemical technique synthesized Cu:ZnO shows resistive characteristics when annealed at 450^{o}C, and the same film shows ferroelectric characteristics when annealed at 800^{o}C. It unveils the dual capacity of the chemically synthesized Cu:ZnO for ferroelectric material and a forming free low power RRAM device [155]. Moreover, it shows the effect of post-annealing temperature [191] on chemically synthesized Cu:ZnO. Dongale *et al.* [192] also used a simple aqueous chemical route to synthesize nanostructured ZnO nanorods thin film. The developed device shows the low operating voltage. A thermal reaction model was used to study the outcome of temperature on the ZnO-based RRAM device. The result suggests that the CF temperature increases rapidly and influences the device memory window. Moreover, the use of chemical deposition-based techniques for the development of RRAM indicates the significance of the method for the synthesis of ZnO-based RRAM with a multi switching layer, good transmittance, and ability to control the thickness of the deposited layers.

Employing the control of substrate temperature when doing the sputtering process is a moral way of regulating the V_O content of ZnO film and enhancing the film's crystallization. Hsu *et al.* [193] reported ZnO-based RRAM fabricated under a 50 W low frequency power, and a film's temperature of 25 - 160^{o}C lacks resistive switching characteristics but possesses high conduction currents. Moreover, optimal values of 240 - 320^{o}C are shown to be more appropriate for attaining the resistive behaviours for ZnO-based RRAM with 10 - 250 μm spaces. Furthermore, an extremely low conduction current was observed at a higher 400^{o}C and with vague electrical characteristics. Moreover, the regular resistive feature is witnessed after ∼ 200 cycles for a substrate's temperature of 240^{o}C, and sweep-voltage of ±3 V, as shown in Fig. 15(a) by Hsu *et al.* [193]. But, this substrate's endurance for a read-voltage of −0.4 V produces a memory window of −4.17, as demonstrated by Fig. 15(b) [193]. Similarly, Wu *et al.* [194] show three different resistance states using two dissimilar sweep-voltages of 4 V and 5 V. They reveal the likelihood of obtaining a ZnO-based multi-bit RRAM device. Also, it demonstrates the possibility of controlling HRS/LRS via controlling the sweep-voltage.

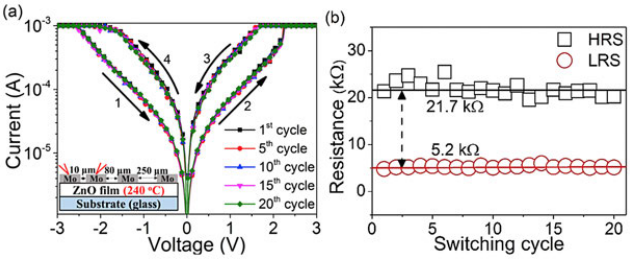

FIGURE 15. Resistive switching behaviour and endurance cycles of ZnO-based RRAM developed at 240^{o}C substrate temperature with an electrode distance of 10 μm. (a) Resistive switching curves after ∼ 200 cycles for a substrate's temperature of 240^{o}C and sweep-voltage of ±3V [193]. (b) Memory window of 4.17 produced at the endurance's read-voltage of −0.4 V [193].

Furthermore, Hsu *et al.* [193] shows in Fig. 16(a) and (b) lower conduction currents and stable device characteristics, but extremely high resistance is witnessed when the electrode's span distance was 80 μm and 320^{o}C substrate's temperature. Also, it reveals that the electrical characteristics for the lateral ZnO-based RRAM with the electrode's span of 10 μm cannot be realized when the temperature of the

substrate is raised to 400^{o}C. It is worth noting that keeping the substrate temperature of 240 - 320^{o}C proved to be useful for fabricating a planar-based ZnO device with an electrode's distance of 10 – 250 μm [193].

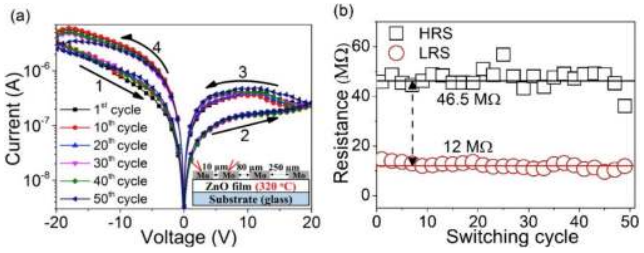

FIGURE 16. Resistive switching behaviour and endurance cycles of ZnO-based RRAM developed at 320^{o}C substrate's temperature with an electrode's distance of 10 μm. (a) Resistive switching curves after ~ 200 cycles for a substrate temperature of 320^{o}C and sweep voltage of ±20V [193]. (b) Memory window of ~ 3.88 produced at the endurance's read voltage 1 V [193].

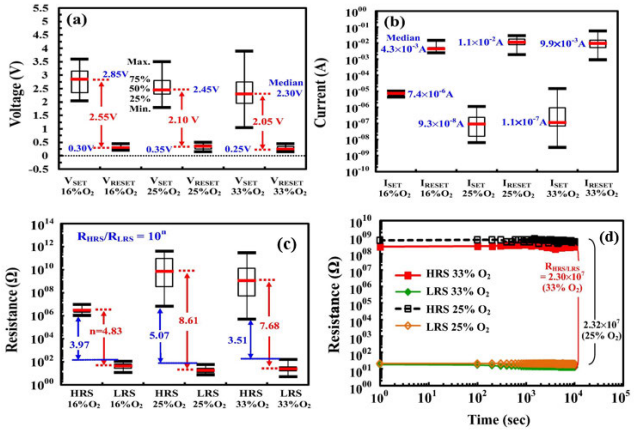

FIGURE 17. Performance of Al/ZnO/Al RRAM at various oxygen flow rations. (a) V_{set} and V_{reset} box plots at various O_2 flow rations. (b) I_{set} and I_{reset} box plots at various O_2 flow rations. (c) HRS and LRS at various O_2 flow rations for AL/ZnO/Al RRAM. (d) The retention behaviour of Al/ZnO/Al RRAM at O_2 flow ratios of 25% and 33% measured at 0.1 V [197].

Similarly, the effect of growth temperature on a ZnO-based RRAM device was demonstrated by Gupta *et al.* [195], which indicates that the films show better crystalline conductivity, electron mobility, and its transparency increases with the increase in the deposition temperature. Another multilayer thin film of ZnO-based device is proposed by Gupta *et al.* [196] that confirms the effect of deposition temperature. Therefore, the choice of suitable substrate temperature during thin film deposition shows tremendous influence on the electrical characteristics, optical/structural properties of a ZnO thin-film.

The effect of oxygen content during the development of ZnO thin-film on the performance characteristics was demonstrated by Lin *et al.* [197], three sets of ZnO based RRAMs were developed under numerous oxygen (O_2) gas flow rations: 33%, 25%, and 16% with [O_2/(O_2 + Ar) = 12 sccm/(24 sccm + 12 sccm)], [O_2/(O_2 + Ar) = 8 sccm/(24 + 8) sccm)] and [O_2/(O_2 + Ar) = 4.6 sccm/(24 + 4.6) sccm)] respectively. Lin *et al.* [197] elaborates the advantage of the ZnO thin film developed under the O_2 flow ratio of 33% as shown in Fig. 17. The 33% device shows low values of the V_{reset}/V_{set} voltages, better resistance ratio, and the retention reliability recorded at 0.1 stress voltage under the O_2 flow ratios of 33% and 25% remains stable for up to 10^4 for both oxygen flow conditions [197]. Therefore, oxygen composition during the deposition of ZnO-based RRAM has a significant effect on the electrical characteristics of the deposited material. The optimal number of V_O/oxygen ions found during the rupture of CF are keys for enhancing the reliability and operation of the ZnO-based RRAM.

Similarly, the room-temperature oxidation process is good in controlling the ZnO defect concentrations. The process allows the ZnO's resistive layer to absorb neutral oxygen particles that significantly enhance the developed film's resistance ratio (ON/OFF) [198]. Also, it should be noted that surface treatment by irradiation with a neutral oxygen beam induces characteristics that stimulate switching in very thin ZnO films and at lower compliance current.

Rapid hydrogen annealing treatment has provided another alternative for achieving improve thin-film crystallinity and vacancy injection layer. Fig. 18 shows an auger electron spectroscopy (AES) depth profiles demonstrated by Sun *et al.* [199]. It shows the depth profiles of ZnO nanorods before and after the annealing treatment. It gives an insight into the change in oxygen concentration noticed after the treatment process, apart from the dramatic increase in resistance ratio, multilevel resistance, and enhanced memory characteristics observed after the formation of injection electrode due to the annealing process [200].

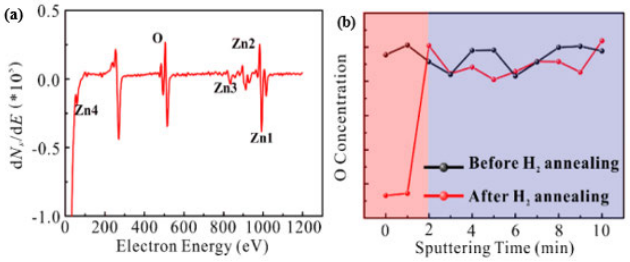

FIGURE 18. Photoluminescence spectra of ZnO Nanorods. (a) surface auger electron spectroscopy (b) surface auger electron spectroscopy depth profiles of ZnO nanorods. The pink region represents the ZnO nanorods' surface part, while the blue region represents the inner region. Reprinted with permission from [199]. Copyright 2015 American Chemical Society.

Radio-frequency (RF) sputtering is a popular method of ejecting microscopic particles of solid material after the material's bombardment by energetic particles of gas or plasma. The effect of the RF sputtering power on the switching characteristics of ZnO-based transparent RRAM was recently demonstrated by Simanjuntak *et al.* [201]. They reveal that device breakdown and vague switching characteristics

may occur when an RRAM device is developed using a low RF power. In contrast, high RF power produces RRAM with enhanced switching characteristics but reduced switching uniformity and reduced stress and strain [202]. Fig. 19(a) and (b) are insets of RRAM devices developed by Simanjuntak *et al.* [201] using a low RF power of 25 W and 50 W, respectively. The designed device failed to produce visible switching behaviour. Instead, it only shows susceptible device breakdown. The insets shown in Fig. 19(c) and (d) are I-V characteristics observed using RF power of 100 W and 200 W demonstrated by Simanjuntak *et al.* [201] respectively. They show a counter-clockwise bipolar switching characteristic and can toggle from LRS to HRS after applying a negative sweep bias voltage.

Therefore, RF sputtering power significantly affects the switching characteristics and structural uniformity [203], [204] of ZnO-based transparent RRAM. Sputtering pressure also plays some vital roles in the fabrication of ZnO-based RRAM. The effect of sputtering pressure was demonstrated recently by Simanjuntak *et al.* [205]. The work reveals that devices developed with a low sputtering pressure show write-once-read-many-times (WORM, non-erasable) memory behaviours [206], [207]. In conclusion, those devices developed with a high sputtering pressure typically show reproducible switching behaviors (rewriteable, erasable) [202], [208]. Interestingly, the permanent physical damage observed in devices developed with low sputtering pressure could be employed for data–security uses against the misuse of data and illegal software/hardware use [205]. Therefore, this opens up a new trend of memory application in securing data and information.

The atomic layer deposition (ALD) offers the technology for uniform materials deposition and design of the device's structures with controllable thickness [209]. Precisely low substrate temperature, but the new approach to this technology called Spatial ALD (SALD) has continued to gain momentum, which is based on separating the precursors in space (physical separation) rather than separating in time (temporal separation) [210]. The reported study [211] on SALD methods using ZnO thin film suggests that the lower substrate temperature limit at constant precursor partial pressures during the deposition lies between 100 - 150^{o}C. Also, the precursor exposure times should be varied from 25 – 400 ms. SALD can also sustain deposition of substrate temperature varied up to 300^{o}C highest limit. The film's refractive index increases when the annealing temperature gets between 300 - 700^{o}C, after which the carrier concentration decreases. The V_O defects are observed to be suppressed [212], and the film resistivity decreases at 800^{o}C. The method support deposition at a fraction of time usually used by the ALD method, high quality of deposition with high throughput, and support area-selective deposition [210]. Li *et al.* [177] recently demonstrated how to precisely control the content of Zn and V_O concentration in an ALD deposited Ga_2O_3/ZnO composite resistive layer via adjusting the number of the composite resistive layer cycles during the ALD

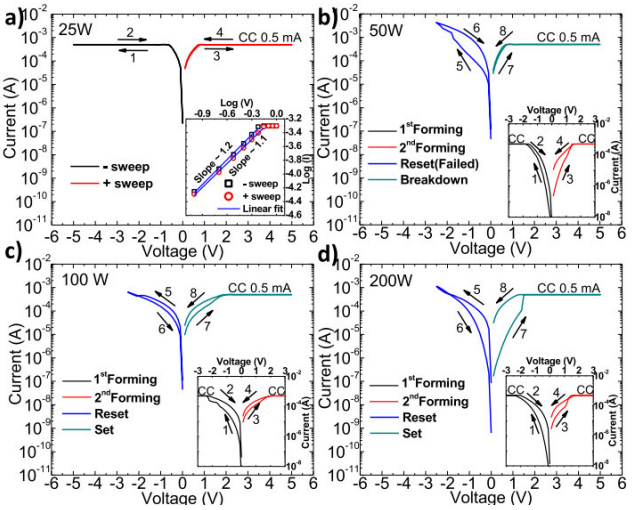

FIGURE 19. Characteristic I-V of AZO/ZnO/ITO/PEN RRAM device developed under various RF powers; (a) Device developed with 25 W RF power, the device shows very-low resistivity and unable to produce switching behavior (b) Device developed using 50 W RF power, the device shows an LRS that leads to its failure even with the application of the negative voltage it refused to switch to the HRS (c) Device made with RF power of 100 W (d) Device developed using RF power of 200 W. The 100 W and 200 W RF power produce devices with counter-clockwise bipolar switching characteristics [201].

process. It was found that $\approx$ 31% content of Zn enhances the resistive switching characteristics of the deposited film, a forming free property, an approximate 1000 resistance ratio, the endurance of 100 cycles, and more than 10^4s retention time were observed [177]. Therefore, ALD and SALD are competent methods for depositing ZnO-based RRAM, yet the techniques are still evolving, and more investigations are required for further consideration.

E. HYBRID LAYER AND ITS SIGNIFICANCE IN ZnO BASED RRAM

Graphene has been one of the materials that have shown great promise in the RRAM application. Graphene is a structure consisting of a crystalline carbon allotrope. Also, Graphene is a 2-dimensional nanomaterial typically used as Graphene oxide (GO) [213]. Moreover, GO is versatile, transparent, not costly, and has a wide surface area; the use of the hybrid structure of organic and inorganic oxides has been studied long ago [214]. Furthermore, graphene can be used in a reduced form to generate good RS characteristics [215]. Also, it can function as an electrode [216] to lower the RESET operational current, thus providing a possible means of dropping the RRAM programming energy.

The organic and inorganic hybrid structure is another way to improve the RS characteristics of the RRAM material [215]. The ZnO/rGO hybrid has exhibited excellent electro-catalytic behaviour for the oxygen reduction reaction used in fuel cells and renewable energy technology [213], [215]. Graphene has been employed along-side other materials in creating a highly transparent and flexible RRAM

device [217], [218] with a transmittance of more than 82 % in the visible field. Therefore, rGO can store oxygen that is needed for the switching of RRAM devices. It was confirmed in [219] that proposed a ZnO-based RRAM structure with a thin rGO coating layer of 13 nm. The insertion of the rGO was revealed to enhance the crystallinity and boost the device switching dynamics [215], [220], [221]. Cardarilli *et al.* [222] demonstrates the diffraction patterns of ZnO with and without rGO as shown in Fig. 20. ZnO and rGO have a good crystalline formation and show hexagonal wurtzite structures. It shows a good hybridization form. From the peaks of Fig. 20(b), it offers the reduction of the GO to rGO due to the absence of other diffraction peaks. The rGO/ZnO hybridization greatly affects the V_O interstitial effect found in the ZnO structure. The composite surface was found to possibly chemisorbed oxygen [222], thus generated quite several vacancy layer/pool that consequently enhances the crystalline of the film and device performance [214], [219], [222]–[224].

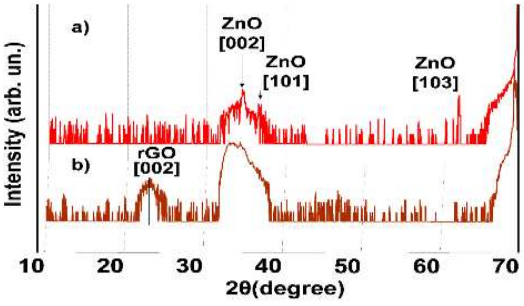

FIGURE 20. X-ray Diffraction pattern of (a) ZnO without rGO (b) Hybrid of ZnO with rGO. The hybridization of the rGO and ZnO greatly enhances the structure and performance of the device [222].

Moreover, Ahmed *et al.* [226] demonstrates the optoelectronic characteristics of ZnO and GO contents using microwave techniques as depicted by Fig. 21. The composite of ZnO-Graphene (GZ) shows improved oxygen contents spectra, as shown in Fig. 21(b) due to the chemisorption process at the GZ layer. The change in the ionic state of the surface oxygen results in the peak position shift from 530.6 eV of ZnO to 531.6 eV of GZ composites spectra. Thus, indicating the presence of oxygen atoms at the ZnO surfaces [225]. Also, the formation of the bond by ZnO at the GO sheets is due to the presence of the following functional groups C-O, O-C=O, C=C, and C=O as shown in Fig. 21(c) and (d) show the disappearance of C=O peak (284.3 eV) and peak at (288.3 eV) that indicates the reduction of GO to rGO [226]. Therefore, the bonding between the ZnO and GO is a promising one. It shows an evenly distributed crystalline structure, V_O healed ZnO composites, and enhanced photo-catalyst film for future optoelectronic memory applications.

Furthermore, to demonstrate the significance of GO capping layer in ZnO based RRAM device. Lin *et al.* [219] studies the switching characteristics of ZnO without GO

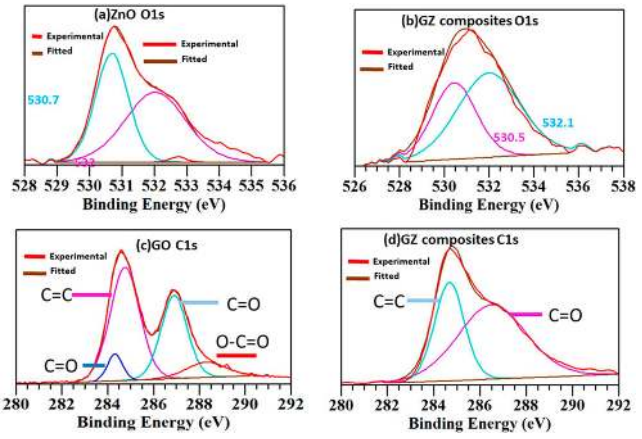

FIGURE 21. O1s and C1s core levels spectra of ZnO, GO and GZ (a) ZnO composite showing the O1s core level spectra (b) GZ composites showing the O1s core level spectra (c) The GO composite showing the C1s core level spectra (d) The GZ composite showing the C1s core level spectra. The insets show the distribution of the binding energy (eV) related to the ZnO nanoparticles' hybridisation with GO composites. Thus, (a), (b), (c) and (d) elucidates the oxidation of the oxygen atoms in the stoichiometric of GZ composites [226].

as Al/ZnO/Al, ZnO with GO as Al/ZnO/rGO/Al, and Al/rGO/ZnO/Al RRAM structures as shown in Fig. 22. Devices with the rGO capping layer show better-switching abilities than those without the rGO, as observed from the I-V switching characteristics as seen in Fig. 22(a), (b), (c) and (d) [219]. The device in Fig. 22(e) and (f) has the most stable switching curve. However, inserting a capping layer of rGO in the structure between the ZnO and electrodes may enhance the overall switching characteristics due to the oxygen storage reservoir nature of the rGO layer [215], [218], [221]. Still, more investigations are needed to elucidate the influence of GO capping layer properties on the ZnO switching characteristics under the various bottom and top electrodes. The resistive switching characteristics of ZnO with rGO capping layer RRAM devices are shown in Table. 3.

The use of ZnO–Graphene quantum dots (GQDs) nanocomposite was demonstrated by Ji *et al.* [229]. The composites acted as charge trap sites that result in better switching characteristics; their one-diode-one-resistor (1D1R) design may effectively cater to cross-talk issues between an array of memory cells as elaborated in [229] and shown in Fig. 23(a) and (b). Furthermore, the use of Schottky diode in 1D1R crossbar memory devices in tackling the cross-talk or sneak paths issues has superior advantages over the use of PN junction diode [233]. The insertion of ZnO nanorods (ZNs) in the GO sheet using Al and indium tin oxide (ITO) coated polyethylene terephthalate (ITOPET) substrate as top and a bottom electrode, respectively. Thus could significantly enhance the V_O storage and lower the operating voltage [228], the inset shown in Fig. 23(c) shows the structure with the embedded ZNs and Fig. 23(d) demonstrates the improvement in the structure's operational voltage with ZNs compared to those without ZNs as elaborated by Khurana *et al.* [228]. Besides, using vertically grown

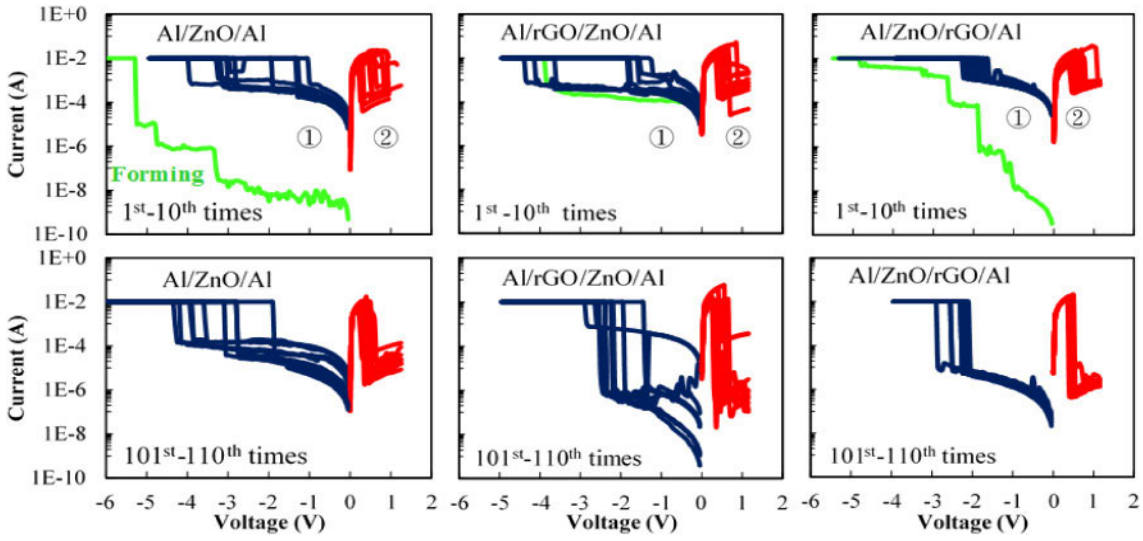

FIGURE 22. I-V Switching characteristics (a) without rGO at up to 10th times (b) without rGO between 101th to 110th times (c) with rGO/ZnO at up to 10th times (d) with rGO/ZnO between 101th to 110th times (e) with ZnO/rGO at up to 10th times (f) with ZnO/rGO between 101th to 110th times. From the insets shown in the figure, the cooperation of the rGO in the ZnO film offers the layer's ability to enhance the device's switching dynamics [219].

TABLE 3. ZnO with GO capping layer found in the literature.

Structure	Mode	CC (mA)	V_f(V)	V_{set}(V)	V_{reset}(V)	Endurance (cycles)	Retention (seconds)	ON/OFF ratio	Ref
ITO/graphene/ZnO/ITO	B	5	4	-1	∼-2,5	100	104/85^{o}C	7000	[220]
Al/rGO/ZnO/Al	B	10	6	NS	NS	10^3	$\sim10^4$	10^5	[219]
Al/ZnO/rGO/FTO	B	100	NS	4.5	-4.5	NA	NA	40	[222]
Ag/ZnO-rGO/FTO	B	200	NS	4	-5	NA	NA	NS	[227]
Al/GOZNs/ITOPET	B	2	∼5	2.1	-2	200	$\sim10^4$	100	[228]
Al/PS:ZnO-GQDs/Al	U	NS	NS	NS	NS	10^2	10^4	$\sim10^3$	[229]
Pt/ZnO-Graphene/Pt	B	∼1	NS	∼5	∼-5	NS	NS	3.11@350^{o}C	[230]
Al/ZnO-GQD/Pt	B	20	FF	0.88	-0.82	10^3	10^4	10^3	[231]
Pt/GO/ZnONRs/GO/ZnONRs/ITO	B	NS	NS	∼4	∼-4	NS	NS	NS	[232]
Pt/GO/ZnONRs/GO/ZnONRs/GO/ZnONRs/ITO				∼5.8	∼-5.8	1000	5×10^4	3.3×10^5	

CC: compliance current, V_f: forming voltage, FF: forming free, B: bipolar, U: unipolar, NA: data not available and NS: not specified

one-dimensional ZNs as a guided filament for RS proved to be effective [232], [234].

However, developing it horizontally in the GO sheets may maximize the contact area between the films [235], reducing the operating voltage compared to using GO alone [226]. It is worth noting that GO film embedded with ZNs with a weight ratio of 15:1 (ZnO:GQD) tends to exhibit ultra-low operating power of approximately 75% lower than a device with pure ZnO nanocomposite. It may operate with the RESET and SET operating powers of 8.79×10^4 and 2.56×10^4, respectively [231], whereas those developed with ZnO:GQD weight ratio of 35:1 shows similar operating characteristics to pure ZnO nanocomposite. Therefore, ZnO:GQD composite weight ratio significantly influences the device switching dynamics. Attention should be paid to the composite weight ratio during device development for better uniformity and switching enhancement to realizing the practical application of the future next-generation memory [232], [236]. Moreover, an increase in the number of layers of the composite may decrease the OFF current. Still, the ON current would remain constant due to the enhanced uniformity, sufficient V_O, and space charge effect, consequently conserving the ON current that improved the ON/OFF ratio [232].

F. TRANSPARENT/FLEXIBLE ZnO BASED RRAM

Silicon is the basic material that grips the largest portion of the silicon-based fabrication technology of nonvolatile memory devices. However, its opacity seems to be a challenge to realizing transparent nonvolatile memory [237]. The indispensable of transparent nonvolatile memories for invisible devices makes it necessary to delve into the realization of this emerging technology field and perceive the actualization of the fully-integrated see-through memory devices [91]. Recently, transparent RRAM (T-RRAM) structures were proposed using various materials. These materials are wide or large direct bandgap switching insulator films and possess high transmittance in visible light. T-RRAM active layers are normally sandwiched between transparent conducting oxides (TCO) electrodes like the indium-tin-oxide (ITO), fluorine-doped tin oxide (FTO), and doped ZnO. Some of the T-RRAM structures found in the literature are AZO/ZnO/ITO [205], Hafnium Oxide

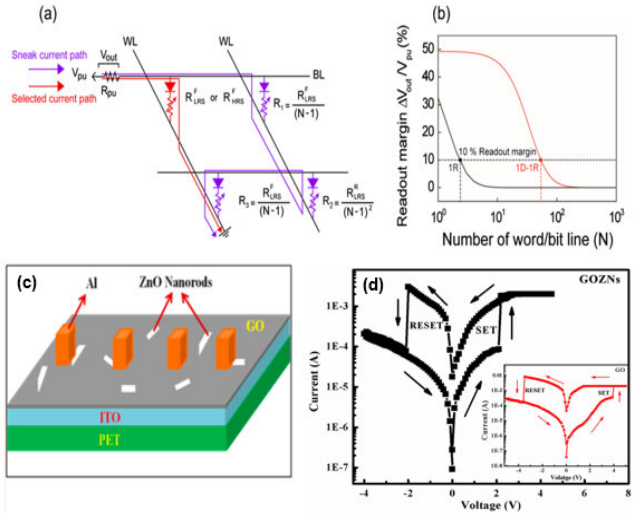

FIGURE 23. (a) An N × N 1D1R equivalent cross-bar array showing a worse case read state [229]. (b) An N × N cross-bar array normalized readout margin plotted against the number of word/bit lines. The purple colour line denotes the unselected cells. It is assumed to be in LRS, it may cause read error when selected cells are in HRS, and the R_2 can decide the total resistance of the sneak current due to reverse biased 1D found in 1D1R array structure [229]. (c) The Al/GOZNs/ITOPET RRAM device's representation shows the inserted ZNs in the GO film [228]. (d) The typical I-V switching characteristics plots of the Al/GOZNs/ITOPET and Al/GO/ITOPET RRAM devices. The device was first activated by applying a positive bias voltage of 5 V with a compliance current of 2 mA, then sweeping the device around 5 V to −5 V to reset the device at −2 V and set it at 2.1 V. Whereas, the device without ZNs that set at 3.9 V and reset at −3.5 V. Thus, lower operating voltage realized in Al/GOZNs/ITOPET due to the embedded ZNs [228].

(HfO_2) in ITO/HfO_x/ITO/PET, Magnesium-doped Zinc Oxide (MZO) in ITO/ZnO:Mg/FTO/glass, Europium oxide (Eu_2O_3) in ITO/Eu_2O_3/ITO/PET, CeO in ITO/CeO_2/ITO. The Silicon carbonitride (SiCN) in ITO/SiCN/AZO, SiO_2 in ITO/SiOx/ITO, Tantalum oxide (TaO) in ITO/TaO_x/AlN/ITO, TiO_2 in ITO/TiO_2/FTO. The IGZO in Cu/α-IGZO/p^+-Si, Gallium-doped ZnO (GZO) in ITO/GZO/ITO, aluminium-zinc oxide (AZO) in ITO/AZO/ITO/glass, aluminium nitride (AlN) in ITO/AlN/ITO. Also, the application of natural biomaterials like egg albumen in Ag/egg albumen/ITO/PET, organic oxide like GO in ITO/rGO/ITO, perovskite $ZnSnO_3$ via polyvinyl alcohol (PVOH) in Ag/PVOHZnSnO$_3$/Ag and Al-chelated gelatin (ACG) in ITO/ACG/ITO [205], [237]–[252]. But, ZnO is attractive to many optoelectronic processes, also possesses a high absorption rate in the ultraviolet (UV) range. Excitingly, ZnO has shown a lot of promising characteristics. ZnO's wide bandgap energy 3.1-3.3 eV gives it good transparency in the visible range at room temperature. 3.28-3.30 eV as polycrystalline, and at a temperature of 4 K, it can reach up to 3.44 eV [253].

Fabrication parameters strongly regulate the growth and conduction properties of TCO [254], [255]. Nevertheless, some studies have shown that the modification and manipulation of the TCO electrodes may trigger the oxygen vacancy concentration, thus, enhancing the device performance [242], [256], [257]. Various methods were proposed to deposit ZnO switching layer on TCO electrodes, like the solution-processed (sol-gel) method [167], [189], [246], [258]–[260], high-power pulse laser deposition (PLD) [238], [261]–[263], atomic layer deposition (ALD) [264], thermal–roll lamination technique [265], hydrothermal growth [266], RF magnetron sputtering [53], [151], [202], [205], [267]–[270], metal-organic chemical vapor deposition [271]–[273].

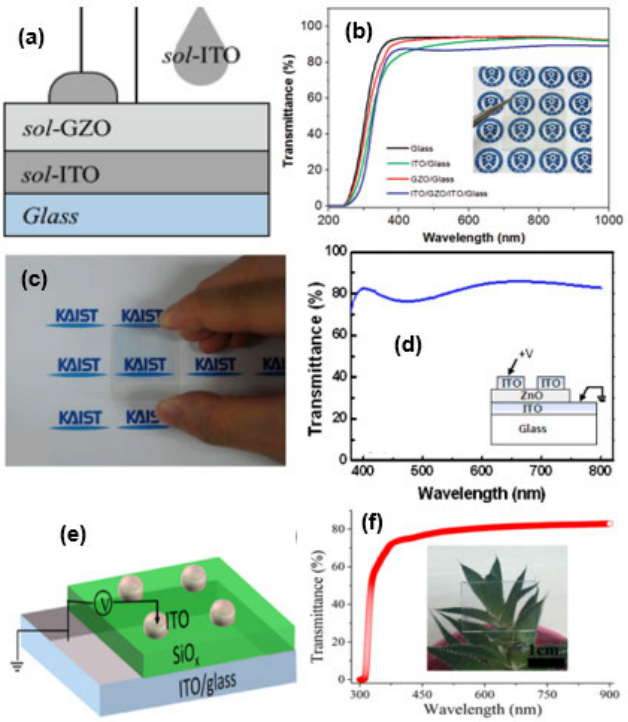

FIGURE 24. UV-transmittance of various structures (a) The structure of the developed device. (b) The glass transmittance is shown in black color, ITO/glass in green color, GZO/glass in red color, and ITO/GZO/ITO/glass in blue colour. It should be noted that the ITO electrodes were spin-coated four times until their thickness reached 30 nm [246]. (c) The schematic of the developed device [274]. (d) The transmittance of the structure ITO/ZnO/ITO shows the visible region's transmittance [274]. (e) The structure of ITO/SiO_x/ITO/glass RRAM device developed in [242]. (f) The transmittance of the structure ITO/SiO_x/ITO/glass showing the optical image and transmittance obtained in the visible-region [242].

The introduction of gallium into zinc oxide shows to improve the transmittance of the film. Kim *et al.* [246] shows 93.5% intensity of the transmittance in GZO/glass is greater than 90.6% realized in ITO/glass at 550nm as shown in Fig. 24(a) and (b). Thus, GZO/glass and ITO/glass are good candidates for see-through RRAM application. They proposed a sandwich structure of ITO/GZO/ITO which shows the transmittance of 86.5% at 550 nm, and this is better when compared with the transmittance of 81% at 600 nm obtained in the structure of ITO/ZnO/ITO described in [273] as shown in Fig. 24(c) and (d). Also, Qian *et al.* [242] elaborates a transmittance of $\sim$ 82% at $\sim$ 600 nm obtained in ITO/SiO_x/ITO as shown in Fig. 24(e) and (f). Thus, the GZO layer's use between the ITO electrodes significantly results in a fully transparent device, apart from

TABLE 4. The transparent ZnO-based RRAM structures.

Structure	Optical Transmittance (%)	CC (mA)	V_f(V)	V_{set}(V)	V_{reset}(V)	Endurance (cycles)	Retention (seconds)	ON/OFF ratio	Ref
AZO/ZnO/ITO@0.11Pa	74.87@ 550 nm	1	-2	NS	NS	NS	NA	NA	[205]
@0.2Pa	73.91@ 550 nm		-5	NS	NS	NS	$\sim 10^4$		
@0.4Pa	74.71@ 550 nm		NS	$\sim$2	-3	100	$\sim 10^4$		
@0.8Pa	74.35@ 550 nm		NS	NS	NS	100	NA		
Ag/$Zn_{1-x}Pr_xO$/FTO	92@ 388 nm	10	7.3	0.8	1.2	NA	NA	2.35	[167]
ITO/$Zn_{1-x}Co_xO$/ITO	$\sim$85@ 550 nm	5	3	1.2	-1.5	5×10^3	NA	2	[151]
AZO/(200W)ZnO/ITO	$\sim$73	0.5	NS	1.5	-2.5	>100	NS	NS	[201]
ITO/graphene/ZnO/ITO	75.6	5	4	$\sim$1	$\sim$-2.5	100	10^4	20	[220]
ITO/ZnO:Al/ITO	$\sim$80@$\sim$600 nm	10	$\sim$2.3	$\sim$0.5	$\sim$-0.5	300	NA	NA	[261]
AZO/ZnO:Mg/AZO	$\sim$73@ $\sim$600	1	-6	$\sim$3	$\sim$-4	10^3	10^5	3	[247]
ITO/ZnO/PCMO/ITO	84.6@590 nm	10	FF	$\sim$-2.6	$\sim$2.3	2.5×10^3	NA	10^4	[263]
GZO/ZnO/GZO	$\sim$80@$\sim$500 nm	10	3.5	$\sim$2.2	$\sim$1.6	NA	NA	$\sim$10	[262]
ITO/EVA:ZnO NPs/ITO	70.6@$\sim$600 nm	1	NS	NS	NS	NA	4×10^4	10^3	[265]
ITO/GZO/ZnO/ITO	$\sim$80@ $\sim$600	10	$\sim$3	14	-12	7000	NS	200	[266]
AZO/ZnO/ITO	NS	1	2	1.3	-1.5	>50	NA	NS	[53]
ITO/ZnO/ITO	88@$\sim$575 nm	5	2.7	1.6	-2.4	2500	10^4	NS	[268]
ITO/IGZO/ITO	$\sim$75	10	FF	$\sim$-1	$\sim$3.5	10^2	10^4	32	[270]
GZO/Ga_2O_3/ZnO/Ga_2O_3/GO	92@$\sim$570 nm	20	FF	14	-12	50	10^5	10^2	[271]
ITO/ZnO/ITO	81	15	3.2	2.6	1.8	10^2	$\sim 10^2$	10^3	[273]
GZO/ZnO_2/ZnO/ITO	87.4	1	$\sim$5.5	$\sim$1.5	-1.7	250	7000	$\sim$30	[274]
AZO/ZnO/ITO	80@$\sim$550 nm	10	$\sim$4.5	1.7	-2	$>10^4$	NS	NS	[256]

CC: compliance current, V_f: forming voltage, FF: forming free, B: bipolar, U: unipolar, NA: data not available and NS: not specified

enhancing the device's switching dynamics. The summary of the ZnO-based T-RRAM switching characteristics is shown in Table. 4.

Two devices exhibit the highest transmittance at 92% each, as shown in Table. 4, the praseodymium (Pr) doped ZnO film and the ITO free multiple structures of GZO/Ga_2O_3/ZnO/Ga_2O_3/GZO transparent device. The Pr-doped ZnO thin films developed by Kao *et al.* [167] show an optical transmittance of 92% at 388 nm wavelength absorption edges and are red-shifted with the increase of Pr content, while a pure ZnO film displays transmittance above 92% with a sharp wavelength absorption edge at 380 nm, as shown in Fig. 25(a). However, the film of $Zn_{1-x}Pr_xO$ exhibits decreased bandgap from 3.293 to 3.264 eV as Pr's content increased between $x = 0.00$ to $x = 0.04$, as shown in Fig. 25(b) [167]. Nevertheless, this decrease was due to the increase in the porosity defects and the decrease in Pr doped ZnO films' grain size. Thus, this further shows a decrease in the bandgap that was confirmed by the optical transmittance scattering up the film. Moreover, the best LRS/HRS ratio could be obtained when a 4% content of Pr was doped to ZnO thin film [167]. The ITO-free device of GZO/Ga_2O_3/ZnO/Ga_2O_3/GZO also exhibited a transmittance of 92% in the visible region; the device shows long retention good memory window [271].

From the structures shown in Table. 4, it can be seen that devices that are ITO-based electrodes show optical transmittance between 73% to 88% in the visible light region. Decisively, structures with optical transmittance within 80% and above in the visible region are considered fully transparent devices. Those with transmittance within 7% are normal-transparent devices, and those below 70% transmittance in the visible region are termed semi-transparent devices [275], [276].

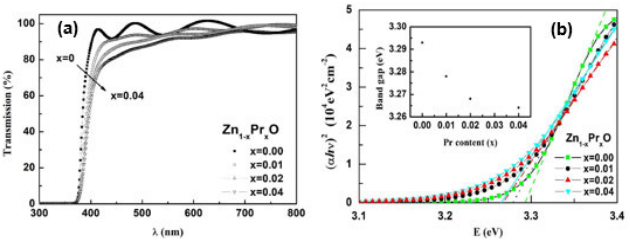

FIGURE 25. (a) The inset of the transmittance (%) spectra of ZnO and $Zn_{1-x}Pr_xO$ films measured as a function of the wavelength (nm), the absorption edges decreases with the increase in the Pr content [167]. (b) The relationship between the Pr-content Vs the bandgap energy and the inset shows the rise in Pr content on the bandgap energy and the device resistance [167].

The fabrication of RRAM devices on a polymer substrate, metal foil, and stainless steel offer the potential to develop flexible nonvolatile memory know as flexible RRAM (FRRAM). This potential may be seen as the refurbishment of flexible embedded technologies that could lead to the realization of flexible, stretchable, and soft memories. Hence, this could get us closer to sci-fi developments [228], [277], [278], where future nanoelectronic devices are fully integrated into our outfits and activities.

FRRAM of polymer substrate-based normally have its electrode coated with a polymer substrate [228], [259], some of the polymer substrate used are polyethylene terephthalate (PET) [228], [279]–[283], Kapton [284], polyethylene naphthalate (PEN) [285], [286], polyimide (PI) [234], polyethersulfone (PES) [234], [287]. Nevertheless, other flexible materials were also used, like stainless steel used in [30], [288], a plastic substrate [289], and metal foil used in [290]. Table. 5 shows the summary of the ZnO-based FRRAM found in the literature.

TABLE 5. The flexible ZnO-based RRAM structures.

Structure	Bending cycles (times)	Radii (mm)	ON/OFF ratio	CC (mA)	V_f (V)	V_{set} (V)	V_{reset} (V)	Endurance (cycles)	Retention (seconds)	Ref
Au/ZnO/Stainless steel	NA	NA	NA	30	NS	±1.0-2.0	±0.5-0.8	100	NA	[30]
Al/GOZNs/ITOPET	10^3	6	$\sim10^2$	2	NS	2.1	-2	200	10^4/RT	[228]
PET/rGO/ZnO NRs/Au	1000	6	$\sim10^3$	NS	NS	3	∼-3	NA	10^4	[279]
Cu/ZnO:Mg/ITO/PET	10^3	20	30	1	2.6	∼1	∼-1.5	10^2	10^4	[280]
Al/ZnO-GO-PVA/Al/PET (ZnO:GO=1:15)	80	NA	NS	$\sim10\times10^{-2}$	NA	∼1	∼-1	NS	2×10^3	[281]
ZnO/Ag/ZnO/PET	2500	8.1	NS	2	∼4.5	∼2.2	∼1.2	10^5	10^5	[282]
Al_2O_3/Ag/Al_2O_3/PET				0.5	∼4	∼2.4	∼0.9			
TaN/Al_2O_3:Ag:ZnO/ITO/PET	NS	NS	NA	∼10	NA	∼1	∼-3	NA	10^4	[283]
Al/Mn:ZnO/HfO_2/Ti/Pt/Kapton	500	11	∼70	NS	NS	5	-5	50	NA	[284]
Ag/ZnO/Ti/PET	NA	NA	NA	10	NS	∼1.45	∼-1.5	NA	NA	[285]
GZO/GZO(H)/GZO/PEN	NA	NA	NA	0.1	∼1.7	1.5	-2	20	NA	[286]
Au/ZnONR/Au/PI	100	20	∼10	50	∼1.7	0.84±0.04	0.23±0.02	>10	10^4/RT	[234]
Al/ZnO/Al/plastic	10^5	NS	∼10	5	FF	∼2	∼0.5	10^4	NA	[160]
ITO/ZnO/ITO/Ag/ITO/PES	10^4	20	>10	10	3.4	1.5	0.6	200	10^5/85^{o}C	[287]
Ta/Ta_2O_{5-x}/Al_2O_3/$InGaZnO_4$/ stainless steel	1000	15	NA	NS	NS	NS	NS	NA	NA	[288]
Cu/IGZO/Cu/plastic	10^5	15	10^2	3	FF	∼1.5	∼0.5	150	NS	[289]
Ti/AZTO/Pt/metal foil	NS	20	NS	1	NS	∼1.1	-0.7	NA	NA	[290]

CC: compliance current, V_f: forming voltage, FF: forming free, B: bipolar, U: unipolar, NA: data not available and NS: not specified

The archetypal photograph of the Ag/ZnO/Ti/PET FRRAM device is elaborated by Sun *et al.* [285] as shown in Fig. 26(a) and (b), the device is developed on the PET substrate. The flexibility does not obstruct the resistive performance of the device [285]. Since mechanical flexibility is key to bendable NVM, other memory characteristics should also be preserved in various angles and situations during and after repetitive mechanical bends. Moreover, Hmar [281] demonstrates bendable non-volatile memory in Fig. 26(c), he shows an inset and a photograph of Al/ZnO-GO-PVA/Al/PET substrate under various bending angles. It demonstrates the mechanical flexibility and endurance of the ZnO embedded GO/PVA composite for flexible NVM application [281]. The durability performance of PET/rGO/ZnONRs/Au device with a negligible degradation after 1000 bending cycles is shown in Fig. 26(d) [279]. Hence, it shows reliable mechanical robustness of ZnO nanorod (NR) based FRRAM. The significance of a device with ZnO NR over the one with ZnO thin film was demonstrated using Au/ZnO NR/Au/PI structure [234].

It worth noting that, ZnO NR shows better bending performance than ZnO film. Park *et al.* [234] shows schematic illustrations before bending ZnO based RRAM devices with ZnO thin film and ZnO NR as shown in Fig. 27(a) and (b) respectively. Also, they illustrates in Fig. 27(c) and (d) the devices during bending, the device with ZnO NR showing better uniform CF paths before and after bending. ZnO NR allows the device to reproduce RS operation within a confined distribution compared to a thin-film device. Hence, this may be attributed to the NR device's radius being similar to the CF radius [291]. Furthermore, the CF in thin-film devices is usually formed contrarily after every switching cycle, leading to dissimilar resistance states and cracks during operation under bending situations [234]. Hence, this may lead to inaccurate memory operations. Therefore, the use of NR is superior to the use of thin-film in FRRAM, since vertically localized NRs

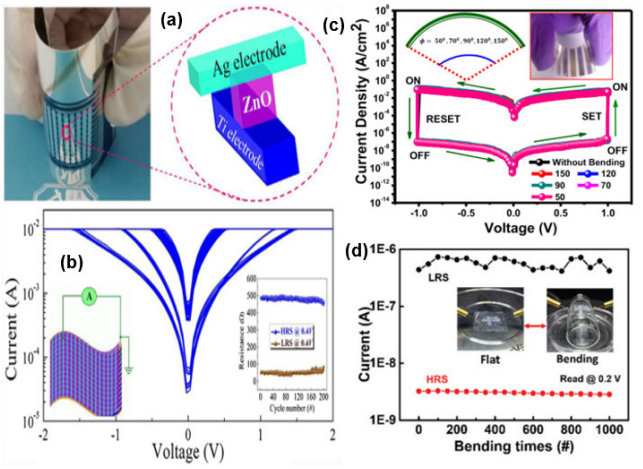

FIGURE 26. (a) The inset of Ag/ZnO/Ti/PET structure and its photograph (b) I-V characteristics of Ag/ZnO/Ti/PET structure with experimental test setup and HRS/LRS resistance ration [285]. (c) The inset depicts I-V switching characteristics taken at various bending angles (180^o with no turning, 150^o, 120^o, 90^o, 70^o, 50^o) of the Al/ZnO-GO-PVA/Al/PET substrate [281]. (d) The PET/rGO/ZnO NRs/Au flexible memory device and its endurance performance after multiple bending cycles, the inset demonstrate continual bending distortions and release states using a bending radius of 6 mm [279].

are not likely to form cracks and inaccurate operation [292] and less affected by bending situation as shown in Fig. 27(d). Hence, the TE or BE substrate's flexibility is not the only determinant of the reliability of FRRAM, but the resistive layer should be considered as well [228], [234], [279].

The use of stainless steel (SS) in FRRAM may help the mechanical flexibility of the FRRAM device, and SS material has high tensile strength, very durable, corrosion-resistant, and temperature resistant. It has an excellent anti-pull capacity [293], [294]. SS is used as an alternative material to another traditional flexible substrate in Ta/Ta_2O_{5-x}/Al_2O_3/$InGaZnO_4$/SS material [288]. The device shows unaffected performance under 200N tensile force

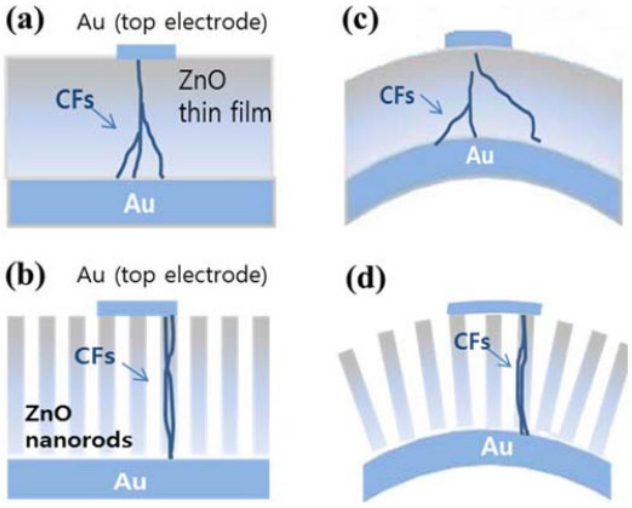

FIGURE 27. (a) The schematic of CF formation in a device with ZnO thin film before bending (b) The diagram of CF formation in a device with ZnO NR before bending (c) Schematic of the CF during bending of the device with ZnO thin film (d) Schematic of the device with ZnO NR during bending. This figure demonstrates the significance of using ZnO NR over ZnO thin film since CF formation in NR is normally guided by the NR's radius and shows no cracks during switching operation under bending situations [234].

and 1000 bending times. Thus, SS material should be employed when developing a FRRAM device with good tensile strength. But tensile strain (up) is not the only mechanical parameter that signifies the reliability of the FRRAM device, compressive strain (down) should also be taking into account [295]. However, further research on the mechanical flexibility under various bending situations and the RS characteristics of ZnO-based FRRAM are necessary to realize future bendable nonvolatile memory.

G. ZnO BASED RRAM FOR SYNAPTIC APPLICATION

The principle of designing bio-inspired computational cognitive adaptive devices has been studied long ago [296], [297]. In 2008, the emergence of the Darpa Synapse [298] program triggered the current resumption of interest in developing electronic systems that mimic the brain's ability to conduct energy-efficient and fault-tolerant reckoning in a compacted scope. However, research activities in this sector have been rising rapidly since then. Research on the human brain system has contributed to neuromorphic computing, a new revolutionary technology. In the design and development of the computational device, this system emulates how the brain functions, the memristor's ability to vary and memorize its conductance level due to the change in the polarity/strength of the applied signal and its nanoscale capability makes it a preferred candidate for building bio-inspired cognitive computational systems. For this reason, several designs and developments of neuromorphic adaptive plastic scalable electronics (SYNAPSE) based on memristor have been offered by different authors nowadays [46], [299]. Among memristor devices, RRAM possesses greater advantages for non-volatile synapse applications.

It is well known in the literature, ZnO has a direct and wide bandgap [96] that makes it possible to detect visible-blind ultraviolet (UV) [300], [301]. Interestingly, optical signals are usually used to modulate neural activity [302] in biological systems. Therefore, it is pertinent to investigate the optically influenced synaptic response based on the ZnO RRAM device, and its realization remains unclear [303]. Hence, in this section, we will discuss the artificial synapses realized in ZnO-based RRAM.

An optically modulated artificial synapse based on ZnO NRs was reported by Zhou *et al.* [303]. They proposed that not only electrical response can stimulate artificial synapses but also optical modulation is practicable. They utilized the high surface state densities of ZnO NRs that sufficiently provide Pt/ZnO/FTO's developed structure with high photo-response that produce optical shielding effect unshielded on the application of electric pulses. Thus, this process provides capabilities for massive data processing for artificial neural networks (ANNs). Interestingly, Zhou *et al.* [303] demonstrates that ZnO NR exhibits a very high photo-to-dark current ratio of 10^4 compared to 70 obtained in ZnO thin film as shown in Fig. 28. Fig. 28(a) shows how synaptic plasticity was modulated using optical stimuli when some sets of identical electric spikes are applied, showing the paired-pulse facilitation (PPF) effect. Fig. 28(b) shows how the PPF value was realized by the pulses' interval, which confirms the device's synaptic plasticity is optically modulated and is analogous to the biological phenomenon seen in optogenetics [304].

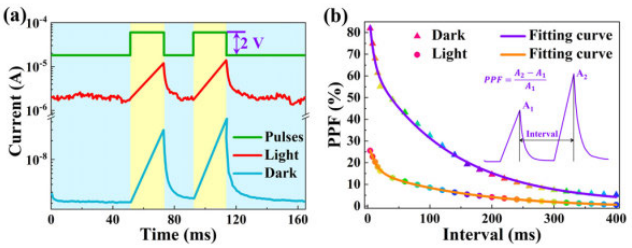

FIGURE 28. Optical dominance on the PPF function realized in ZnO NRs showing the actual depiction of PPF. (a) The electrical PPF response is showing the process under darkness and illumination. (b) The description of the PPF values concerning interval, the inset shows how the conditions influenced the PPF values [303].

Identical double pulsing (DP) scheme for linearity and training epoch was proposed in [268] on (ITO)/ZnO/ITO structure. The proposed scheme improved the device linearity and training epochs from 0.83 to 0.44 with a broad dynamic range of 200 having 320 conductance states as shown in Fig. 29(a) – (c) by Chandrasekaran *et al.* [268]. Fig. 29(d) – (f) shows the AZO/ZnO/ITO flexible-transparent device's synaptic performance described by Simanjuntak *et al.* [53]. The device showed good stability after several repeated potentiation and depression more than 30 times. The device's low programming voltage (1.5 V) that modulated the conductance is a good indication that

the device is logic-compatible [53]. It is important to note that the strain-induced piezo-phototronic effect found in ZnO films offers some advantages in the level of regulation in modulating the synaptic roles in multi-levels. A piezo-phototronic-based triggered synaptic device was reported in [305] as shown in Fig. 29(g); they harness the silver nanowires (AgNWs) with a ZnO thin film and proposed ZnO/AgNWs/PET device. The well-established AgNWs setup is the core of the structure, and it offers effective charge collection [306]. On the other hand, ZnO thin film with no AgNWs setup couldn't provide a reasonable photo-response after the application of several strains [307]. The device activation by some set of UV light pulses is given Fig. 29(g).

The magnitude of the SET voltage is found to be dependent on resistive layer thickness [178], so is the synaptic property found in Al/ZnO/SS device [308]. The hydrothermally grown device shows potentials for bipolar asymmetrical I-V switching characteristics. Thus, a bidirectional synapse data transfer bus may be realized. The device synaptic weight characteristics with various sweep rates at the positive and negative bias are given in Fig. 30(a) – (b) as described by N. B. Mullani *et al.* [308]. The inset shown in Fig. 30(a) delineates that only device A2 with an active layer thickness of 1337 nm displays a risen synaptic weights, but other devices A1, A3, and A4 with active layer thicknesses of 906 nm 3344 nm, and 5045 nm, respectively. It shows decaying synaptic weights in line with the sweeping rate in the positive bias region. But, they indicates in Fig. 30(b) all devices that offer decaying weights in the negative bias region with an improved A2 synaptic weight. And this may be attributed to the disordered morphology of the device. Therefore, this demonstrates how the thickness of the active layer influenced the device's synaptic weight properties. Ag dopant effect on the switching effects is shown in the hydrothermally developed Aluminium/silver-zinc oxide/SS device (Al/Ag:ZnO/SS) [309]. Additionally, the device shows memristor fingerprint effects where the magnitude of the SET voltage is relatively dependent on the level of concentration of the Ag dopant. Moreover, T. D. Dongale *et al.* [309] shows in Fig. 30(c) – (d) the device synaptic weight characteristics at positive and negative bias regions with various sweep rates, respectively. The pure ZnO active layer and Ag-doped active layers of 1%, 2%, and 3%. Therefore, these results vividly show the Ag-doping effect on the devices' synaptic weight behavior, and the 2% Ag-doped active layer demonstrates higher synaptic weights in both regions. This is attributed to the uniform Ag-doping and well-aligned NR structure, whereas 1% and 3% show an increase in the leakage current due to their non-uniform Ag-doping and grain boundary effect [310]. The 2% Ag-doped device shows quasi-reverse rectifying characteristics. Interestingly, this kind of behavior is usually used in the unidirectional data flow that could improve neuromorphic architecture's computational abilities [311].

The synaptic capabilities of ZnO-based RRAM found in the published literature are shown in Table. 6. Device switching and synaptic performances could be improved after neutral oxygen irradiation [267]; this technique is also known as neutral beam oxidation (NBO). NBO can neutralize oxygen plasma [312] by charge exchange collision. NBO helps enhance surface oxidation, increasing the amount of oxygen interstitial at the TE of the ZnO interface. Thus, this is valuable towards improving the switching and synaptic weight linearity [267].

H. SNEAK CURRENT ISSUES

Some difficulties have distorted the realization of crossbar memory architecture. The main practical bottleneck for this array design is the cross-talk interference between adjacent cells due to sneak-path current [314]–[316] that causes error in the read operation [317]. Crossbar array design provides scalability, multiple stacks, and its simplicity makes it a smart architecture. Therefore, numerous approaches have been proposed to resolve the sneak current path issue like the diode-based approach, volatile switches, nonlinear devices, Mott transition, threshold switches, and the use of carbon nanotube field-effect transistor (CNTFET) in a 1T1R configuration [233], [318]. Sneak current path issue also suffered ZnO-based crossbar architecture [319], [320]. Thus, this section will provide various approaches to suppress the current sneak issue for the ZnO-based RRAM devices.

In the diode-based approach, there are two main methods. The Schottky contact diode and the multi-layered PN junction diode, but the Schottky diode approach has a very low forward voltage drop and easy to produce than the PN junction approach [321]. Gül [233] proposed one Schottky diode-one resistor (1D1R) device using Ag/ZnO/Al structure, as shown in Fig. 31. The corresponding simplified circuit of the worst-case read pattern used to provide the device's anti-crosstalk features is shown in Fig. 31(a). And the read-voltage margin is plotted against the crossbar-line number as shown in Fig. 31(b), and the inset shows how the read-voltage margin decreases with the increase in the crossbar-line number. Thus, demonstrate that the device could be a good candidate for a crossbar RRAM device application.

It is worth noting that the nanowires' one-dimensional (NWs) structure makes it superb at outlining a device's direction. Fig. 32 shows a p-n ZnO NWs based RRAM device vertically developed on Ta_2O_5 by Chen *et al.* [319]. Fig. 32(a) shows the Au/Ta_2O_5/Au device's I-V characteristics without the p-n ZnO NWs film that only demonstrates typical unipolar behaviors. But after the p-n ZnO NWs film's growth with an asymmetric barrier, the device demonstrates the characteristics of 1D1R, as shown in Fig. 32(b). The schematic structure and the equivalent circuit of the device are depicted in Fig. 32(c); the crossbar schematic that portrays the vertically grown ZnO p-n junction is shown in Fig. 32(d). The junction acts as an oxygen storage layer during CFs formation, apart from its superb rectifying performance. Thus, the insertion of vertically grown ZnO p-n junction is positive as the basic material for building a high-density crossbar array

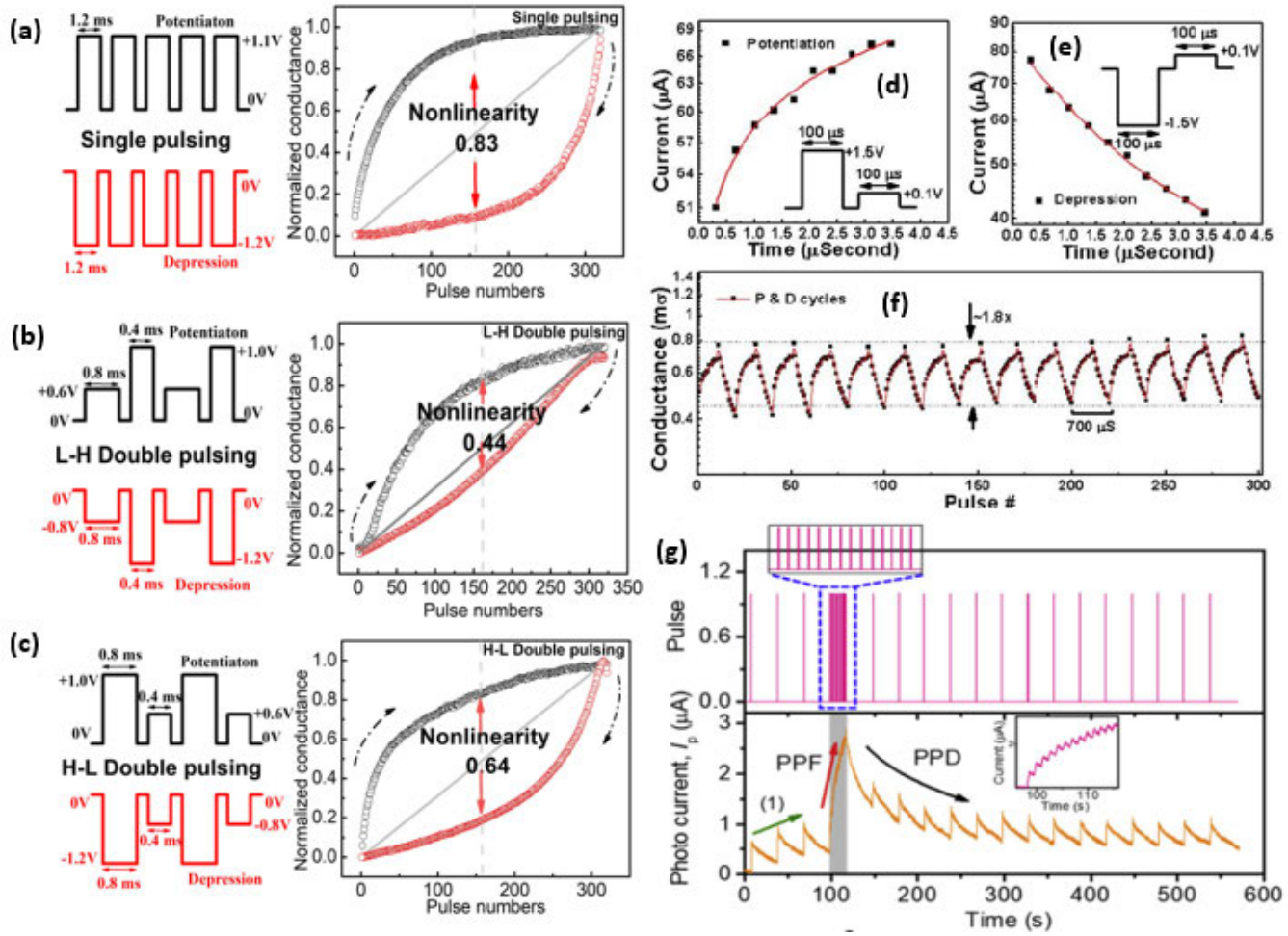

FIGURE 29. (a) Single-pulse operation scheme of ITO/ZnO/ITO device showing potentiation and depression states of the pulse scheme and normalized conductance (b) Single-pulse operation scheme of ITO/ZnO/ITO device showing Low-High 0.44 DP and normalized conductance state (c) Double pulse operation scheme of ITO/ZnO/ITO device showing High-Low 0.64 DP and normalized conductance state. The insets shown in (a), (b), and (c) are better described in [268]. (d) Potentiation characteristics of AZO/ZnO/ITO device after the deployment of identical pulses positive amplitude. (e) The depression characteristics of AZO/ZnO/ITO device after the deployment of identical pulses negative amplitude. (f) The conductance against the pulse showing the repeated potentiation and depression. Thus, it offers the stability of the device that goes for over 30 times. The insets shown in (d), (e), and (f) are [53]. (g) The UV pulse period of the PPF and paired-pulse depression (PPD) induction and post-synaptic currents of ZnO/AgNWs/PET device activated by a set of UV light pulses [305].

RRAM. The device has a low leakage and devices with such potentials could be essential in the future combination of 5G with artificial intelligence (AI) applications.

Typically, to elude sneak path current, several techniques were studies as depicted in Fig. 33. Some of the techniques used are transistor, diode, or selector usually are joint with the RRAM resistor. Using diode to each cell of the memory as one diode one memristor (1D1M) is seen as an alternative for reducing the sneak path current [322], as shown in Fig. 33(a). However, using diodes to the array may add capacitive loads and increase the system delay [323]. Also, the memristor's writing process needs two distinct polarities, which means this method will also distort the writing process. Therefore, a 3D crossbar array arrangement with one new diode-added is proposed to enable a smooth write operation and mend the integration density, as shown in Fig. 33(b) [323]. The design requires more area per cell, and it is still blurred that 3D alignment for four crossbars could eliminate the current sneak issue. The unfolded architecture approach demonstrated in [322] is another perspective for sneak path current solutions; the method requires a separate column for each memristor, as shown in Fig. 33(c). But this method tends to occupy more cell area than using an array with just one row. Moreover, the design requires more area per cell, and it is still blurred that 3D alignment for four crossbars could eliminate the current sneak issue.

The process of using one transistor one memory (1T1M) was also considered as one of the best alternatives for the realization of a sneak path current free high-density crossbar memristor device [324], as shown in Fig. 33(d). Still, transistors are considered to behave as leaky valves, and transistor gating constrains the 3D stacking of RRAM crossbar arrays.

TABLE 6. The Synaptic potentials for ZnO-based RRAM structures.

Structure	ON/OFF ratio	Endurance (cycles)	Neuromorphic computing applications	Ref
Pt/ZnO.NRs/FTO	10^4	250	Optically tuned synaptic devices for secured communications	[303]
AZO/ZnO/ITO	2	>50	Demonstration of the synaptic potentiation and depression characteristics	[53]
ZnO/Ag-nanowires/PET	1	100	Photonic artificial synapse with control on artificial learning and modulation	[209]
Al/ZnO/SS	NA	NS	Human forgetting curves	[212]
Al/Ag:ZnO/SS	NA	NS	Synaptic weighted sum process carried out on Ag:ZnO with unidirectional synapse capabilities	[213]
Al_2O_3/TiN/ZnO	69.7	NA	Thorough operational processes and analysis carried out on ZnO based RRAM with synapse capabilities	[216]
Ag/ZnO–rGO/FTO	NS	NA	The realization of spike-timing-dependent plasticity on a custom made PCB circuit	[227]
ITO/ZnO/ITO	NA	2500	Demonstration of the synaptic potentiation and depression characteristics on ZnO-based transparent resistive device for artificial neural networks in wearable electronic applications	[268]
Cu/α-IGZO/p+-Si	NS	NA	Operational processes and analysis carried out on bilayer IGZO based RRAM with synapse capabilities	[245]
TaN/Al_2O_3:Ag:ZnO/ITO	NS	NA	Operational processes and analysis carried out on Al_2O_3:ZnO based RRAM with synapse capabilities	[283]
TiN/ZnO/W	7742	NA	Operational processes and analysis carried out on ZnO based RRAM with synapse capabilities	[313]
AZO/ZnO/ITO	NS	2000	Synaptic weighted sum process carried out on the ZnO-based transparent memristor device using a method capable of controlling other synaptic parameters	[267]

NA: data not available and NS: not specified

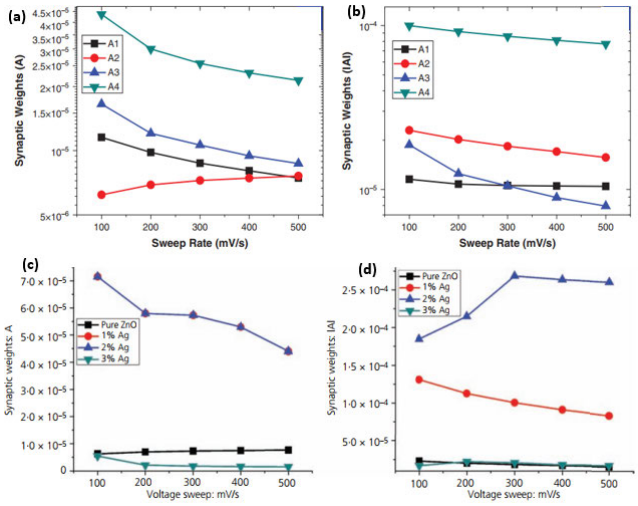

FIGURE 30. (a) Synaptic weight characteristics of Al/ZnO/SS device at positive bias against sweep rate [308]. (b) Synaptic weight characteristics at the negative bias [308]. (c) Synaptic weight characteristics of Al/ZnO/SS and Al/Ag:ZnO/SS devices at positive bias against sweep rate [309]. (d) Synaptic weight characteristics at the negative bias [309].

A complimentary memristor's approach is used in [325], and complementary resistive switches (CRSs) for crossbar array are also proposed in [326] that can reconstruct their data after being destroyed. But these approaches are a bit complex, and their reading techniques seem difficult. The multistage reading approach is introduced by the HP Labs crew in [327] using a straightforward yet long algorithm to suppress sneak path issues. The approach requires many sensing elements and takes a lot of time, and maybe ineffective at large array sizes.

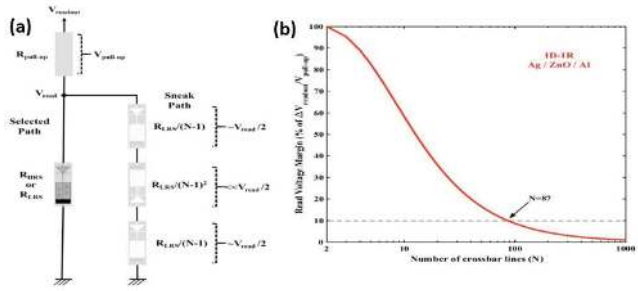

FIGURE 31. (a) The equivalent circuit of 1D1R Ag/ZnO/Al device for the worst-case scenario (b) the normalized read-voltage margin is showing its dependency on the number of crossbar lines for Ag/ZnO/Al device [233].

Interestingly, a memristor as a three-terminal device possesses a transistor's advantages as a gate device and can be termed as better gates compared to diodes or transistors. A gating using a three-terminal memristor device is demonstrated by Zidan *et al.* [315] as shown in Fig. 33 (e) and (f). The approach provides a structure of the memristor gated array. Each cell is gated with a memristor device, as shown in Fig. 33(e) while Fig. 33(f) shows the worst-case power consumption against the array size. A theoretic-based technique for combating sneak path current is proposed in [328]. The technique demonstrates an error correction coding across the arrays, which could be done when multiple 2D arrays are arranged like layers of 3D architecture. Though the techniques still require further extensions and have not been fully materialized, it avoids incorporating additional non-linear elements that may further add unwelcome disturbances.

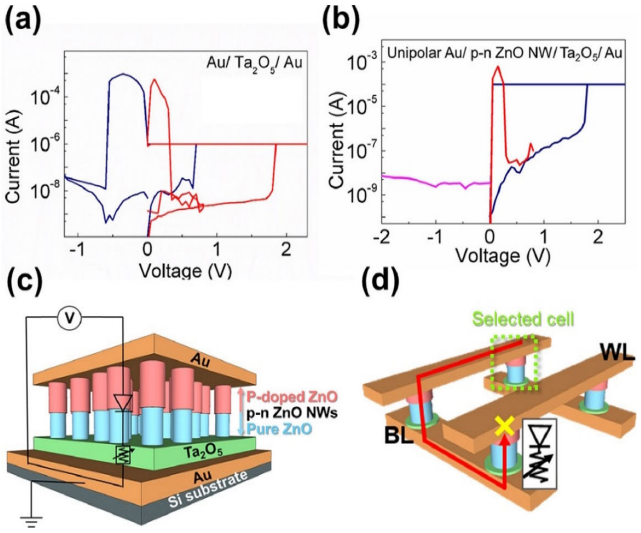

FIGURE 32. (a) The I-V characteristics of Au/Ta_2O_5/Au RRAM device. (b) The reverse bias I-V characteristic of Au/p-n ZnO NWs/Ta_2O_5/Au device. (c) The schematic structure of Au/p-n ZnO NWs/Ta_2O_5/Au device and its equivalent circuit. (d) The crossbar array schematic of the Au/p-n ZnO NWs/Ta_2O_5/Au device showing a reduced leakage current. The insertion of the p-n ZnO NWs junction could greatly prevent the manifestation of leakage current that normally disturbs the adjacent cells [319].

Integrating additional non-linear devices and developing additional thin-film layers to the memristor element may change its characteristics and add unintentional disturbances. Thus, theoretical-based algorithms may be the next alternative. Still, attention needs to be paid to the algorithm's complexity and execution difficulty and how effective it should function on high-density arrays.

I. MULTIFUNCTION OF ZnO BASED RRAM DEVICES

ZnO's potential to be fabricated on a wide morphological setting makes it a multifunctional material [91]–[93]; it has great potential in numerous wide electronic applications [89]–[92]. Its large exciton binding energy gives it the potential for optoelectronic application [96]. Using the advantages of a ZnO NWs Willander *et al.* [329] developed an electrochemical intracellular nano-sensor for human cell activity monitoring. They have grown ZnO on a coated micro-electrodes together with Ag/AgCl reference electrode, and the developed prototype recorded a safe penetration of human fat cells along with cell pH. Thus, a ZnO NWs sensor's small size makes them suitable for sensing in nano-settings for intracellular sensing of biological and physiological species. Interestingly, if this kind of function could be incorporated with data storage in a single device, it may be seen as a breakthrough in nano-electronic circuitry.

Sensor signal could be referred to as the deviation of conductivity, voltage, current or resistance, and chemical gas react with the oxygen ion present in ZnO to release electrons [330]. Chemical gases are toxic, volatile, and combustible. Hence the detection of these gases is necessary for secure working environments [331]. ZnO nanostructure is used in other sensors like pH, humidity, and ultraviolet (UV) sensing [330]. Its versatile properties include biocompatibility, piezoelectricity, surface area, good conductivity, and nontoxicity [332], [333]. ZnO-based nanostructured exhibits significant lead in nano-devices. Also, it was considered a great candidate in optoelectronic applications [334]. It has attracted significant attention, of its potentials have not been explored yet. Therefore, all these potentials are properly exploited and harmonized with data storage applications on a single architecture. Thus, multifunctional devices may transform microelectronic designs. But much work needs to be done. Due to insufficient knowledge and understanding of the properties and their relationship, only a few successes were registered. Therefore, attention should be paid to understanding their properties' relationship for the appropriate harmonization and design. And for the application of these future nano-electronic multifunctional devices.

The recent development in wearable memories and computing devices (WMCs) makes it necessary to focus attention on ZnO-based nanostructures. Therefore, with ZnO's vast potentials, the realization of ZnO-based WMC devices is indisputable. WMC devices found application in various areas like flexible electronic, smartwatches and clothes, wearable devices, stretchable, soft electronic and so on [277], [335]. For instance, ZnO NR-based flexible RRAM has the capability of being rooted in WMC flexible devices. In this regard, the flexibility is anticipated not to hinder its operational stability in a real scenario subjected to numerous bending stress and strain [234], [279]–[286]. Fig. 34 shows a ZnO NRs based flexible device developed using three steps process: seeding, annealing, and growth (SAG) method as elaborated by Reddy *et al.* [336]; the method was employed to enhance the performance of the processes realized in [337], [338]. Fig. 34(a-c) demonstrates the capabilities of ZnO NRs based flexible devices for WMC applications [336].

Recently Zhou *et al.* [279] developed 1D ZnO NRs based flexible RRAM using a 2D rGO hybrid nanostructure. The device exhibits good endurance, high ON/OFF ratio, and good mechanical flexibility, as shown in Fig. 35(a-f) [279]. Also, Sun *et al.* [285] developed a flexible RRAM device based on ZnO film. The Ag/ZnO/Ti/PET devices exhibit good memory capabilities, and their good flexibility makes them suitable for WMC applications.

Furthermore, Wang *et al.* [289] developed Cu/α-IGZO/Cu sandwich structure on a flexible plastic substrate to demonstrate the ZnO's mechanical flexibility when sandwiching with other compounds. The good memory characteristics show a high transmittance of $\sim$ 85% in the visible region as shown in Fig. 36(a-d) [289]. In particular, Fig. 36(c) shows the device's performance during flat and bending states. Their 2.5 cm long developed device underwent bending of various angles and up to 10^5 times, as shown in Fig. 36(d). The device's good performance and flexibility were attributed to the known properties of α-IGZO [245], [339], [340].

The transparent memory is popularly called invisible memory [268]; they have recently attracted great attention

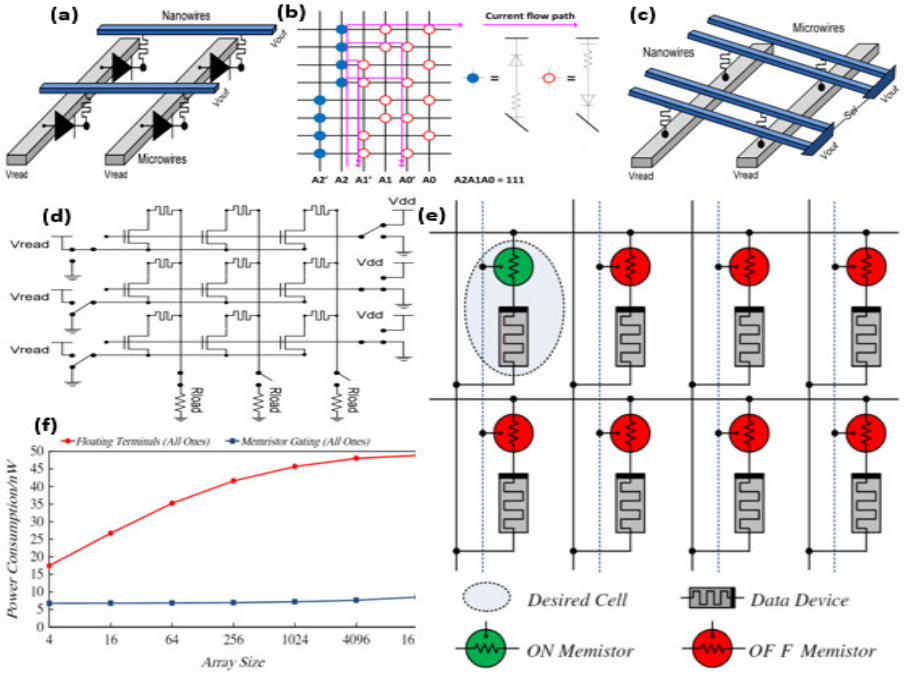

FIGURE 33. (a) The layout of a 2 × 2 1D1M memory array arrangement [322]. (b) A diode-added memristor crossbar array structure [323]. (c) the layout of a 2 × 2 unfolded crossbar memory array arrangement [322]. (d) The layout of 1T1M crossbar array memory structure with top element activated for read operation [324]. (e) The structure of the memristor gated array with a selected cell in green. Note that all cells that are not selected will have a resistance higher than R_{off} while the resistance of the selected cell that is open depends on the data device resistance. (f) The average power consumption against the array size. (e) and (f) [315].

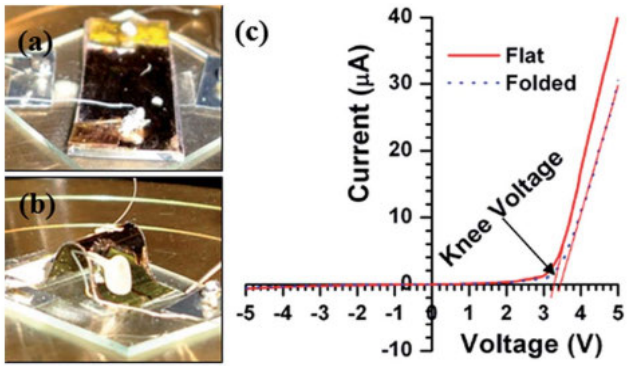

FIGURE 34. The snapshots of the developed flexible p-n junction. (a) Snapshot under the flat scenario. (b) Snapshot under bending scenario (fold states). (c) I-V characteristics curves of the device. [336].

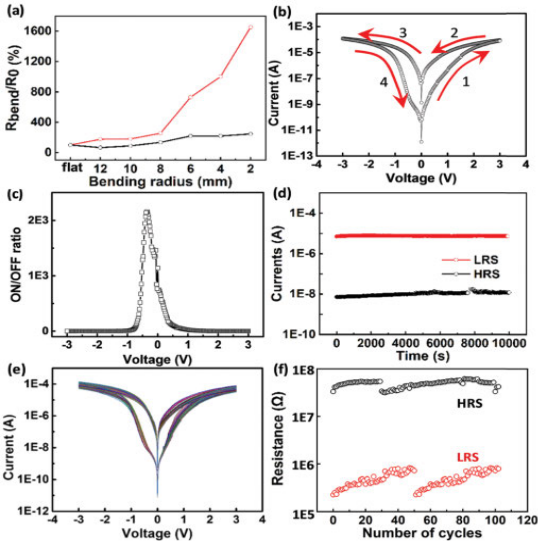

FIGURE 35. (a) Sheet resistance dependency on the bending radius for the rGO, ITO black, and red line, respectively. (b) I-V behaviours exhibited by flat PET/rGO/ZnO NRs/Au RRAM device. (c) The ON/OFF current and voltage relationship of the PET/rGO/ZnO NRs/Au RRAM device. (d) Retention behaviour at a bias of 0.2 V of PET/rGO/ZnO NRs/Au RRAM device. (e) The repeated I-V characteristics result in 100 cycles. (f) The evolution of HRS and LRS of PET/rGO/ZnO NRs/Au. Thus, this demonstrates the potential of ZnO NRs based RRAM for the WMC flexible device [279].

due to their potential application in transparent displays, UV detectors, invisible data and energy storage, and solar cells [341]. Interestingly, it will be great if an invisible device is incorporated with a data storage capability. Kim *et al.* [246] developed a fully transparent memory device using ITO/GaZnO(GZO)/ITO structure with 86.5% transmittance in the visible region at 550 nm. An invisible memory device could also exhibit synaptic behavior that can mimic the brain's typical synaptic features [342]. The memristor's analog features are beneficial to demonstrate the potentiation and depression due to its gradual increase and decrease nature of the conductance state. ZnO-based invisible-synapse memory was demonstrated recently in [268]; the device was developed using ZnO dielectric layer sandwiched between indium tin

TABLE 7. The performance and multifunctional potentials of ZnO based RRAM devices.

Structure	V_f	V_{set} (V)	V_{reset} (V)	Retention (seconds)	Endurance (cycles)	Functional type	Ref
AZO/ZnO/ITO	2	1.3	-1.5	>50	NS	Exhibits synaptic potentiation and depression characteristics for use in neuromorphic systems	[263]
Au/ZnO/Stainless steel	NS	±1.0-2.0	±0.5-0.8	>100	NA	Possess resistive switching and flexibility for use in future flexible RRAM application	[53]
AZO/ZnO/ITO	∼4.5	1.7	-2	$>10^4$	NS	Demonstrates resistive switching and transparent characteristics for use in invisible memory devices	[256]
GZO/ZnO/GZO	3.5	∼2.2	∼1.6	NS	NS	Novel transparent RRAM devices for use in transparent memory application	[30]
ZnO/Ag/ZnO/PET	∼4.5	∼2.2	∼1.2	10^5	10^5	Exhibit flexibility and transparent characteristics for potential use in flexible-invisible memory	[282]
AZO/ZnO/ITO	NS	1.5	-2.5	>100	NS	Resistive switching and transparent memory for use in the transparent devices	[201]
Au/ZnO NR/Au/PI	∼1.7	0.84±0.04	0.23±0.02	>100	10^4/RT	Exhibit resistive process and flexibility for potential use in flexible RRAM application	[234]
Al/ZnO/Al/plastic	FF	∼2	∼0.5	10^4	10^5	Exhibit resistive switching and flexibility properties for use in flexible memory devices	[349]
ITO/ZnO/ITO	2.7	1.6	-2.7	2500	10^4	Demonstration of the synaptic potentiation and depression characteristics and transparent behaviors	[268]
Cu/ZnO:Mg/ITO/PET	2.6	∼1	∼-1.5	10^2	10^4	Good resistive switching and flexibility for potential use in flexible memory	[280]
Au/ZnO NR/Au	NS	1.5	2	NA	NS	Light-Induced switching property for potential application in photoconductivity memory devices or photodetector	[250]
TiN/ZnO(6±1)/W	3	1.5	NS	NS	NS	Possess synapse capabilities	[313]
AZO/ZnO:Mg/AZO	-6	∼3	∼-4	10^3	10^5	Exhibits transparent characteristics	[261]
Ag/ZnO/Ti/PET	NS	∼1.45	∼-1.5	200	NA	Exhibit resistive switching and flexibility characteristics for potential application in fixable and wearable electronic devices	[285]
Pt/CZO/NSTO	NS	2.5	-4	NS	10^3	Exhibit multifunctional characteristics of resistive switching, photoelectricity, and ferromagnetism	[345]
AZO/ZnO/ITO	NS	1	-2.3	2000	NS	Exhibited both transparent and synaptic characteristics	[267]

V_f: forming voltage, FF: forming free, B: bipolar, U: unipolar, NA: data not available and NS: not specified

oxide electrodes. It shows more than 88% transmittance, stable memory operations, and two memory window orders that give it the potential for synapse application. It would be great if a memory device is embedded with a synapse capability; this would be seen as a great addition to the realization of WMC devices. Also, ZnO's potential as an excellent photoelectric material, if combined with a data storage capacity, may be seen as an addition to the WMC devices [250]. The UV illumination was reported to be responsible for the decrease in the Pt/ZnO/Pt device's resistance, and this happened as a result of oxygen photo-desorption that destroy the device surface defects [343]. On the other hand, it was demonstrated using the TiN/ZnO/ITO structure that the decrease in the resistance was attributed to the release of extra oxygen ions and radicals due to the breaking down of Zn-O bonds [344]. Table. 7 provides the performance and multifunctional potentials of ZnO-based RRAM devices found in the literature.

Recently, Luo *et al.* [345] shows how the resistance of Pt/CZO/NSTO heterostructure was affected due to the UV illumination as shown in Fig. 37. The device's HRS under UV illumination is about 100 times less than the one with no UV illumination. This process was attributed to the photo-generated carriers and V_O migration to the junction region stimulated by the electric field [345], [346]. The energy band diagram shown in Fig. 37 demonstrates the formation of n– n+ Schottky junction at the CZO/NSTO film interface. So, when the device comes under UV illumination, the trapped electrons were excited to the conduction band, and the barrier height was reduced [345]. Moreover, Fig. 37(a) and (b) shows that Pt/CZO/NSTO device's

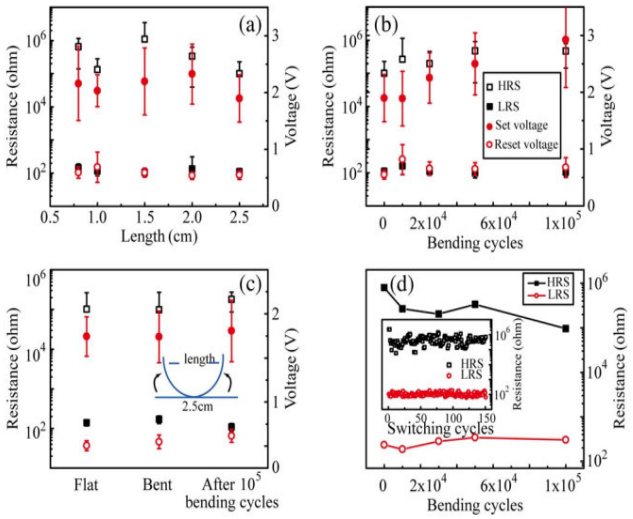

FIGURE 36. (a) The average HRS/LRS resistances and the voltages under different bending scenarios. (b) The HRS/LRS resistances and voltages under various bending cycles and different times. (c) The performance for flat and bent devices and continuous bending of 10^5 cycles. (d) The bending cycles and resistance state variations, and the inset shows the LRS and HRS values taken in 150 RS cycles after 10^5 bending times [289]. The device is subjected to a continuous bending test of 10^5 times in (b) and (d). Also bent up to a length of 1.5 cm. The legend shown in (b) is valid to (a) and (c) [289].

photosensitivity in the HRS is subjected to the interface-states. Thus, this kind of device's operation may be stable in a real scenario when subjected to numerous wavelengths of light. Interestingly, this potential may pave the way for developing devices whose light sensitivity does not obstruct their memory capabilities.

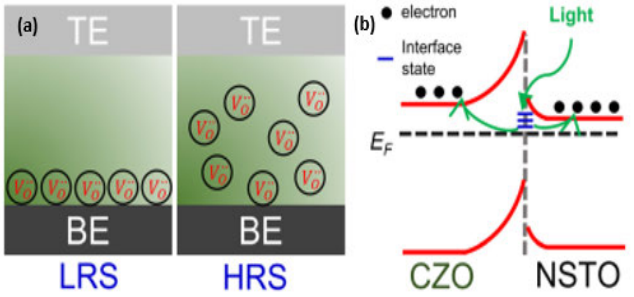

FIGURE 37. (a) Sketch of the resistive switching process observed in the Pt/CZO/NSTO heterostructure. (b) The equivalent energy band diagram is demonstrating the formation of n – n+ Schottky junction [345].

Furthermore, the IGZO RRAM could be employed in a system-on-panel display application for embedding in a transparent system [347]. ZnO demonstrates a lot of potentials among other BMOs apart from its multifunctional RRAM capabilities.

ZnO-based RRAM has performed quite reasonably among other BMOs. It offers quite sufficient endurance, acceptable retention, reasonable operational power, and good memory window, yet low operation current, ultra-thin and fast operation speed is still great challenges of the ZnO-based RRAM [83], [91], [348], [349]. The switching layer is anticipated to scale down to as thin as 1× nm [345]. The maximum theoretical scalability is restricted by multiples of $2e^2/h$ known as discrete Landauer conductance levels [51]. It is worth noting that larger resistive switching devices cannot be directly scaled down to smaller resistive switching devices because the operating mechanism depends on the size of the RRAM device [350].

III. CONCLUSION

This review paper provides a brief outline of the emerging memory devices. Emerging memories face several challenges due to scaling functionality and dimension of CMOS, but the RRAM device's emergence is seen as a liberation of the bedevil challenges. An overview of the brief historical trend of the RRAM device is presented, right from the discovery of the device in the laboratory up to the realization of recent advancements of ultra-low-power embedded RRAM technology. Detailed highlights on the RRAM structure, working mechanism, and operations have been shown. Several native point defects associated with the ZnO structure hinder its material characteristics. Moreover, the genesis of conductivity in ZnO n-type is the manifestation of V_O and zinc interstitials. Thus, it's challenging to reproduce reliable p-type doping, and several efforts have been made, yet the issue is still open for further investigation. The use of suitable electrodes, interfacial layer, doping the switching layer, multilayered or hybrid structure, controlled deposition parameters, and development techniques were shown to enhance ZnO-based RRAM switching characteristics still requires more investigations. ZnO NRs show better mechanical robustness than ZnO thin film, the mechanical flexibility and good switching operations are vital for realizing bendable nonvolatile memories. Therefore, further explorations are required to see the actualization of this trend. Synaptic roles reported in ZnO-based RRAM device is a step towards building bio-inspired cognitive computational systems. The realization of crossbar memory architecture is still facing a lot of challenges. The sneak current path issue still suffered ZnO-based crossbar architecture. Hence, further research is needed to resolve these challenges. It is quite motivating to explore the multifunctional nonvolatile memories. But, most of the studies are still not much in this area. Furthermore, this article's discussion points out the promising potentials and future of ZnO-based RRAM devices. Therefore, the improvement of new device concepts, suitable fabrication techniques, and standardized testing systems may enhance and simplify research and development procedures for the near future.

REFERENCES

[1] D. B. Strukov, G. S. Snider, D. R. Stewart, and R. S. Williams, "The missing memristor found," *Nature*, vol. 453, no. 7191, pp. 80–83, May 2008.

[2] J. S. Meena, S. M. Sze, U. Chand, and T.-Y. Tseng, "Overview of emerging nonvolatile memory technologies," *Nanosc. Res. Lett.*, vol. 9, no. 1, pp. 1–33, 2014.

[3] R. Bez and A. Pirovano, "Non-volatile memory technologies: Emerging concepts and new materials," *Mater. Sci. Semicond. Process.*, vol. 7, nos. 4–6, pp. 349–355, 2004.

[4] Grand View Research. (Feb. 2015). *Next Generation Memory Market Size: Global Industry Report, 2020*. Accessed: May 10, 2021. [Online]. Available: https://www.grandviewresearch.com/industry-analysis/next-generation-memory-market

[5] D. Kahng and S. M. Sze, "A floating gate and its application to memory devices," *Bell Syst. Tech. J.*, vol. 46, no. 6, pp. 1288–1295, Jul. 1967.

[6] R. Bez, E. Camerlenghi, A. Modelli, and A. Visconti, "Introduction to flash memory," *Proc. IEEE*, vol. 91, no. 4, pp. 489–502, Apr. 2003.

[7] W. J. Gallagher and S. S. P. Parkin, "Development of the magnetic tunnel junction MRAM at IBM: From first junctions to a 16-Mb MRAM demonstrator chip," *IBM J. Res. Develop.*, vol. 50, no. 1, pp. 5–23, Jan. 2006.

[8] M. Wuttig and N. Yamada, "Phase-change materials for rewriteable data storage," *Nature Mater.*, vol. 6, pp. 824–832, Nov. 2007.

[9] T. Kawahara, K. Ito, R. Takemura, and H. Ohno, "Spin-transfer torque RAM technology: Review and prospect," *Microelectron. Rel.*, vol. 52, no. 4, pp. 613–627, Apr. 2012.

[10] Y. T. Evgeny and K. Hermann, "Tunneling across a ferroelectric," *Science*, vol. 313, no. 5784, pp. 181–183, 2006. [Online]. Available: https://digitalcommons.unl.edu/cgi/viewcontent.cgi?article=1021&context=physicstsymbal, doi: 10.1126/science.1126230.

[11] R. Waser and M. Aono, "Nanoionics-based resistive switching memories," *Nanosci. Technol., Collection Rev. From Nature J.*, vol. 6, pp. 158–165, Nov. 2007.

[12] D. S. Jeong, R. Thomas, R. S. Katiyar, J. F. Scott, H. Kohlstedt, A. Petraru, and C. S. Hwang, "Emerging memories: Resistive switching mechanisms and current status," *Rep. Prog. Phys.*, vol. 75, no. 7, Jul. 2012, Art. no. 076502.

[13] D. Ielmini, "Resistive switching memories based on metal oxides: Mechanisms, reliability and scaling," *Semicond. Sci. Technol.*, vol. 31, no. 6, May 2016, Art. no. 063002.

[14] B. Hoefflinger, "ITRS: The international technology roadmap for semiconductors," in *Chips*. Berlin, Germany: Springer, 2020, pp. 161–174.

[15] W. Zhuang, W. Pan, B. D. Ulrich, J. J. Lee, L. Stecker, A. Burmaster, D. R. Evans, S. T. Hsu, M. Tajiri, A. Shimaoka, K. Inoue, T. Naka, N. Awaya, A. Sakiyama, Y. Wang, S. Q. Liu, N. J. Wu, and A. Ignatiev, "Novel colossal magnetoresistive thin film nonvolatile resistance random access memory (RRAM)," in *IEDM Tech. Dig.*, Dec. 2002, pp. 193–196.

[16] H. Akinaga and H. Shima, "Resistive random access memory (ReRAM) based on metal oxides," *Proc. IEEE*, vol. 98, no. 12, pp. 2237–2251, Dec. 2010.

[17] L. O. Chua, "Memristor-the missing circuit element," *IEEE Trans. Circuit Theory*, vol. CT-18, no. 5, pp. 507–519, Sep. 1971.

[18] T. W. Hickmott, "Low-frequency negative resistance in thin anodic oxide films," *J. Appl. Phys.*, vol. 33, no. 9, pp. 2669–2682, 1962.

[19] N. M. Bashara and P. H. Nielsen, "Memory effects in thin film negative resistance structures," in *Proc. Annu. Rep. Conf. Electr. Insul.*, Nov. 1963, pp. 29–32.

[20] D. Lamb and P. Rundle, "A non-filamentary switching action in thermally grown silicon dioxide films," *Brit. J. Appl. Phys.*, vol. 18, no. 1, p. 29, 1967.

[21] K. B. Jung, J. W. Lee, Y. D. Park, J. R. Childress, S. J. Pearton, M. Jenson, and A. T. Hurst, "Electron cyclotron resonance plasma etching of materials for magneto-resistive random access memory applications," *J. Electron. Mater.*, vol. 26, no. 11, pp. 1310–1313, Nov. 1997.

[22] S. Q. Liu, N. J. Wu, and A. Ignatiev, "Electric-pulse-induced reversible resistance change effect in magnetoresistive films," *Appl. Phys. Lett.*, vol. 76, no. 19, pp. 2749–2751, 2000.

[23] S. T. Hsu and W.-W. Zhuang, "Electrically programmable resistance cross point memory," U.S. Patent 6 531 371, Mar. 11, 2003. [Online]. Available: https://patents.google.com/patent/US6531371B2/en

[24] S. Seo, M. J. Lee, D. H. Seo, E. J. Jeoung, D. S. Suh, Y. S. Joung, I. K. Yoo, I. R. Hwang, S. H. Kim, I. S. Byun, J.-S. Kim, J. S. Choi, and B. H. Park, "Reproducible resistance switching in polycrystalline NiO films," *Appl. Phys. Lett.*, vol. 85, no. 23, pp. 5655–5657, 2004.

[25] I. G. Baek, M. S. Lee, S. Sco, M. J. Lee, D. H. Seo, D.-S. Suh, J. C. Park, S. O. Park, H. S. Kim, I. K. Yoo, U.-I. Chung, and J. T. Moon, "Highly scalable non-volatile resistive memory using simple binary oxide driven by asymmetric unipolar voltage pulses," in *IEDM Tech. Dig.*, Dec. 2004, pp. 587–590.

[26] I. G. Baek, D. C. Kim, M. J. Lee, H.-J. Kim, E. K. Yim, M. S. Lee, J. E. Lee, S. E. Ahn, S. Seo, J. H. Lee, J. C. Park, Y. K. Cha, S. O. Park, H. S. Kim, I. K. Yoo, U. Chung, J. T. Moon, and B. I. Ryu, "Multi-layer cross-point binary oxide resistive memory (OxRRAM) for post-NAND storage application," in *IEDM Tech. Dig.*, Dec. 2005, pp. 750–753.

[27] M.-J. Lee, Y. Park, B.-S. Kang, S.-E. Ahn, C. Lee, K. Kim, W. Xianyu, G. Stefanovich, J.-H. Lee, S.-J. Chung, Y.-H. Kim, C.-S. Lee, J.-B. Park, I.-G. Baek, and I.-K. Yoo, "2-stack 1D-1R cross-point structure with oxide diodes as switch elements for high density resistance RAM applications," in *IEDM Tech. Dig.*, Dec. 2007, pp. 771–774.

[28] K. Aratani, K. Ohba, T. Mizuguchi, S. Yasuda, T. Shiimoto, T. Tsushima, T. Sone, K. Endo, A. Kouchiyama, S. Sasaki, A. Maesaka, N. Yamada, and H. Narisawa, "A novel resistance memory with high scalability and nanosecond switching," in *IEDM Tech. Dig.*, Dec. 2007, pp. 783–786.

[29] E. Vogel, "Technology and metrology of new electronic materials and devices," *Nature Nanotechnol.*, vol. 2, no. 1, pp. 25–32, Jan. 2007.

[30] S. Lee, H. Kim, D.-J. Yun, S.-W. Rhee, and K. Yong, "Resistive switching characteristics of ZnO thin film grown on stainless steel for flexible non-volatile memory devices," *Appl. Phys. Lett.*, vol. 95, no. 26, Dec. 2009, Art. no. 262113.

[31] C. J. Chevallier, C. H. Siau, S. F. Lim, S. R. Namala, M. Matsuoka, B. L. Bateman, and D. Rinerson, "A 0.13 μm 64 Mb multi-layered conductive metal-oxide memory," in *IEEE Int. Solid-State Circuits Conf. (ISSCC) Dig. Tech. Papers*, Feb. 2010, pp. 260–261.

[32] W. Otsuka, K. Miyata, M. Kitagawa, K. Tsutsui, T. Tsushima, H. Yoshihara, T. Namise, Y. Terao, and K. Ogata, "A 4 Mb conductive-bridge resistive memory with 2.3 GB/s read-throughput and 216 MB/s program-throughput," in *IEEE Int. Solid-State Circuits Conf. (ISSCC) Dig. Tech. Papers*, Feb. 2011, pp. 210–211.

[33] A. Kawahara, R. Azuma, Y. Ikeda, K. Kawai, Y. Katoh, Y. Hayakawa, K. Tsuji, S. Yoneda, A. Himeno, and K. Shimakawa, "An 8 Mb multi-layered cross-point ReRAM macro with 443 MB/s write throughput," *IEEE J. Solid-State Circuits*, vol. 48, no. 1, pp. 178–185, Jan. 2013.

[34] C. Mellor. (Feb. 2012). *Rambus Drops $35m for Unity Semiconductor*. Accessed: May 20, 2021. [Online] Available: https://shorturl.at/uN078

[35] L. Mearian. (Aug. 2013). *Next-Gen Storage Wars: In the Battle of RRAM vs 3D NAND Flash, All of Us are Winners*. Accessed: May 20, 2021. [Online] Available: https://shorturl.at/iwF49

[36] C. Mellor. (Nov. 2013). *HP 100TB Memristor Drives by 2018—If You're Lucky, Admits Tech Titan*. Accessed: May 20, 2021. [Online] Available: https://shorturl.at/nEGPQ

[37] (Jun. 2013). *Headquarters News: Panasonic Starts World's First Mass Production of ReRAM Mounted Microcomputers*. Accessed: May 20, 2021. [Online]. Available: https://shorturl.at/hksuH

[38] T.-Y. Liu *et al.*, "A 130.7 mm^2 2-layer 32 Gb ReRAM memory device in 24 nm technology," in *IEEE Int. Solid-State Circuits Conf. (ISSCC) Dig. Tech. Papers*, Feb. 2013, pp. 210–211.

[39] R. Fackenthal, M. Kitagawa, W. Otsuka, K. Prall, D. Mills, K. Tsutsui, J. Javanifard, K. Tedrow, T. Tsushima, Y. Shibahara, and G. Hush, "A 16 Gb ReRAM with 200 MB/s write and 1 GB/s read in 27 nm technology," in *IEEE Int. Solid-State Circuits Conf. (ISSCC) Dig. Tech. Papers*, Feb. 2014, pp. 338–339.

[40] M. Ueki, K. Takeuchi, T. Yamamoto, A. Tanabe, N. Ikarashi, M. Saitoh, T. Nagumo, H. Sunamura, M. Narihiro, K. Uejima, K. Masuzaki, N. Furutake, S. Saito, Y. Yabe, A. Mitsuiki, K. Takeda, T. Hase, and Y. Hayashi, "Low-power embedded ReRAM technology for IoT applications," in *Proc. Symp. VLSI Technol. (VLSI Technol.)*, Jun. 2015, pp. T108–T109.

[41] Q. Luo, X. Xu, H. Liu, H. Lv, T. Gong, S. Long, Q. Liu, H. Sun, W. Banerjee, L. Li, J. Gao, N. Lu, and M. Liu, "Super non-linear RRAM with ultra-low power for 3D vertical nano-crossbar arrays," *Nanoscale*, vol. 8, pp. 15629–15636, Aug. 2016.

[42] S. Yoneda, S. Ito, Y. Hayakawa, Z. Wei, S. Muraoka, R. Yasuhara, K. Kawashima, A. Himeno, and T. Mikawa, "Newly developed process integration technologies for highly reliable 40 nm ReRAM," *Jpn. J. Appl. Phys.*, vol. 58, no. SB, Apr. 2019, Art. no. SBBB06.

[43] (Sep. 2019). *FUJITSU Released World's Largest Density 8 Mbit ReRAM Product*. Accessed: May 20, 2021. [Online] Available: https://shorturl.at/cwGOT

[44] P. Clarke. (Jun. 2017). *Report: TSMC to Offer Embedded ReRAM in 2019*. Accessed: May 20, 2021. [Online] Available: https://www.eenewsanalog.com/news/report-tsmcoffer-embedded-reram-2019

[45] TSMC Report. (2019). *TSMC Annual Report 2019 (I)*. Accessed: May 20, 2021. [Online] Available: https://shorturl.at/mqCO2

[46] X. Hong, D. J. Loy, P. A. Dananjaya, F. Tan, C. Ng, and W. Lew, "Oxide-based RRAM materials for neuromorphic computing," *J. Mater. Sci.*, vol. 53, no. 12, pp. 8720–8746, 2018.

[47] L. Zhu, J. Zhou, Z. Guo, and Z. Sun, "An overview of materials issues in resistive random access memory," *J. Mater.*, vol. 1, no. 4, pp. 285–295, 2015.

[48] F. Pan, S. Gao, C. Chen, C. Song, and F. Zeng, "Recent progress in resistive random access memories: Materials, switching mechanisms, and performance," *Mater. Sci. Eng. R, Rep.*, vol. 83, pp. 1–59, Sep. 2014.

[49] B. Gao, S. Yu, N. Xu, L. F. Liu, B. Sun, X. Y. Liu, R. Q. Han, J. F. Kang, B. Yu, and Y. Y. Wang, "Oxide-based RRAM switching mechanism: A new ion-transport-recombination model," in *IEDM Tech. Dig.*, Dec. 2008, pp. 1–4.

[50] U. Russo, D. Ielmini, C. Cagli, A. L. Lacaita, S. Spiga, C. Wiemer, M. Perego, and M. Fanciulli, "Conductive-filament switching analysis and self-accelerated thermal dissolution model for reset in NiO-based RRAM," in *IEDM Tech. Dig.*, Dec. 2007, pp. 775–778.

[51] R. Waser, R. Dittmann, G. Staikov, and K. Szot, "Redox-based resistive switching memories–nanoionic mechanisms, prospects, and challenges," *Adv. Mater.*, vol. 21, nos. 25–26, pp. 2632–2663, Jul. 2009.

[52] F. Pan, C. Chen, Z.-S. Wang, Y.-C. Yang, J. Yang, and F. Zeng, "Non-volatile resistive switching memories-characteristics, mechanisms and challenges," *Prog. Natural Sci., Mater. Int.*, vol. 20, pp. 1–15, Nov. 2010.

[53] F. M. Simanjuntak, S. Chandrasekaran, F. Gapsari, and T. Y. Tseng, "Switching and synaptic characteristics of AZO/ZnO/ITO valence change memory device," *IOP Conf. Ser., Mater. Sci. Eng.*, vol. 494, Mar. 2019, Art. no. 012027.

[54] D. Xu, Y. Xiong, M. Tang, B. Zeng, and Y. Xiao, "Bipolar and unipolar resistive switching modes in Pt/$Zn_{0.99}Zr_{0.01}$O/Pt structure for multi-bit resistance random access memory," *Appl. Phys. Lett.*, vol. 104, no. 18, 2014, Art. no. 183501.

[55] S. Murali, J. S. Rajachidambaram, S.-Y. Han, C.-H. Chang, G. S. Herman, and J. F. Conley, Jr., "Resistive switching in zinc–tin-oxide," *Solid-State Electron.*, vol. 79, pp. 248–252, Jan. 2013.

[56] Z. Wang, W. Zhu, A. Du, L. Wu, Z. Fang, X. A. Tran, W. Liu, K. Zhang, and H.-Y. Yu, "Highly uniform, self-compliance, and forming-free ALD HfO_2-based RRAM with Ge doping," *IEEE Trans. Electron Devices*, vol. 59, no. 4, pp. 1203–1208, Apr. 2012.

[57] K. Tsunoda, K. Kinoshita, H. Noshiro, Y. Yamazaki, T. Iizuka, Y. Ito, A. Takahashi, A. Okano, Y. Sato, T. Fukano, M. Aoki, and Y. Sugiyama, "Low power and high speed switching of Ti-doped NiO ReRAM under the unipolar voltage source of less than 3 V," in *IEDM Tech. Dig.*, Dec. 2007, pp. 767–770.

[58] R. Huang, K. Sun, K. S. Kiang, K. A. Morgan, and C. H. de Groot, "Forming-free resistive switching of tunable ZnO films grown by atomic layer deposition," *Microelectron. Eng.*, vol. 161, pp. 7–12, Aug. 2016.

[59] Z. Fang, H. Y. Yu, X. Li, N. Singh, G. Q. Lo, and D. L. Kwong, "HfO_x/TiO_x/HfO_x/TiO_x multilayer-based forming-free RRAM devices with excellent uniformity," *IEEE Electron Device Lett.*, vol. 32, no. 4, pp. 566–568, Apr. 2011.

[60] N. Banno, T. Sakamoto, N. Iguchi, H. Sunamura, K. Terabe, T. Hasegawa, and M. Aono, "Diffusivity of Cu ions in solid electrolyte and its effect on the performance of nanometer-scale switch," *IEEE Trans. Electron Devices*, vol. 55, no. 11, pp. 3283–3287, Nov. 2008.

[61] R. Govindaraj, R. Kesavamoorthy, R. Mythili, and B. Viswanathan, "The formation and characterization of silver clusters in zirconia," *J. Appl. Phys.*, vol. 90, pp. 958–963, Jun. 2001.

[62] Y. Li, S. Long, M. Zhang, Q. Liu, L. Shao, S. Zhang, Y. Wang, Q. Zuo, S. Liu, and M. Liu, "Resistive switching properties of Au/ZrO_2/Ag structure for low-voltage nonvolatile memory applications," *IEEE Electron Device Lett.*, vol. 31, no. 2, pp. 117–119, Dec. 2009.

[63] F. Zhuge, B. Hu, C. He, X. Zhou, Z. Liu, and R.-W. Li, "Mechanism of nonvolatile resistive switching in graphene oxide thin films," *Carbon*, vol. 49, no. 12, pp. 3796–3802, Oct. 2011.

[64] A. Makarov, V. Sverdlov, and S. Selberherr, "Modeling of the SET and RESET process in bipolar resistive oxide-based memory using Monte Carlo simulations," in *Proc. Int. Conf. Numer. Methods Appl.* Berlin, Germany: Springer, 2010, pp. 87–94.

[65] M. Bocquet, D. Deleruyelle, H. Aziza, C. Muller, J.-M. Portal, T. Cabout, and E. Jalaguier, "Robust compact model for bipolar oxide-based resistive switching memories," *IEEE Trans. Electron Devices*, vol. 61, no. 3, pp. 674–681, Mar. 2014.

[66] V. Karpov, D. Niraula, and I. Karpov, "Thermodynamic analysis of conductive filaments," *Appl. Phys. Lett.*, vol. 109, no. 9, Aug. 2016, Art. no. 093501.

[67] B. Traore, P. Blaise, E. Vianello, L. Perniola, B. De Salvo, and Y. Nishi, "HfO_2-based RRAM: Electrode effects, Ti/HfO_2 interface, charge injection, and oxygen (O) defects diffusion through experiment and *ab initio* calculations," *IEEE Trans. Electron Devices*, vol. 63, no. 1, pp. 360–368, Jan. 2016.

[68] M. Villena, F. Jiménez-Molinos, J. Roldán, J. Suñé, S. Long, X. Lian, F. Gámiz, and M. Liu, "An in-depth simulation study of thermal reset transitions in resistive switching memories," *J. Appl. Phys.*, vol. 114, no. 14, 2013, Art. no. 144505.

[69] M. C. Aguilera-Morillo, A. M. Aguilera, F. Jiménez-Molinos, and J. B. Roldán, "Stochastic modeling of random access memories reset transitions," *Math. Comput. Simul.*, vol. 159, pp. 197–209, May 2019.

[70] J. S. Lee, S. Lee, and T. W. Noh, "Resistive switching phenomena: A review of statistical physics approaches," *Appl. Phys. Rev.*, vol. 2, no. 3, 2015, Art. no. 031303.

[71] F. Zahoor, T. Z. Azni Zulkifli, and F. A. Khanday, "Resistive random access memory (RRAM): An overview of materials, switching mechanism, performance, multilevel cell (MLC) storage, modeling, and applications," *Nanosc. Res. Lett.*, vol. 15, no. 1, pp. 1–26, Dec. 2020.

[72] S. Yu and H.-S. P. Wong, "Characterization and modeling of the conduction and switching mechanisms of HfO_x based RRAM," *MRS Online Library*, vol. 1631, no. 1, pp. 1–2, 2014.

[73] S. Yu and H.-S. P. Wong, "A phenomenological model for the reset mechanism of metal oxide RRAM," *IEEE Electron Device Lett.*, vol. 31, no. 12, pp. 1455–1457, Dec. 2010.

[74] Y. S. Zhi, P. G. Li, P. C. Wang, D. Y. Guo, Y. H. An, Z. P. Wu, X. L. Chu, J. Q. Shen, W. H. Tang, and C. R. Li, "Reversible transition between bipolar and unipolar resistive switching in Cu_2O/Ga_2O_3 binary oxide stacked layer," *AIP Adv.*, vol. 6, no. 1, Jan. 2016, Art. no. 015215.

[75] F. Zahoor, T. Z. A. Zulkifli, F. A. Khanday, and S. A. Z. Murad, "Carbon nanotube and resistive random access memory based unbalanced ternary logic gates and basic arithmetic circuits," *IEEE Access*, vol. 8, pp. 104701–104717, 2020.

[76] F. Zahoor, F. A. Hussin, T. Z. A. Zulkifli, F. A. Khanday, U. B. Isyaku, and A. A. Fida, "Resistive random access memory (RRAM) based unbalanced ternary inverter," *Solid State Technol.*, vol. 63, no. 6, pp. 4245–4255, 2020.

[77] USFAD Administration: Center for Food Safety and Applied Nutrition. *Food Additive Status List*. Accessed: May 20, 2021. [Online] Available: https://shorturl.at/avBRV

[78] P. R. Gandhi, C. Jayaseelan, R. R. Mary, D. Mathivanan, and S. R. Suseem, "Acaricidal, pediculicidal and larvicidal activity of synthesized ZnO nanoparticles using momordica charantia leaf extract against blood feeding parasites," *Exp. Parasitol.*, vol. 181, pp. 47–56, Oct. 2017.

[79] J. W. Rasmussen, E. Martinez, P. Louka, and D. G. Wingett, "Zinc oxide nanoparticles for selective destruction of tumor cells and potential for drug delivery applications," *Expert Opinion Drug Del.*, vol. 7, no. 9, pp. 1063–1077, Sep. 2010.

[80] Z. Sharifi-Heris, L. Amiri Farahani, and S. B. Hasanpoor-Azghadi, "A review study of diaper rash dermatitis treatments," *J. Client-Centered Nursing Care*, vol. 4, no. 1, pp. 1–12, Oct. 2018.

[81] V. Galstyan, M. Bhandari, V. Sberveglieri, G. Sberveglieri, and E. Comini, "Metal oxide nanostructures in food applications: Quality control and packaging," *Chemosensors*, vol. 6, no. 2, p. 16, Apr. 2018.

[82] G. Deak, F. D. Dumitru, M. A. Moncea, A. M. Panait, A. G. Baraitaru, M. V. Olteanu, M. G. Boboc, and S. Stanciu, "Synthesis of ZnO nanoparticles for water treatment applications," *Int. J. Conservation Sci.*, vol. 10, no. 2, pp. 343–350, 2019.

[83] M. Laurenti, S. Porro, C. F. Pirri, C. Ricciardi, and A. Chiolerio, "Zinc oxide thin films for memristive devices: A review," *Crit. Rev. Solid State Mater. Sci.*, vol. 42, no. 2, pp. 153–172, Mar. 2017.

[84] V. Galstyan, E. Comini, C. Baratto, G. Faglia, and G. Sberveglieri, "Nanostructured ZnO chemical gas sensors," *Ceram. Int.*, vol. 41, no. 10, pp. 14239–14244, Dec. 2015.

[85] S. Pearton, D. Norton, K. Ip, Y. Heo, and T. Steiner, "Recent advances in processing of ZnO," *J. Vac. Sci. Technol. B, Microelectron. Nanometer Struct. Process., Meas., Phenomena*, vol. 22, no. 3, pp. 932–948, 2004.

[86] W.-Y. Chang, Y.-C. Lai, T.-B. Wu, S.-F. Wang, F. Chen, and M.-J. Tsai, "Unipolar resistive switching characteristics of ZnO thin films for nonvolatile memory applications," *Appl. Phys. Lett.*, vol. 92, no. 2, Jan. 2008, Art. no. 022110.

[87] Y. Tu, S. Chen, X. Li, J. Gorbaciova, W. P. Gillin, S. Krause, and J. Briscoe, "Control of oxygen vacancies in ZnO nanorods by annealing and their influence on ZnO/PEDOT:PSS diode behaviour," *J. Mater. Chem. C*, vol. 6, no. 7, pp. 1815–1821, 2018.

[88] A. Kołodziejczak-Radzimska and T. Jesionowski, "Zinc oxide—From synthesis to application: A review," *Materials*, vol. 7, no. 4, pp. 2833–2881, 2014.

[89] C. Jin, R. Narayan, A. Tiwari, H. Zhou, A. Kvit, and J. Narayan, "Epitaxial growth of zinc oxide thin films on silicon," *Mater. Sci. Eng., B*, vol. 117, no. 3, pp. 348–354, Mar. 2005.

[90] Y. E. Lee, Y. J. Kim, and H. J. Kim, "Thickness dependence of microstructural evolution of ZnO films deposited by RF magnetron sputtering," *J. Mater. Res.*, vol. 13, no. 5, pp. 1260–1265, May 1998.

[91] F. M. Simanjuntak, D. Panda, K.-H. Wei, and T.-Y. Tseng, "Status and prospects of ZnO-based resistive switching memory devices," *Nanosc. Res. Lett.*, vol. 11, no. 1, pp. 1–31, Dec. 2016.

[92] D. Panda and T.-Y. Tseng, "One-dimensional ZnO nanostructures: Fabrication, optoelectronic properties, and device applications," *J. Mater. Sci.*, vol. 48, no. 20, pp. 6849–6877, Oct. 2013.

[93] A. B. Djurišić and Y. H. Leung, "Optical properties of ZnO nanostructures," *Small*, vol. 2, nos. 8–9, pp. 944–961, Aug. 2006.

[94] K. Denishev, "Some metal oxides and their applications for creation of microsystems (MEMS) and energy harvesting devices (EHD)," *J. Phys., Conf. Ser.*, vol. 764, Oct. 2016, Art. no. 012003.

[95] M. R. Zakaria, S. Johari, M. H. Ismail, and U. Hashim, "Characterization of zinc oxide (ZnO) piezoelectric properties for surface acoustic wave (SAW) device," in *Proc. EPJ Web Conf.*, vol. 162, Nov. 2017, p. 01055.

[96] J. Cui and U. Gibson, "Low-temperature fabrication of single-crystal ZnO nanopillar photonic bandgap structures," *Nanotechnology*, vol. 18, no. 15, Apr. 2007, Art. no. 155302.

[97] Y. Zhang, T. Nayak, H. Hong, and W. Cai, "Biomedical applications of zinc oxide nanomaterials," *Current Mol. Med.*, vol. 13, no. 10, pp. 1633–1645, 2013.
[98] H. Mirzaei and M. Darroudi, "Zinc oxide nanoparticles: Biological synthesis and biomedical applications," *Ceram. Int.*, vol. 43, no. 1, pp. 907–914, Jan. 2017.
[99] J. Bourgoin and M. Lannoo, *Point Defects in Semiconductors II* (Springer Series in Solid-State Sciences), vol. 35. Heidelberg, Germany: Springer-Verlag, 1983.
[100] A. Alkauskas, M. D. McCluskey, and C. G. Van de Walle, "Tutorial: Defects in semiconductors—Combining experiment and theory," *J. Appl. Phys.*, vol. 119, no. 18, May 2016, Art. no. 181101.
[101] M. Lannoo and J. Bourgoin, *Point Defects in Semiconductors I: Theoretical Aspects*. Berlin, Germany: Springer, 1981.
[102] S. T. Pantelides, *Deep Centers in Semiconductors*. Boca Raton, FL, USA: CRC Press, 1992.
[103] Q. Hou, X. Jia, Z. Xu, C. Zhao, and L. Qu, "Effects of Li doping and point defect on the magnetism of ZnO," *Ceram. Int.*, vol. 44, no. 2, pp. 1376–1383, Feb. 2018.
[104] A. Janotti and C. Van de Walle, "Native point defects in ZnO," *Phys. Rev. B, Condens. Matter*, vol. 76, no. 16, Oct. 2007, Art. no. 165202.
[105] A. Kohan, G. Ceder, D. Morgan, and C. G. V. D. Walle, "First-principles study of native point defects in ZnO," *Phys. Rev. B, Condens. Matter*, vol. 61, no. 22, p. 15019, 2000.
[106] C. S. Fuller, "The chemistry of imperfect crystals," *J. Amer. Chem. Soc.*, vol. 86, no. 20, pp. 4514–4515, 1964.
[107] A. Janotti and C. G. Van de Walle, "New insights into the role of native point defects in ZnO," *J. Cryst. Growth*, vol. 287, no. 1, pp. 58–65, 2006.
[108] X. Chen, Q. Xie, and J. Li, "Significantly improved photoluminescence properties of ZnO thin films by lithium doping," *Ceram. Int.*, vol. 46, no. 2, pp. 2309–2316, Feb. 2020.
[109] K. H. Tam, C. K. Cheung, Y. H. Leung, A. B. Djurišic, C. C. Ling, C. D. Beling, S. Fung, W. M. Kwok, W. K. Chan, D. L. Phillips, L. Ding, and W. K. Ge, "Defects in ZnO nanorods prepared by a hydrothermal method," *J. Phys. Chem. B*, vol. 110, no. 42, pp. 20865–20871, 2006.
[110] L. E. Greene, M. Law, J. Goldberger, F. Kim, J. C. Johnson, Y. Zhang, R. J. Saykally, and P. Yang, "Low-temperature wafer-scale production of ZnO nanowire arrays," *Angew. Chem.*, vol. 115, no. 26, pp. 3139–3142, 2003.
[111] M. Gomi, N. Oohira, K. Ozaki, and M. Koyano, "Photoluminescent and structural properties of precipitated ZnO fine particles," *Jpn. J. Appl. Phys.*, vol. 42, no. 2R, p. 481, 2003.
[112] A. B. Djurišic, Y. H. Leung, K. H. Tam, Y. F. Hsu, L. Ding, W. K. Ge, Y. C. Zhong, K. S. Wong, W. K. Chan, H. L. Tam, K. W. Cheah, W. M. Kwok, and D. L. Phillips, "Defect emissions in ZnO nanostructures," *Nanotechnology*, vol. 18, no. 9, 2007, Art. no. 095702.
[113] Q. Hou, Y. Liu, C. Li, and H. Tao, "Effect of VZn/VO on stability, magnetism, and electronic characteristic of oxygen ions for Li-doped ZnO," *J. Supercond. Novel Magnetism*, vol. 32, no. 7, pp. 1859–1869, Jul. 2019.
[114] L. Zhu and W. Zeng, "Room-temperature gas sensing of ZnO-based gas sensor: A review," *Sens. Actuators A, Phys.*, vol. 267, pp. 242–261, Nov. 2017.
[115] Z. S. Hosseini, A. I. Zad, and A. Mortezaali, "Room temperature H_2S gas sensor based on rather aligned ZnO nanorods with flower-like structures," *Sens. Actuators B, Chem.*, vol. 207, pp. 865–871, Feb. 2015.
[116] R. S. Ganesh, E. Durgadevi, M. Navaneethan, V. Patil, S. Ponnusamy, C. Muthamizhchelvan, S. Kawasaki, P. Patil, and Y. Hayakawa, "Low temperature ammonia gas sensor based on Mn-doped ZnO nanoparticle decorated microspheres," *J Alloys Compounds*, vol. 721, pp. 182–190, Oct. 2017.
[117] M. Das and D. Sarkar, "One-pot synthesis of zinc oxide–polyaniline nanocomposite for fabrication of efficient room temperature ammonia gas sensor," *Ceram. Int.*, vol. 43, no. 14, pp. 11123–11131, Oct. 2017.
[118] S. Bhatia, N. Verma, and R. K. Bedi, "Ethanol gas sensor based upon ZnO nanoparticles prepared by different techniques," *Result Phys.*, vol. 7, pp. 801–806, Feb. 2017.
[119] H. S. Hassan, A. Kashyout, I. Morsi, A. Nasser, and A. Raafat, "Fabrication and characterization of nano-gas sensor arrays," *AIP Conf.*, vol. 1653, Apr. 2015, Art. no. 020042.
[120] H. Y. Peng, G. P. Li, J. Y. Ye, Z. P. Wei, Z. Zhang, D. D. Wang, G. Z. Xing, and T. Wu, "Electrode dependence of resistive switching in Mn-doped ZnO: Filamentary versus interfacial mechanisms," *Appl. Phys. Lett.*, vol. 96, no. 19, May 2010, Art. no. 192113.
[121] J. Zhao, F. Liu, J. Sun, H. Huang, Z. Hu, and X. Zhang, "Low power consumption bipolar resistive switching characteristics of ZnO-based memory devices," *Chin. Opt. Lett.*, vol. 10, no. 1, 2012, Art. no. 013102.
[122] X. Wang, H. Qian, L. Guan, W. Wang, B. Xing, X. Yan, S. Zhang, J. Sha, and Y. Wang, "Influence of metal electrode on the performance of ZnO based resistance switching memories," *J. Appl. Phys.*, vol. 122, no. 15, Oct. 2017, Art. no. 154301.
[123] N. Xu, L. F. Liu, X. Sun, C. Chen, Y. Wang, D. D. Han, X. Y. Liu, R. Q. Han, J. F. Kang, and B. Yu, "Bipolar switching behavior in TiN/ZnO/Pt resistive nonvolatile memory with fast switching and long retention," *Semicond. Sci. Technol.*, vol. 23, no. 7, Jul. 2008, Art. no. 075019.
[124] C.-L. Lin, C.-C. Tang, S.-C. Wu, S.-R. Yang, Y.-H. Lai, and S.-C. Wu, "Resistive switching characteristics of zinc oxide (ZnO) resistive RAM with Al metal electrode," in *Proc. 4th IEEE Int. Nanoelectron. Conf.*, Jun. 2011, pp. 1–2.
[125] S. Seo, M. J. Lee, D. C. Kim, S. E. Ahn, B.-H. Park, Y. S. Kim, I. K. Yoo, I. S. Byun, I. R. Hwang, S. H. Kim, J.-S. Kim, J. S. Choi, J. H. Lee, S. H. Jeon, S. H. Hong, and B. H. Park, "Electrode dependence of resistance switching in polycrystalline NiO films," *Appl. Phys. Lett.*, vol. 87, no. 26, Dec. 2005, Art. no. 263507.
[126] K.-J. Lee, L.-W. Wang, T.-K. Chiang, and Y.-H. Wang, "Effects of electrodes on the switching behavior of strontium titanate nickelate resistive random access memory," *Materials*, vol. 8, no. 10, pp. 7191–7198, Oct. 2015.
[127] W. H. Xue, W. Xiao, J. Shang, X. X. Chen, X. J. Zhu, L. Pan, H. W. Tan, W. B. Zhang, Z. H. Ji, G. Liu, X.-H. Xu, J. Ding, and R.-W. Li, "Intrinsic and interfacial effect of electrode metals on the resistive switching behaviors of zinc oxide films," *Nanotechnology*, vol. 25, no. 42, Oct. 2014, Art. no. 425204.
[128] A. Kumar and M. S. Baghini, "Experimental study for selection of electrode material for ZnO-based memristors," *Electron. Lett.*, vol. 50, no. 21, pp. 1547–1549, Oct. 2014.
[129] Z.-J. Liu, J.-C. Chou, S.-Y. Wei, J.-Y. Gan, and T.-R. Yew, "Improved resistive switching of textured ZnO thin films grown on Ru electrodes," *IEEE Electron Device Lett.*, vol. 32, no. 12, pp. 1728–1730, Dec. 2011.
[130] D.-Y. Lee, S.-Y. Wang, and T.-Y. Tseng, "Ti-induced recovery phenomenon of resistive switching in ZrO_2 thin films," *J. Electrochem. Soc.*, vol. 157, no. 7, p. G166, 2010.
[131] J. Wang, Z. Song, K. Xu, and M. Liu, "Rectifying switching characteristics of Pt/ZnO/Pt structure based resistive memory," *J. Nanosci. Nanotechnol.*, vol. 10, no. 11, pp. 7088–7091, Nov. 2010.
[132] S. Pi, C. Li, H. Jiang, W. Xia, H. Xin, J. J. Yang, and Q. Xia, "Memristor crossbar arrays with 6-nm half-pitch and 2-nm critical dimension," *Nature Nanotechnol.*, vol. 14, pp. 35–39, Nov. 2018.
[133] A. I. Maaroof and B. L. Evans, "Onset of electrical conduction in Pt and Ni films," *J. Appl. Phys.*, vol. 76, no. 2, pp. 1047–1054, Jul. 1994.
[134] A. Younis, D. Chu, and S. Li, "Bi-stable resistive switching characteristics in Ti-doped ZnO thin films," *Nanosc. Res. Lett.*, vol. 8, no. 1, pp. 1–6, 2013.
[135] H. Xu, D. H. Kim, Z. Xiahou, Y. Li, M. Zhu, B. Lee, and C. Liu, "Effect of Co doping on unipolar resistance switching in Pt/Co:ZnO/Pt structures," *J. Alloys Compounds*, vol. 658, pp. 806–812, Feb. 2016.
[136] R. Sridhar, C. Manoharan, S. Ramalingam, S. Dhanapandian, and M. Bououdina, "Spectroscopic study and optical and electrical properties of Ti-doped ZnO thin films by spray pyrolysis," *Spectrochim. Acta A, Mol. Biomolecular Spectrosc.*, vol. 120, pp. 297–303, Feb. 2014.
[137] H. Li, Q. Chen, X. Chen, Q. Mao, J. Xi, and Z. Ji, "Improvement of resistive switching in ZnO film by Ti doping," *Thin Solid Films*, vol. 537, pp. 279–284, Jun. 2013.
[138] S.-C. Qin, R.-X. Dong, and X.-L. Yan, "Memristive behavior of ZnO film with embedded Ti nano-layers," *Appl. Phys. A, Solids Surf.*, vol. 116, no. 1, pp. 1–7, Jul. 2014.
[139] J.-L. Chung, J.-C. Chen, and C.-J. Tseng, "Electrical and optical properties of TiO_2-doped ZnO films prepared by radio-frequency magnetron sputtering," *J. Phys. Chem. Solids*, vol. 69, nos. 2–3, pp. 535–539, Feb. 2008.
[140] Y. C. Lin, C. Y. Hsu, S. K. Hung, and D. C. Wen, "Influence of TiO_2 buffer layer and post-annealing on the quality of Ti-doped ZnO thin films," *Ceram. Int.*, vol. 39, no. 5, pp. 5795–5803, Jul. 2013.
[141] S. A. Bidier, M. R. Hashim, A. M. Al-Diabat, and M. Bououdina, "Effect of growth time on Ti-doped ZnO nanorods prepared by low-temperature chemical bath deposition," *Phys. E, Low-Dimensional Syst. Nanostruct.*, vol. 88, pp. 169–173, Apr. 2017.

[142] D. Vanderbilt, "Soft self-consistent pseudopotentials in a generalized eigenvalue formalism," *Phys. Rev. B, Condens. Matter*, vol. 41, p. 7892, Apr. 1990.
[143] B.-Z. Lin, L. Zhou, S. U. Yuldashev, D.-J. Fu, and T.-W. Kang, "Optical and ferromagnetic properties of Cr doped ZnO nanorods," *Appl. Surf. Sci.*, vol. 315, pp. 124–130, Oct. 2014.
[144] Y. M. Hu, S. S. Li, and C. H. Chia, "Correlation between saturation magnetization and surface morphological features in $Zn_{1-x}Cr_xO$ thin films," *Appl. Phys. Lett.*, vol. 98, no. 5, Jan. 2011, Art. no. 052503.
[145] O. Gürbüz and M. Okutan, "Structural, electrical, and dielectric properties of Cr doped ZnO thin films: Role of Cr concentration," *Appl. Surf. Sci.*, vol. 387, pp. 1211–1218, Nov. 2016.
[146] A. Meng, J. Xing, Z. Li, and Q. Li, "Cr-doped ZnO nanoparticles: Synthesis, characterization, adsorption property, and recyclability," *ACS Appl. Mater. Interfaces*, vol. 7, no. 49, pp. 27449–27457, Dec. 2015.
[147] K. Vijayalakshmi and D. Sivaraj, "Enhanced antibacterial activity of Cr doped ZnO nanorods synthesized using microwave processing," *RSC Adv.*, vol. 5, no. 84, pp. 68461–68469, 2015.
[148] S.-S. Li and Y.-K. Su, "Improvement of the performance in Cr-doped ZnO memory devices via control of oxygen defects," *RSC Adv.*, vol. 9, no. 6, pp. 2941–2947, 2019.
[149] D. L. Xu, Y. Xiong, M. H. Tang, B. W. Zeng, J. Q. Li, L. Liu, L. Q. Li, S. A. Yan, and Z. H. Tang, "Bipolar resistive switching behaviors in Cr-doped ZnO films," *Microelectron. Eng.*, vol. 116, pp. 22–25, Mar. 2014.
[150] A. Manivasaham, K. Ravichandran, and K. Subha, "Light intensity effects on the sensitivity of ZnO:Cr gas sensor," *Surf. Eng.*, vol. 33, no. 11, pp. 866–876, Nov. 2017.
[151] F. M. Simanjuntak, O. K. Prasad, D. Panda, C.-A. Lin, T.-L. Tsai, K.-H. Wei, and T.-Y. Tseng, "Impacts of Co doping on ZnO transparent switching memory device characteristics," *Appl. Phys. Lett.*, vol. 108, no. 18, May 2016, Art. no. 183506.
[152] X. Li, Y. Shi, J. Li, Y. Bai, J. Jia, Y. Li, and X. Xu, "The dissimilar resistive switching properties in ZnO–Co and ZnO films," *Mater. Res. Exp.*, vol. 4, no. 3, Mar. 2017, Art. no. 036407.
[153] J. I. Langford and A. Wilson, "Scherrer after sixty years: A survey and some new results in the determination of crystallite size," *J. Appl. Crystallogr.*, vol. 11, no. 2, pp. 102–113, 1978.
[154] L.-C. Chang, H.-L. Kao, and K.-H. Liu, "Effect of annealing treatment on the electrical characteristics of Pt/Cr-embedded ZnO/Pt resistance random access memory devices," *J. Vac. Sci. Technol. A, Vac. Surf. Films*, vol. 32, no. 2, 2014, Art. no. 02B119.
[155] P. K. R. Boppidi, P. M. P. Raj, S. Challagulla, S. R. Gollu, S. Roy, S. Banerjee, and S. Kundu, "Unveiling the dual role of chemically synthesized copper doped zinc oxide for resistive switching applications," *J. Appl. Phys.*, vol. 124, no. 21, Dec. 2018, Art. no. 214901.
[156] K.-C. Chuang, H.-T. Chung, C.-Y. Chu, J.-D. Luo, W.-S. Li, Y.-S. Li, and H.-C. Cheng, "Impact of AlO_x layer on resistive switching characteristics and device-to-device uniformity of bilayered HfO_x-based resistive random access memory devices," *Jpn. J. Appl. Phys.*, vol. 57, no. 6S3, Jun. 2018, Art. no. 06KC01.
[157] J. J. Yang, D. B. Strukov, and D. R. Stewart, "Memristive devices for computing," *Nature Nanotechnol.*, vol. 8, no. 1, pp. 13–24, 2013.
[158] A. Carvalho, A. Alkauskas, A. Pasquarello, A. K. Tagantsev, and N. Setter, "A hybrid density functional study of lithium in ZnO: Stability, ionization levels, and diffusion," *Phys. Rev. B, Condens. Matter*, vol. 80, no. 19, Nov. 2009, Art. no. 195205.
[159] A. Igityan, Y. Kafadaryan, N. Aghamalyan, S. Petrosyan, G. Badalyan, V. Vardanyan, M. Nersisyan, R. Hovsepyan, A. Palagushkin, and B. Kryzhanovsky, "Resistivity switching properties of Li-doped ZnO films deposited on LaB_6 electrode," *Thin Solid Films*, vol. 595, pp. 92–95, Nov. 2015.
[160] M.-S. Kim, Y. H. Hwang, S. Kim, Z. Guo, D.-I. Moon, J.-M. Choi, M.-L. Seol, B.-S. Bae, and Y.-K. Choi, "Effects of the oxygen vacancy concentration in InGaZnO-based resistance random access memory," *Appl. Phys. Lett.*, vol. 101, no. 24, Dec. 2012, Art. no. 243503.
[161] M. H. Tang, Z. Q. Zeng, J. C. Li, Z. P. Wang, X. L. Xu, G. Y. Wang, L. B. Zhang, S. B. Yang, Y. G. Xiao, and B. Jiang, "Resistive switching behavior of La-doped ZnO films for nonvolatile memory applications," *Solid-State Electron.*, vol. 63, no. 1, pp. 100–104, Sep. 2011.
[162] Y. Han, K. Cho, S. Park, and S. Kim, "The effects of Mn-doping and electrode material on the resistive switching characteristics of $ZnO_{x\,S(1-x)}$ thin films on plastic," *Trans. Electr. Electron. Mater.*, vol. 15, no. 1, pp. 24–27, 2014.
[163] H. Yang, Z. Li, L. Tang, G. Li, Q. Sun, and S. Ren, "Improved magnetism in Mn-doped ZnO thin films by inserting ZnO layer," *IOP Conf. Ser., Mater. Sci. Eng.*, vol. 562, Aug. 2019, Art. no. 012075.
[164] T.-H. Huang, P.-K. Yang, W.-Y. Chang, J.-F. Chien, C.-F. Kang, M.-J. Chen, and J.-H. He, "Eliminating surface effects via employing nitrogen doping to significantly improve the stability and reliability of ZnO resistive memory," *J. Mater. Chem. C*, vol. 1, no. 45, pp. 7593–7597, 2013.
[165] W.-K. Hsieh, R. W. Chuang, and S.-J. Chang, "Two-bit-per-cell resistive switching memory device with a Ti/MgZnO/Pt structure," *RSC Adv.*, vol. 5, no. 107, pp. 88166–88170, 2015.
[166] X. Chen, W. Hu, S. Wu, and D. Bao, "Complementary switching on TiN/MgZnO/ZnO/Pt bipolar memory devices for nanocrossbar arrays," *J. Alloys Compounds*, vol. 615, pp. 566–568, Dec. 2014.
[167] M.-C. Kao, H.-Z. Chen, K.-H. Chen, J.-B. Shi, J.-H. Weng, and K.-P. Chen, "Resistive switching behavior and optical properties of transparent Pr-doped ZnO based resistive random access memory," *Thin Solid Films*, vol. 697, Mar. 2020, Art. no. 137816.
[168] Y. She, Y. Peng, B. Tang, W. Hu, J. Qiu, X. Tang, and D. Bao, "Bipolar resistive switching effects with self-compliance and multilevel storage characteristics in Ag/MgZnO/Si structures," *Ceram. Int.*, vol. 44, pp. S11–S14, Nov. 2018.
[169] L. Zhang, H. Huang, C. Ye, K.-C. Chang, R. Zhang, Q. Xia, X. Wei, W. Wei, and W. Wang, "Exploration of highly enhanced performance and resistive switching mechanism in hafnium doping ZnO memristive device," *Semicond. Sci. Technol.*, vol. 33, no. 8, Aug. 2018, Art. no. 085013.
[170] X. Chen, G. Wu, and D. Bao, "Resistive switching behavior of $Pt/Mg_{0.2}Zn_{0.8}O/Pt$ devices for nonvolatile memory applications," *Appl. Phys. Lett.*, vol. 93, no. 9, 2008, Art. no. 093501.
[171] X. Zhao, Y. Li, C. Ai, and D. Wen, "Resistive switching characteristics of Li-doped ZnO thin films based on magnetron sputtering," *Materials*, vol. 12, no. 8, p. 1282, Apr. 2019.
[172] M. C. Kim, K. Y. Lim, C. O. Kim, and S.-H. Choi, "Effect of doping concentration on resistive switching behaviors of Cu-doped ZnO films," *J. Korean Phys. Soc.*, vol. 59, no. 2, pp. 304–307, Aug. 2011.
[173] S.-S. Li and Y.-K. Su, "Oxygen-vacancy induced resistive switching effect in Mn-doped ZnO memory devices," *Phys. Status Solidi (RRL)-Rapid Res. Lett.*, vol. 13, no. 2, Feb. 2019, Art. no. 1800453.
[174] J.-W. Zhao, J. Sun, H.-Q. Huang, F.-J. Liu, Z.-F. Hu, and X.-Q. Zhang, "Effects of ZnO buffer layer on GZO RRAM devices," *Appl. Surf. Sci.*, vol. 258, no. 10, pp. 4588–4591, Mar. 2012.
[175] X. Li, J. Jia, Y. Li, Y. Bai, J. Li, Y. Shi, L. Wang, and X. Xu, "Realization of resistive switching and magnetoresistance in ZnO/ZnO-Co composite materials," *Sci. Rep.*, vol. 6, no. 1, pp. 1–8, Sep. 2016.
[176] F. Gul and H. Efeoglu, "ZnO and ZnO_{1-x} based thin film memristors: The effects of oxygen deficiency and thickness in resistive switching behavior," *Ceram. Int.*, vol. 43, no. 14, pp. 10770–10775, 2017.
[177] X. Li, J.-G. Yang, H.-P. Ma, Y.-H. Liu, Z.-G. Ji, W. Huang, X. Ou, D. W. Zhang, and H.-L. Lu, "Atomic layer deposition of Ga_2O_3/ZnO composite films for high-performance forming-free resistive switching memory," *ACS Appl. Mater. Interfaces*, vol. 12, no. 27, pp. 30538–30547, 2020.
[178] F. Du, Y. Li, X. Li, J. Yang, Y. Bai, Z. Quan, C. Liu, and X. Xu, "Resistive switching and its modulating ferromagnetism and magnetoresistance of a ZnO-Co/SiO_2-Co film," *J. Magn. Magn. Mater.*, vol. 489, Nov. 2019, Art. no. 165445.
[179] G. Chen, C. Song, and F. Pan, "Improved resistive switching stability of $Pt/ZnO/CoO_x/ZnO/Pt$ structure for nonvolatile memory devices," *Rare Met.*, vol. 32, no. 6, pp. 544–549, Dec. 2013.
[180] H. Li, X. Lv, J. Xi, X. Wu, Q. Mao, Q. Liu, and Z. Ji, "Effects of TiO_x interlayer on resistance switching of $Pt/TiO_x/ZnO/n^+$-Si structures," *Surf. Rev. Lett.*, vol. 21, no. 5, 2014, Art. no. 1450061.
[181] C.-H. Huang, J.-S. Huang, S.-M. Lin, W.-Y. Chang, J.-H. He, and A.-L. Chueh, "ZnO_{1-x} nanorod arrays/ZnO thin film bilayer structure: From homojunction diode and high-performance memristor to complementary 1D1R application," *ACS Nano*, vol. 6, no. 9, pp. 8407–8414, 2012.
[182] D. Xu, Y. Xiong, M. Tang, B. Zeng, Y. Xiao, J. Li, L. Liu, S. Yan, Z. Tang, L. Wang, X. Zhu, and R. Li, "Improvement of resistive switching performances in ZnLaO film by embedding a thin ZnO buffer layer," *ECS Solid State Lett.*, vol. 2, no. 9, pp. Q69–Q71, Jun. 2013.

[183] X. Chen, W. Hu, S. Wu, and D. Bao, "Stabilizing resistive switching performances of TiN/MgZnO/ZnO/Pt heterostructure memory devices by programming the proper compliance current," *Appl. Phys. Lett.*, vol. 104, no. 4, Jan. 2014, Art. no. 043508.

[184] Y. Huang, Z. Shen, Y. Wu, M. Xie, Y. Hu, S. Zhang, X. Shi, and H. Zeng, "CuO/ZnO memristors via oxygen or metal migration controlled by electrodes," *AIP Adv.*, vol. 6, no. 2, Feb. 2016, Art. no. 025018.

[185] K. Bejtka, G. Milano, C. Ricciardi, C. F. Pirri, and S. Porro, "TEM nanostructural investigation of Ag-conductive filaments in polycrystalline ZnO-based resistive switching devices," *ACS Appl. Mater. Interfaces*, vol. 12, no. 26, pp. 29451–29460, Jul. 2020.

[186] A. Jilani, M. S. Abdel-Wahab, and A. H. Hammad, "Advance deposition techniques for thin film and coating," in *Modern Technologies for Creating the Thin-Film Systems and Coatings*, vol. 2. Rijeka, Croatia: InTech, 2017, pp. 137–149.

[187] D. G. Ayana, V. Prusakova, C. Collini, M. V. Nardi, R. Tatti, M. Bortolotti, L. Lorenzelli, A. Chiappini, A. Chiasera, M. Ferrari, L. Lunelli, and S. Dirè, "Sol–gel synthesis and characterization of undoped and Al-doped ZnO thin films for memristive application," *AIP Adv.*, vol. 6, no. 11, Nov. 2016, Art. no. 111306.

[188] S. Salam, M. Islam, and A. Akram, "Sol–gel synthesis of intrinsic and aluminum-doped zinc oxide thin films as transparent conducting oxides for thin film solar cells," *Thin Solid Films*, vol. 529, pp. 242–247, Feb. 2013.

[189] K. N. Tonny, R. Rafique, A. Sharmin, M. S. Bashar, and Z. H. Mahmood, "Electrical, optical and structural properties of transparent conducting Al doped ZnO (AZO) deposited by sol–gel spin coating," *AIP Adv.*, vol. 8, no. 6, Jun. 2018, Art. no. 065307.

[190] D. C. Agarwal, U. B. Singh, S. Gupta, R. Singhal, P. K. Kulriya, F. Singh, A. Tripathi, J. Singh, U. S. Joshi, and D. K. Avasthi, "Enhanced room temperature ferromagnetism and green photoluminescence in Cu doped ZnO thin film synthesised by neutral beam sputtering," *Sci. Rep.*, vol. 9, no. 1, pp. 1–12, Dec. 2019.

[191] S. Paul, P. G. Harris, C. Pal, A. K. Sharma, and A. K. Ray, "Low cost zinc oxide for memristors with high on–off ratios," *Mater. Lett.*, vol. 130, pp. 40–42, Sep. 2014.

[192] T. D. Dongale, K. V. Khot, S. S. Mali, P. S. Patil, P. K. Gaikwad, R. K. Kamat, and P. N. Bhosale, "Development of Ag/ZnO/FTO thin film memristor using aqueous chemical route," *Mater. Sci. Semicond. Process.*, vol. 40, pp. 523–526, Dec. 2015.

[193] C.-C. Hsu, W.-C. Ting, and Y.-T. Chen, "Effects of substrate temperature on resistive switching behavior of planar ZnO resistive random access memories," *J. Alloys Compounds*, vol. 691, pp. 537–544, Jan. 2017.

[194] S.-C. Wu, H.-T. Feng, M.-J. Yu, I.-T. Wang, and T.-H. Hou, "Multi-bit-per-cell a-IGZO TFT resistive-switching memory for system-on-plastic applications," in *IEDM Tech. Dig.*, Dec. 2012, pp. 3–5.

[195] R. K. Gupta, K. Ghosh, R. Patel, and P. K. Kahol, "Properties of ZnO/W-doped In_2O_3/ZnO multilayer thin films deposited at different growth temperatures," *J. Phys. D, Appl. Phys.*, vol. 41, no. 21, Nov. 2008, Art. no. 215309.

[196] R. K. Gupta, K. Ghosh, and P. K. Kahol, "Effect of substrate temperature on properties of multilayer thin film based on ZnO and Mo-doped indium oxide," *Appl. Surf. Sci.*, vol. 256, no. 5, pp. 1538–1541, Dec. 2009.

[197] C.-L. Lin, C.-C. Tang, S.-C. Wu, P.-C. Juan, and T.-K. Kang, "Impact of oxygen composition of ZnO metal-oxide on unipolar resistive switching characteristics of Al/ZnO/Al resistive RAM (RRAM)," *Microelectron. Eng.*, vol. 136, pp. 15–21, Mar. 2015.

[198] F. M. Simanjuntak, T. Ohno, and S. Samukawa, "Neutral oxygen beam treated ZnO-based resistive switching memory device," *Appl. Electron. Mater.*, vol. 1, no. 1, pp. 18–24, Jan. 2019.

[199] Y. Sun, X. Yan, X. Zheng, Y. Liu, Y. Zhao, Y. Shen, Q. Liao, and Y. Zhang, "High on–off ratio improvement of ZnO-based forming-free memristor by surface hydrogen annealing," *ACS Appl. Mater. Interfaces*, vol. 7, no. 13, pp. 7382–7388, Apr. 2015.

[200] S. Lee, J.-B. Park, M.-J. Lee, and J. J. Boland, "Multilevel resistance in ZnO nanowire memristors enabled by hydrogen annealing treatment," *AIP Adv.*, vol. 6, no. 12, Dec. 2016, Art. no. 125010.

[201] F. M. Simanjuntak, T. Ohno, and S. Samukawa, "Influence of RF sputter power on ZnO film characteristics for transparent memristor devices," *AIP Adv.*, vol. 9, no. 10, Oct. 2019, Art. no. 105216.

[202] S. Sharma and C. Periasamy, "Effect of sputtering power on structural and optical properties of ZnO thin films grown by RF sputtering technique," *J. Nanoelectron. Optoelectron.*, vol. 10, no. 2, pp. 205–210, Apr. 2015.

[203] M. Zhang, N. Liao, P. Chen, and W. Xue, "Effect of sputtering power on nano-mechanical properties of ZnO film," *Int. J. Mater. Struct. Integrity*, vol. 9, no. 4, pp. 236–243, 2015.

[204] Y. M. Hu, J. Y. Li, N. Y. Chen, C. Y. Chen, T. C. Han, and C. C. Yu, "Effect of sputtering power on crystallinity, intrinsic defects, and optical and electrical properties of Al-doped ZnO transparent conducting thin films for optoelectronic devices," *J. Appl. Phys.*, vol. 121, no. 8, Feb. 2017, Art. no. 085302.

[205] F. M. Simanjuntak, T. Ohno, and S. Samukawa, "Film-nanostructure-controlled inerasable-to-erasable switching transition in ZnO-based transparent memristor devices: Sputtering-pressure dependency," *ACS Appl. Electron. Mater.*, vol. 1, no. 11, pp. 2184–2189, Nov. 2019.

[206] K. Onlaor, T. Thiwawong, and B. Tunhoo, "Electrical switching and conduction mechanisms of nonvolatile write-once-read-many-times memory devices with ZnO nanoparticles embedded in polyvinylpyrrolidone," *Organic Electron.*, vol. 15, no. 6, pp. 1254–1262, Jun. 2014.

[207] C.-C. Hsu, C.-C. Tsao, and Y.-S. Lin, "Write-once-read-many-times characteristic of InZnO oxide semiconductor," *IEEE Trans. Electron Devices*, vol. 65, no. 3, pp. 978–985, Mar. 2018.

[208] A. H. N. Melo and M. A. Macêdo, "Permanent data storage in ZnO thin films by filamentary resistive switching," *PLoS ONE*, vol. 11, no. 12, Dec. 2016, Art. no. e0168515.

[209] P. O. Oviroh, R. Akbarzadeh, D. Pan, R. A. M. Coetzee, and T. C. Jen, "New development of atomic layer deposition: Processes, methods and applications," *Sci. Technol. Adv. Mater.*, vol. 20, no. 1, pp. 465–496, 2019.

[210] C. M. de la Huerta, V. Nguyen, J.-M. Dedulle, D. Bellet, C. Jiménez, and D. Muñoz-Rojas, "Influence of the geometric parameters on the deposition mode in spatial atomic layer deposition: A novel approach to area-selective deposition," *Coatings*, vol. 9, no. 1, p. 5, Dec. 2018.

[211] C. R. Ellinger and S. F. Nelson, "Selective area spatial atomic layer deposition of ZnO, Al_2O_3, and aluminum-doped ZnO using poly(vinyl pyrrolidone)," *Chem. Mater.*, vol. 26, no. 4, pp. 1514–1522, Feb. 2014.

[212] M.-J. Zhao, Z.-T. Sun, Z.-X. Zhang, X.-P. Geng, W.-Y. Wu, S.-Y. Lien, and W.-Z. Zhu, "Suppression of oxygen vacancy defects in sALD-ZnO films annealed in different conditions," *Materials*, vol. 13, no. 18, p. 3910, Sep. 2020.

[213] G. Yang, L. Li, W. B. Lee, and M. C. Ng, "Structure of graphene and its disorders: A review," *Sci. Technol. Adv. Mater.*, vol. 19, no. 1, pp. 613–648, Dec. 2018.

[214] S. Porro, E. Accornero, C. F. Pirri, and C. Ricciardi, "Memristive devices based on graphene oxide," *Carbon*, vol. 85, pp. 383–396, Apr. 2015.

[215] X.-F. Wang, H.-M. Zhao, Y. Yang, and T.-L. Ren, "Graphene resistive random memory—The promising memory device in next generation," *Chin. Phys. B*, vol. 26, no. 3, Mar. 2017, Art. no. 038501.

[216] H. Tian, H.-Y. Chen, T.-L. Ren, C. Li, Q.-T. Xue, M. A. Mohammad, C. Wu, Y. Yang, and H.-S.-P. Wong, "Cost-effective, transfer-free, flexible resistive random access memory using laser-scribed reduced graphene oxide patterning technology," *Nano Lett.*, vol. 14, no. 6, pp. 3214–3219, Jun. 2014.

[217] J. Liu, Z. Yin, X. Cao, F. Zhao, L. Wang, W. Huang, and H. Zhang, "Fabrication of flexible, all-reduced graphene oxide non-volatile memory devices," *Adv. Mater.*, vol. 25, no. 2, pp. 233–238, Jan. 2013.

[218] S. Dugu, S. P. Pavunny, T. B. Limbu, B. R. Weiner, G. Morell, and R. S. Katiyar, "A graphene integrated highly transparent resistive switching memory device," *APL Mater.*, vol. 6, no. 5, May 2018, Art. no. 058503.

[219] C.-L. Lin, W.-Y. Chang, Y.-L. Huang, P.-C. Juan, T.-W. Wang, K.-Y. Hung, C.-Y. Hsieh, T.-K. Kang, and J.-B. Shi, "Resistance switching behavior of ZnO resistive random access memory with a reduced graphene oxide capping layer," *Jpn. J. Appl. Phys.*, vol. 54, no. 4S, Apr. 2015, Art. no. 04DJ08.

[220] P.-K. Yang, W.-Y. Chang, P.-Y. Teng, S.-F. Jeng, S.-J. Lin, P.-W. Chiu, and J.-H. He, "Fully transparent resistive memory employing graphene electrodes for eliminating undesired surface effects," *Proc. IEEE*, vol. 101, no. 7, pp. 1732–1739, Jul. 2013.

[221] G. Khanal, S. Acciarito, G. C. Cardarilli, A. Chakraborty, L. Di Nunzio, R. Fazzolari, A. Cristini, G. Susi, and M. Re, "ZnO–rGO composite thin film resistive switching device: Emulating biological synapse behavior," in *Proc. Int. Conf. Appl. Electron. Pervading Ind., Environ. Soc.* Cham, Switzerland: Springer, 2016, pp. 117–123.

[222] G. C. Cardarilli, G. M. Khanal, L. Di Nunzio, M. Re, R. Fazzolari, and R. Kumar, "Memristive and memory impedance behavior in a photo-annealed ZnO–rGO thin-film device," *Electronics*, vol. 9, no. 2, p. 287, 2020.

[223] F. Hui, E. Grustan-Gutierrez, S. Long, Q. Liu, A. K. Ott, A. C. Ferrari, and M. Lanza, "Graphene and related materials for resistive random access memories," *Adv. Electron. Mater.*, vol. 3, no. 8, Aug. 2017, Art. no. 1600195.
[224] T. N. T. A. Aziz, A. B. Rosli, M. M. Yusoff, S. H. Herman, and Z. Zulkifli, "Transparent hybrid ZnO-graphene film for high stability switching behavior of memristor device," *Mater. Sci. Semicond. Process.*, vol. 89, pp. 68–76, Jan. 2019.
[225] M. Chen, X. Wang, Y. H. Yu, Z. L. Pei, X. D. Bai, C. Sun, R. F. Huang, and L. S. Wen, "X-ray photoelectron spectroscopy and auger electron spectroscopy studies of Al-doped ZnO films," *Appl. Surf. Sci.*, vol. 158, nos. 1–2, pp. 134–140, May 2000.
[226] G. Ahmed, M. Hanif, K. Mahmood, R. Yao, H. Ning, D. Jiao, M. Wu, J. Khan, and Z. Liu, "Lattice defects of ZnO and hybrids with GO: Characterization, EPR and optoelectronic properties," *AIP Adv.*, vol. 8, no. 2, Feb. 2018, Art. no. 025218.
[227] G. M. Khanal, S. Acciarito, G. C. Cardarilli, A. Chakraborty, L. D. Nunzio, R. Fazzolari, A. Cristini, M. Re, and G. Susi, "Synaptic behaviour in ZnO–rGO composites thin film memristor," *Electron. Lett.*, vol. 53, no. 5, pp. 296–298, Mar. 2017.
[228] G. Khurana, P. Misra, N. Kumar, and R. S. Katiyar, "Tunable power switching in nonvolatile flexible memory devices based on graphene oxide embedded with ZnO nanorods," *J. Phys. Chem. C*, vol. 118, no. 37, pp. 21357–21364, Sep. 2014.
[229] Y. Ji, S.-A. Lee, A.-N. Cha, M. Goh, S. Bae, S. Lee, D. I. Son, and T.-W. Kim, "Resistive switching characteristics of ZnO–graphene quantum dots and their use as an active component of an organic memory cell with one diode-one resistor architecture," *Organic Electron.*, vol. 18, pp. 77–83, Mar. 2015.
[230] T. N. T. A. Aziz, A. B. Rosli, M. M. Yusoff, S. H. Herman, and Z. Zulkifli, "The effect of ZnO growth temperature on the memristive behaviour of hybrid ZnO-graphene thin film," *Int. J. Electr. Electron. Syst. Res.*, vol. 12, pp. 1–10, Jun. 2018.
[231] T. Chen, Y. Gao, W. Chen, and X. Zhao, "Improved resistive memory based on ZnO–graphene hybrids through redox process of graphene quantum dots," *Phys. Status Solidi (RRL)-Rapid Res. Lett.*, vol. 13, no. 9, Sep. 2019, Art. no. 1900153.
[232] G. Anoop, V. Panwar, T. Y. Kim, and J. Y. Jo, "Resistive switching in ZnO nanorods/graphene oxide hybrid multilayer structures," *Adv. Electron. Mater.*, vol. 3, no. 5, May 2017, Art. no. 1600418.
[233] F. Gül, "Addressing the sneak-path problem in crossbar RRAM devices using memristor-based one Schottky diode-one resistor array," *Results Phys.*, vol. 12, pp. 1091–1096, Mar. 2019.
[234] S. Park, J. H. Lee, H.-D. Kim, S. M. Hong, H.-M. An, and T. G. Kim, "Resistive switching characteristics of sol–gel based ZnO nanorods fabricated on flexible substrates," *Phys. Status Solidi (RRL)-Rapid Res. Lett.*, vol. 7, no. 7, pp. 493–496, Jul. 2013.
[235] Y. Yang and T. Liu, "Fabrication and characterization of graphene oxide/zinc oxide nanorods hybrid," *Appl. Surf. Sci.*, vol. 257, no. 21, pp. 8950–8954, Aug. 2011.
[236] M. M. Rehman, H. M. M. U. Rehman, J. Z. Gul, W. Y. Kim, K. S. Karimov, and N. Ahmed, "Decade of 2D-materials-based RRAM devices: A review," *Sci. Technol. Adv. Mater.*, vol. 21, no. 1, pp. 147–186, Jan. 2020.
[237] L. Shi, D. Shang, J. Sun, and B. Shen, "Bipolar resistance switching in fully transparent ZnO:Mg-based devices," *Appl. Phys. Exp.*, vol. 2, no. 10, Oct. 2009, Art. no. 101602.
[238] J. Shang, W. Xue, Z. Ji, G. Liu, X. Niu, X. Yi, L. Pan, Q. Zhan, X.-H. Xu, and R.-W. Li, "Highly flexible resistive switching memory based on amorphous-nanocrystalline hafnium oxide films," *Nanoscale*, vol. 9, no. 21, pp. 7037–7046, 2017.
[239] R. Aluguri, R. Sailesh, D. Kumar, and T.-Y. Tseng, "Characteristics of flexible and transparent Eu_2O_3 resistive switching memory at high bending condition," *Nanotechnology*, vol. 30, no. 4, Jan. 2019, Art. no. 045202.
[240] M. Ismail and S. Kim, "Negative differential resistance effect and dual bipolar resistive switching properties in a transparent Ce-based devices with opposite forming polarity," *Appl. Surf. Sci.*, vol. 530, Nov. 2020, Art. no. 147284.
[241] D. Kumar, R. Aluguri, U. Chand, and T.-Y. Tseng, "Conductive bridge random access memory characteristics of SiCN based transparent device due to indium diffusion," *Nanotechnology*, vol. 29, no. 12, Mar. 2018, Art. no. 125202.
[242] K. Qian, X. Han, H. Li, T. Chen, and P. S. Lee, "Uncovering the indium filament revolution in transparent bipolar ITO/SiO_x/ITO resistive switching memories," *ACS Appl. Mater. Interfaces*, vol. 12, no. 4, pp. 4579–4585, 2019.
[243] S. Rajasekaran, F. M. Simanjuntak, D. Panda, S. Chandrasekaran, R. Aluguri, A. Saleem, and T.-Y. Tseng, "Fast, highly flexible, and transparent TaO_x-based environmentally robust memristors for wearable and aerospace applications," *ACS Appl. Electron. Mater.*, vol. 2, no. 10, pp. 3131–3140, 2020.
[244] L. Zou, W. Hu, W. Xie, and D. Bao, "Uniform resistive switching properties of fully transparent TiO_2-based memory devices," *J. Alloys Compounds*, vol. 693, pp. 1180–1184, Feb. 2017.
[245] S. Bang, M.-H. Kim, T.-H. Kim, D. K. Lee, S. Kim, S. Cho, and B.-G. Park, "Gradual switching and self-rectifying characteristics of Cu/α-IGZO/p^+-Si RRAM for synaptic device application," *Solid-State Electron.*, vol. 150, pp. 60–65, Dec. 2018.
[246] A. Kim, K. Song, Y. Kim, and J. Moon, "All solution-processed, fully transparent resistive memory devices," *ACS Appl. Mater. Interfaces*, vol. 3, no. 11, pp. 4525–4530, 2011.
[247] H. Yu, M. Kim, Y. Kim, J. Lee, K.-K. Kim, S.-J. Choi, and S. Cho, "Al-doped ZnO as a switching layer for transparent bipolar resistive switching memory," *Electron. Mater. Lett.*, vol. 10, pp. 321–324, Mar. 2014.
[248] C. H. Ho, J. R. D. Retamal, P. K. Yang, C. P. Lee, M. L. Tsai, C. F. Kang, and J.-H. He, "Transparent memory for harsh electronics," *Sci. Rep.*, vol. 7, no. 1, pp. 1–6, Apr. 2017.
[249] J. Zhu, W. Zhou, Z. Wang, H. Xu, Y. Lin, W. Liu, J. Ma, and Y. Liu, "Flexible, transferable and conformal egg albumen based resistive switching memory devices," *RSC Adv.*, vol. 7, no. 51, pp. 32114–32119, 2017.
[250] H.-D. Kim, M. J. Yun, J. H. Lee, K. H. Kim, and T. G. Kim, "Transparent multi-level resistive switching phenomena observed in ITO/RGO/ITO memory cells by the sol–gel dip-coating method," *Sci. Rep.*, vol. 4, no. 1, pp. 1–6, May 2015.
[251] G. U. Siddiqui, M. M. Rehman, and K. H. Choi, "Enhanced resistive switching in all-printed, hybrid and flexible memory device based on perovskite $ZnSnO_3$ via PVOH polymer," *Polymer*, vol. 100, pp. 102–110, Sep. 2016.
[252] Y.-C. Chang and Y.-H. Wang, "Solution-processed Al-chelated gelatin for highly transparent non-volatile memory applications," *Appl. Phys. Lett.*, vol. 106, no. 12, p. 34, 2015.
[253] A. H. Ramelan, S. Wahyuningsih, H. Munawaroh, and R. Narayan, "ZnO wide bandgap semiconductors preparation for optoelectronic devices," *IOP Conf. Ser., Mater. Sci. Eng.*, vol. 176, Feb. 2017, Art. no. 012008.
[254] P.-H. Chen, T.-C. Chang, K.-C. Chang, T.-M. Tsai, C.-H. Pan, C.-C. Shih, C.-H. Wu, C.-C. Yang, W.-C. Chen, J.-C. Lin, M.-H. Wang, H.-X. Zheng, M.-C. Chen, and S. M. Sze, "Effects of plasma treatment time on surface characteristics of indium-tin-oxide film for resistive switching storage applications," *Appl. Surf. Sci.*, vol. 414, pp. 224–229, Aug. 2017.
[255] F.-Y. Jin, K.-C. Chang, T.-C. Chang, T.-M. Tsai, C.-H. Pan, C.-Y. Lin, P.-H. Chen, M.-C. Chen, H.-C. Huang, I. Lo, J.-C. Zheng, and S. M. Sze, "Reducing operation voltages by introducing a low-kswitching layer in indium–tin-oxide-based resistance random access memory," *Appl. Phys. Exp.*, vol. 9, no. 6, Jun. 2016, Art. no. 061501.
[256] F. M. Simanjuntak, D. Panda, T.-L. Tsai, C.-A. Lin, K.-H. Wei, and T.-Y. Tseng, "Enhancing the memory window of AZO/ZnO/ITO transparent resistive switching devices by modulating the oxygen vacancy concentration of the top electrode," *J. Mater. Sci.*, vol. 50, no. 21, pp. 6961–6969, Nov. 2015.
[257] X. Wu, H. Xu, Y. Wang, A. L. Rogach, Y. Shen, and N. Zhao, "General observation of the memory effect in metal-insulator-ITO structures due to indium diffusion," *Semicond. Sci. Technol.*, vol. 30, no. 7, Jul. 2015, Art. no. 074002.
[258] S.-M. Gao, H. Wang, J.-W. Xu, C.-L. Yuan, and X.-W. Zhang, "Effect of annealing temperature on resistance switching behavior of $Mg_{0.2}Zn_{0.8}O$ thin films deposited on ITO glass," *Solid-State Electron.*, vol. 76, pp. 40–43, Oct. 2012.
[259] X. Wu, Z. Xu, Z. Yu, T. Zhang, F. Zhao, T. Sun, Z. Ma, Z. Li, and S. Wang, "Resistive switching behavior of photochemical activation solution-processed thin films at low temperatures for flexible memristor applications," *J. Phys. D, Appl. Phys.*, vol. 48, no. 11, Mar. 2015, Art. no. 115101.
[260] T. Lee, I.-S. Park, Y. C. Jung, S. Seong, S. Y. Kim, and J. Ahn, "Crystallized ZnO films by inserting the inert metal on ITO and their improved on/off current performance," *Mater. Sci. Semicond. Process.*, vol. 97, pp. 85–90, Jul. 2019.

[261] X. Cao, X. Li, X. Gao, X. Liu, C. Yang, R. Yang, and P. Jin, "All-ZnO-based transparent resistance random access memory device fully fabricated at room temperature," *J. Phys. D, Appl. Phys.*, vol. 44, no. 25, 2011, Art. no. 255104.

[262] R. Zhang, J. Miao, F. Shao, W. Huang, C. Dong, X. Xu, and Y. Jiang, "Transparent amorphous memory cell: A bipolar resistive switching in ZnO/$Pr_{0.7}Ca_{0.3}MnO_3$/ITO for invisible electronics application," *J. Non-Crystalline Solids*, vol. 406, pp. 102–106, Dec. 2014.

[263] P. Misra, A. K. Das, and L. M. Kukreja, "Switching characteristics of ZnO based transparent resistive random access memory devices grown by pulsed laser deposition," *Phys. Status Solidi C*, vol. 7, no. 6, pp. 1718–1720, Apr. 2010.

[264] R. Mundle, C. Carvajal, and A. K. Pradhan, "ZnO/Al:ZnO transparent resistive switching devices grown by atomic layer deposition for memristor applications," *Langmuir*, vol. 32, no. 19, pp. 4983–4995, May 2016.

[265] K. Onlaor, T. Thiwawong, and B. Tunhoo, "Bi-stable switching behaviors of ITO/EVA:ZnO NPs/ITO transparent memory devices fabricated using a thermal roll lamination technique," *Organic Electron.*, vol. 31, pp. 19–24, Apr. 2016.

[266] C.-Y. Huang, Y.-T. Ho, C.-J. Hung, and T.-Y. Tseng, "Compact Ga-doped ZnO nanorod thin film for making high-performance transparent resistive switching memory," *IEEE Trans. Electron Devices*, vol. 61, no. 10, pp. 3435–3441, Oct. 2014.

[267] F. M. Simanjuntak, T. Ohno, S. Chandrasekaran, T.-Y. Tseng, and S. Samukawa, "Neutral oxygen irradiation enhanced forming-less ZnO-based transparent analog memristor devices for neuromorphic computing applications," *Nanotechnology*, vol. 31, no. 26, 2020, Art. no. 26LT01.

[268] S. Chandrasekaran, F. M. Simanjuntak, D. Panda, and T.-Y. Tseng, "Enhanced synaptic linearity in ZnO-based invisible memristive synapse by introducing double pulsing scheme," *IEEE Trans. Electron Devices*, vol. 66, no. 11, pp. 4722–4726, Nov. 2019.

[269] J.-L. Wu, H.-Y. Lin, Y.-C. Chen, S.-Y. Chu, C.-C. Chang, C.-J. Wu, and Y.-D. Juang, "Effects of ZnO buffer layer on characteristics of ZnO:Ga films grown on flexible substrates: Investigation of surface energy, electrical, optical, and structural properties," *ECS J. Solid State Sci. Technol.*, vol. 2, no. 4, pp. P115–P119, 2013.

[270] M.-C. Chen, T.-C. Chang, S.-Y. Huang, S.-C. Chen, C.-W. Hu, C.-T. Tsai, and S. M. Sze, "Bipolar resistive switching characteristics of transparent indium gallium zinc oxide resistive random access memory," *Electrochem. Solid-State Lett.*, vol. 13, no. 6, p. H191, 2010.

[271] K. Zheng, X. W. Sun, J. L. Zhao, Y. Wang, H. Y. Yu, H. V. Demir, and K. L. Teo, "An indium-free transparent resistive switching random access memory," *IEEE Electron Device Lett.*, vol. 32, no. 6, pp. 797–799, Jun. 2011.

[272] Y. Wang, "Resistive-switching mechanism of transparent nonvolatile memory device based on gallium zinc oxide," *Phys. Status Solidi A*, vol. 209, no. 2, pp. 364–368, Feb. 2012.

[273] J. W. Seo, J.-W. Park, K. S. Lim, J.-H. Yang, and S. J. Kang, "Transparent resistive random access memory and its characteristics for nonvolatile resistive switching," *Appl. Phys. Lett.*, vol. 93, no. 22, Dec. 2008, Art. no. 223505.

[274] F. M. Simanjuntak, S. Chandrasekaran, C.-C. Lin, and T.-Y. Tseng, "ZnO_2/ZnO bilayer switching film for making fully transparent analog memristor devices," *APL Mater.*, vol. 7, no. 5, May 2019, Art. no. 051108.

[275] P. S. Kalaga, D. Kumar, D. S. Ang, and Z. Tsakadze, "Highly transparent ITO/HfO_2/ITO device for visible-light sensing," *IEEE Access*, vol. 8, pp. 91648–91652, 2020.

[276] J. W. Seo, S. J. Baik, S. J. Kang, and K. S. Lim, "Fabrication of semi-transparent resistive random access memory and its characteristics of nonvolatile resistive switching," *MRS Online Library*, vol. 1292, no. 1, pp. 53–57, 2011.

[277] K. Rajan, E. Garofalo, and A. Chiolerio, "Wearable intrinsically soft, stretchable, flexible devices for memories and computing," *Sensors*, vol. 18, no. 2, p. 367, Jan. 2018.

[278] N. Gergel-Hackett, J. L. Tedesco, and C. A. Richter, "Memristors with flexible electronic applications," *Proc. IEEE*, vol. 100, no. 6, pp. 1971–1978, Jun. 2012.

[279] Z. Zhou, F. Xiu, T. Jiang, J. Xu, J. Chen, J. Liu, and W. Huang, "Solution-processable zinc oxide nanorods and a reduced graphene oxide hybrid nanostructure for highly flexible and stable memristor," *J. Mater. Chem. C*, vol. 7, no. 35, pp. 10764–10768, 2019.

[280] L. Shi, D.-S. Shang, J.-R. Sun, and B.-G. Shen, "Flexible resistance memory devices based on Cu/ZnO:Mg/ITO structure," *Phys. Status Solidi (RRL)-Rapid Res. Lett.*, vol. 4, no. 12, pp. 344–346, Dec. 2010.

[281] J. J. L. Hmar, "Non-volatile resistive switching memory device based on ZnO-graphene oxide embedded in a polymer matrix fabricated on a flexible PET substrate," *Microelectron. Eng.*, vol. 233, Sep. 2020, Art. no. 111436.

[282] B. R. Lee, J. H. Park, T. H. Lee, and T. G. Kim, "Highly flexible and transparent memristive devices using cross-stacked oxide/metal/oxide electrode layers," *ACS Appl. Mater. Interfaces*, vol. 11, no. 5, pp. 5215–5222, Feb. 2019.

[283] D.-T. Wang, Y.-W. Dai, J. Xu, L. Chen, Q.-Q. Sun, P. Zhou, P.-F. Wang, S.-J. Ding, and D. W. Zhang, "Resistive switching and synaptic behaviors of TaN/Al_2O_3/ZnO/ITO flexible devices with embedded Ag nanoparticles," *IEEE Electron Device Lett.*, vol. 37, no. 7, pp. 878–881, Jul. 2016.

[284] H. Zhou, G.-J. Fang, Y. Zhu, N. Liu, M. Li, and X.-Z. Zhao, "Flexible resistive switching memory based on $Mn_{0.20}Zn_{0.80}O$/HfO_2 bilayer structure," *J. Phys. D, Appl. Phys.*, vol. 44, no. 44, 2011, Art. no. 445101.

[285] B. Sun, X. Zhang, G. Zhou, T. Yu, S. Mao, S. Zhu, Y. Zhao, and Y. Xia, "A flexible nonvolatile resistive switching memory device based on ZnO film fabricated on a foldable PET substrate," *J. Colloid Interface Sci.*, vol. 520, pp. 19–24, Jun. 2018.

[286] K. Kinoshita, T. Okutani, H. Tanaka, T. Hinoki, H. Agura, K. Yazawa, K. Ohmi, and S. Kishida, "Flexible and transparent ReRAM with GZO memory layer and GZO-electrodes on large PEN sheet," *Solid-State Electron.*, vol. 58, no. 1, pp. 48–53, Apr. 2011.

[287] J. W. Seo, J.-W. Park, K. S. Lim, S. J. Kang, Y. H. Hong, J. H. Yang, L. Fang, G. Y. Sung, and H.-K. Kim, "Transparent flexible resistive random access memory fabricated at room temperature," *Appl. Phys. Lett.*, vol. 95, no. 13, Sep. 2009, Art. no. 133508.

[288] X. Yan, J. Wang, M. Zhao, X. Li, H. Wang, L. Zhang, C. Lu, and D. Ren, "Artificial electronic synapse characteristics of a Ta/Ta_2O_{5-x}/Al_2O_3/$InGaZnO_4$ memristor device on flexible stainless steel substrate," *Appl. Phys. Lett.*, vol. 113, no. 1, Jul. 2018, Art. no. 013503.

[289] Z. Q. Wang, H. Y. Xu, X. H. Li, X. T. Zhang, Y. X. Liu, and Y. C. Liu, "Flexible resistive switching memory device based on amorphous InGaZnO film with excellent mechanical endurance," *IEEE Electron Device Lett.*, vol. 32, no. 10, pp. 1442–1444, Aug. 2011.

[290] Y.-S. Fan, P.-T. Liu, C.-H. Hsu, and H.-Y. Lai, "P-76: Resistive switching memory device based on amorphous Al-Zn-Sn-O film for flexible electronics application," in *SID Symp. Dig. Tech. Papers*, vol. 43, 2012, pp. 1340–1342.

[291] W.-Y. Chang, C.-A. Lin, J.-H. He, and T.-B. Wu, "Resistive switching behaviors of ZnO nanorod layers," *Appl. Phys. Lett.*, vol. 96, no. 24, 2010, Art. no. 242109.

[292] W. Ong, Q. Low, W. Huang, J. V. Kan, and G. Ho, "Patterned growth of vertically-aligned ZnO nanorods on a flexible platform for feasible transparent and conformable electronics applications," *J. Mater. Chem.*, vol. 22, no. 17, pp. 8518–8524, 2012.

[293] K. J. R. Rasmussen, "Full-range stress–strain curves for stainless steel alloys," *J. Construct. Steel Res.*, vol. 59, no. 1, pp. 47–61, Jan. 2003.

[294] Y. Chen, W. Sun, and T.-M. Chan, "Cyclic stress-strain behavior of structural steel with yieldstrength up to 460 N/mm^2," *Frontiers Struct. Civil Eng.*, vol. 8, no. 2, pp. 178–186, Jun. 2014.

[295] S.-T. Han, Y. Zhou, and V. A. L. Roy, "Towards the development of flexible non-volatile memories," *Adv. Mater.*, vol. 25, pp. 5425–5449, Aug. 2013.

[296] R. Stanford and I. M. Ovshinsky, "Analog models for information storage and transmission in physiological systems," *Mater. Res. Bull.*, vol. 5, no. 8, pp. 681–690, Aug. 1970.

[297] B. Widrow and M. E. Hoff, "Adaptive switching circuits," Electron. Labs, Stanford Univ., Stanford, CA, USA, Tech. Rep. 1553-1, Jun. 1960.

[298] T. Hylton, "Systems of neuromorphic adaptive plastic scalable electronics," in *Proc. DARPA SYNAPSE Bidder's Workshop Teaming Meeting*, 2008, pp. 1–42.

[299] D. Kuzum, S. Yu, and H.-S. P. Wong, "Synaptic electronics: Materials, devices and applications," *Nanotechnology*, vol. 24, no. 38, 2013, Art. no. 382001.

[300] N. Nasiri, R. Bo, L. Fu, and A. Tricoli, "Three-dimensional nano-heterojunction networks: A highly performing structure for fast visible-blind UV photodetectors," *Nanoscale*, vol. 9, no. 5, pp. 2059–2067, 2017.

[301] J. Yun, Y. Lim, H. Lee, G. Lee, H. Park, S. Y. Hong, S. W. Jin, Y. H. Lee, S.-S. Lee, and J. S. Ha, "A patterned graphene/ZnO UV sensor driven by integrated asymmetric micro-supercapacitors on a liquid metal patterned foldable paper," *Adv. Funct. Mater.*, vol. 27, no. 30, Aug. 2017, Art. no. 1700135.

[302] X. Liu, S. Ramirez, P. T. Pang, C. B. Puryear, A. Govindarajan, K. Deisseroth, and S. Tonegawa, "Optogenetic stimulation of a hippocampal engram activates fear memory recall," *Nature*, vol. 484, no. 7394, pp. 381–385, Apr. 2012.
[303] W. Zhou, R. Yang, H.-K. He, H.-M. Huang, J. Xiong, and X. Guo, "Optically modulated electric synapses realized with memristors based on ZnO nanorods," *Appl. Phys. Lett.*, vol. 113, no. 6, Aug. 2018, Art. no. 061107.
[304] K. Deisseroth, "Optogenetics," *Nature Methods*, vol. 8, no. 1, pp. 26–29, 2011.
[305] M. Kumar, J. Kim, and C.-P. Wong, "Transparent and flexible photonic artificial synapse with piezo-phototronic modulator: Versatile memory capability and higher order learning algorithm," *Nano Energy*, vol. 63, Sep. 2019, Art. no. 103843.
[306] W. Wang, X. Pan, X. Peng, Q. Lu, F. Wang, W. Dai, B. Lu, and Z. Ye, "Dual role of Ag nanowires in ZnO quantum dot/Ag nanowire hybrid channel photo thin film transistors," *RSC Adv.*, vol. 8, no. 15, pp. 8349–8354, 2018.
[307] M. Kumar, H.-S. Kim, G.-N. Lee, D. Lim, and J. Kim, "Piezophototronic effect modulated multilevel current amplification from highly transparent and flexible device based on zinc oxide thin film," *Small*, vol. 14, no. 52, Dec. 2018, Art. no. 1804016.
[308] T. D. Dongale, N. B. Mullani, V. B. Patil, R. S. Tikke, P. S. Pawar, S. V. Mohite, A. M. Teli, A. A. Bagade, K. K. Pawar, K. V. Khot, S. S. Shinde, V. L. Patil, S. A. Vanalkar, A. V. Moholkar, P. N. Bhosale, P. S. Patil, and R. K. Kamat, "Mimicking the biological synapse functions of analog memory, synaptic weights, and forgetting with ZnO-based memristive devices," *J. Nanosci. Nanotechnol.*, vol. 18, no. 11, pp. 7758–7766, Nov. 2018.
[309] N. B. Mullani, V. B. Patil, R. S. Tikke, P. S. Pawar, S. V. Mohite, A. A. Bagade, and T. D. Dongale, "Effect of ag doping on hydrothermally grown ZnO thin-film electronic synapse device," *Bioinspired, Biomimetic Nanobiomater.*, vol. 7, no. 2, pp. 82–89, Jun. 2018.
[310] T. D. Dongale, P. S. Pawar, R. S. Tikke, N. B. Mullani, V. B. Patil, A. M. Teli, K. V. Khot, S. V. Mohite, A. A. Bagade, V. S. Kumbhar, K. Y. Rajpure, P. N. Bhosale, R. K. Kamat, and P. S. Patil, "Mimicking the synaptic weights and human forgetting curve using hydrothermally grown nanostructured CuO memristor device," *J. Nanosci. Nanotechnol.*, vol. 18, no. 2, pp. 984–991, Feb. 2018.
[311] S. Li, F. Zeng, C. Chen, H. Liu, G. Tang, S. Gao, C. Song, Y. Lin, F. Pan, and D. Guo, "Synaptic plasticity and learning behaviours mimicked through Ag interface movement in an Ag/conducting polymer/Ta memristive system," *J. Mater. Chem. C.*, vol. 1, no. 34, pp. 5292–5298, Jun. 2013.
[312] T. Ohno, D. Nakayama, T. Okada, and S. Samukawa, "Energy control of neutral oxygen particles passing through an aperture electrode," *Results Phys.*, vol. 8, pp. 169–171, Mar. 2018.
[313] N. A. Shandyba, I. V. Panchenko, R. V. Tominov, V. A. Smirnov, M. I. Pelipenko, E. G. Zamburg, and Y. H. Chu, "Size effect on memristive properties of nanocrystalline ZnO film for resistive synaptic devices," *J. Phys., Conf. Ser.*, vol. 1124, Dec. 2018, Art. no. 081036.
[314] C. Xu, D. Niu, N. Muralimanohar, R. Balasubramonian, T. Zhang, S. Yu, and Y. Xie, "Overcoming the challenges of crossbar resistive memory architectures," in *Proc. IEEE 21st Int. Symp. High Perform. Comput. Archit. (HPCA)*, Feb. 2015, pp. 476–488.
[315] M. A. Zidan, H. A. H. Fahmy, M. M. Hussain, and K. N. Salama, "Memristor-based memory: The sneak paths problem and solutions," *Microelectron. J.*, vol. 44, no. 2, pp. 176–183, 2013.
[316] J. Zhou, K. H. Kim, and W. Lu, "Crossbar RRAM arrays: Selector device requirements during read operation," *IEEE Trans. Electron. Devices*, vol. 61, no. 5, pp. 1369–1376, Mar. 2014.
[317] R. Joshi and J. M. Acken, "Sneak path characterization in memristor crossbar circuits," *Int. J. Electron.*, vol. 44, no. 2, pp. 1–18, 2020.
[318] F. Zahoor, T. Z. A. Zulkifli, F. A. Khanday, and A. A. Fida, "Low-power RRAM device based 1T1R array design with CNTFET as access device," in *Proc. IEEE Student Conf. Res. Develop. (SCOReD)*, Oct. 2019, pp. 280–283.
[319] J.-Y. Chen, M.-C. Wu, Y.-H. Ting, W.-C. Lee, P.-H. Yeh, and W.-W. Wu, "Applications of p-n homojunction ZnO nanowires to one-diode one-memristor RRAM arrays," *Scripta Mater.*, vol. 187, pp. 439–444, Oct. 2020.
[320] J. W. Seo, S. J. Baik, S. J. Kang, Y. H. Hong, J. H. Yang, and K. S. Lim, "A ZnO cross-bar array resistive random access memory stacked with heterostructure diodes for eliminating the sneak current effect," *Appl. Phys. Lett.*, vol. 98, no. 23, 2011, Art. no. 233505.
[321] S. M. Sze, Y. Li, and K. K. Ng, *Physics of Semiconductor Devices*. New York, NY, USA: Wiley, 2021.
[322] H. Manem, G. S. Rose, X. He, and W. Wang, "Design considerations for variation tolerant multilevel CMOS/nano memristor memory," in *Proc. 20th Symp. Great lakes Symp. VLSI (GLSVLSI)*, 2010, pp. 287–292.
[323] W. Fei, H. Yu, W. Zhang, and K. S. Yeo, "Design exploration of hybrid CMOS and memristor circuit by new modified nodal analysis," *IEEE Trans. Very Large Scale Integr. (VLSI) Syst.*, vol. 20, no. 6, pp. 1012–1025, Jun. 2012.
[324] H. Manem and G. S. Rose, "A read-monitored write circuit for 1T1M multi-level memristor memories," in *Proc. IEEE Int. Symp. Circuits Syst. (ISCAS)*, May 2011, pp. 2938–2941.
[325] C.-M. Jung, J.-M. Choi, and K.-S. Min, "Two-step write scheme for reducing sneak-path leakage in complementary memristor array," *IEEE Trans. Nanotechnol.*, vol. 11, no. 3, pp. 611–618, May 2012.
[326] E. Karakulak, R. Mutlu, and E. Uçar, "Reconstructive sensing circuit for complementary resistive switches-based crossbar memories," *TURKISH J. Electr. Eng. Comput. Sci.*, vol. 24, pp. 1371–1383, Mar. 2016.
[327] P. O. Vontobel, W. Robinett, P. J. Kuekes, D. R. Stewart, J. Straznicky, and R. S. Williams, "Writing to and reading from a nano-scale crossbar memory based on memristors," *Nanotechnology*, vol. 20, no. 42, 2009, Art. no. 425204.
[328] Y. Cassuto, S. Kvatinsky, and E. Yaakobi, "Information-theoretic sneak-path mitigation in memristor crossbar arrays," *IEEE Trans. Inf. Theory*, vol. 62, no. 9, pp. 4801–4813, Sep. 2016.
[329] M. Willander, P. Klason, L. L. Yang, S. M. Al-Hilli, Q. X. Zhao, and O. Nur, "ZnO nanowires: Chemical growth, electrodeposition, and application to intracellular nano-sensors," *Phys. Status Solidi C*, vol. 5, no. 9, pp. 3076–3083, May 2008.
[330] A. Wei, L. Pan, and W. Huang, "Recent progress in the ZnO nanostructure-based sensors," *Mater. Sci. Eng. B*, vol. 176, no. 18, pp. 1409–1421, Nov. 2011.
[331] D. Mishra, A. Srivastava, A. Srivastava, and R. K. Shukla, "Bead structured nanocrystalline ZnO thin films: Synthesis and LPG sensing properties," *Appl. Surf. Sci.*, vol. 255, no. 5, pp. 2947–2950, Dec. 2008.
[332] N. P. Shetti, S. D. Bukkitgar, K. R. Reddy, C. V. Reddy, and T. M. Aminabhavi, "ZnO-based nanostructured electrodes for electrochemical sensors and biosensors in biomedical applications," *Biosensors Bioelectron.*, vol. 141, Sep. 2019, Art. no. 111417.
[333] Y. Q. Fu, J. K. Luo, N.-T. Nguyen, A. J. Walton, A. J. Flewitt, X.-T. Zu, Y. Li, G. McHale, A. Matthews, E. Iborra, H. Du, and W. I. Milne, "Advances in piezoelectric thin films for acoustic biosensors, acoustofluidics and lab-on-chip applications," *Prog. Mater. Sci.*, vol. 89, pp. 31–91, Aug. 2017.
[334] Ü. Özgür, H. Daniel, and H. Morkoç, "ZnO devices and applications: A review of current status and future prospects," *Proc. IEEE*, vol. 98, no. 7, pp. 1255–1268, Jul. 2010.
[335] P. Rong, S. Ren, and Q. Yu, "Fabrications and applications of ZnO nanomaterials in flexible functional devices—A review," *Crit. Rev. Anal. Chem.*, vol. 49, no. 4, pp. 336–349, Jul. 2019.
[336] N. K. Reddy, M. Devika, and C. W. Tu, "High-quality ZnO nanorod based flexible devices for electronic and biological applications," *RSC Adv.*, vol. 4, no. 71, pp. 37563–37568, 2014.
[337] A. Zainelabdin, S. Zaman, G. Amin, O. Nur, and M. Willander, "Stable white light electroluminescence from highly flexible polymer/ZnO nanorods hybrid heterojunction grown at 50°C," *Nanosc. Res. Lett.*, vol. 5, no. 9, pp. 1442–1448, Sep. 2010.
[338] K. H. Lee, B. Kumar, H.-J. Park, and S.-W. Kim, "Optimization of an electron transport layer to enhance the power conversion efficiency of flexible inverted organic solar cells," *Nanosc. Res. Lett.*, vol. 5, no. 12, pp. 1908–1912, Dec. 2010.
[339] P. F. Ma, G. D. Liang, Y. M, Wang, Y. P. Li, Q. Xin, Y. X. Li, and A. M. Song, "High-performance InGaZnO-based ReRAMs," *IEEE Trans. Electron Devices*, vol. 66, no. 6, pp. 2600–2605, Jun. 2019.
[340] H.-H. Hsu, C.-Y. Chang, and C.-H. Cheng, "A flexible IGZO thin-film transistor with stacked TiO_2-based dielectrics fabricated at room temperature," *IEEE Electron Device Lett.*, vol. 34, no. 6, pp. 768–770, May 2013.
[341] J. F. Wager, "Transparent electronics," *Science*, vol. 300, no. 5623, pp. 1245–1246, May 2003.
[342] D. Ielmini, "Brain-inspired computing with resistive switching memory (RRAM): Devices, synapses and neural networks," *Microelectron. Eng.*, vol. 190, pp. 44–53, Apr. 2018.

[343] J. R. D. Retamal, C.-F. Kang, C.-H. Ho, J.-J. Ke, W.-Y. Chang, and J.-H. He, "Effect of ultraviolet illumination on metal oxide resistive memory," *Appl. Phys. Lett.*, vol. 105, no. 25, Dec. 2014, Art. no. 253111.
[344] C.-C. Shih, K.-C. Chang, T.-C. Chang, T.-M. Tsai, R. Zhang, J.-H. Chen, K.-H. Chen, T.-F. Young, H.-L. Chen, J.-C. Lou, T.-J. Chu, S.-Y. Huang, D.-H. Bao, and S. M. Sze, "Resistive switching modification by ultraviolet illumination in transparent electrode resistive random access memory," *IEEE Electron Device Lett.*, vol. 35, no. 6, pp. 633–635, Jun. 2014.
[345] Z. Luo, L. Pei, M. Li, Y. Zhu, S. Xie, X. Cheng, J. Liu, H. Ding, and R. Xiong, "Electric field-induced resistive switching, magnetism, and photoresponse modulation in a Pt/$Co_{0.03}Zn_{0.97}O$/Nb:$SrTiO_3$ multifunction heterostructure," *Appl. Phys. Lett.*, vol. 112, no. 15, 2018, Art. no. 153504.
[346] A. Bera, H. Peng, J. Lourembam, Y. Shen, X. W. Sun, and T. Wu, "A versatile light-switchable nanorod memory: Wurtzite ZnO on perovskite $SrTiO_3$," *Adv. Funct. Mater.*, vol. 23, no. 39, pp. 4977–4984, Oct. 2013.
[347] A. Kiazadeh and J. Deuermeier, "Flexible and transparent RRAM devices for system on panel (SOP) application," in *Advances in Non-Volatile Memory and Storage Technology*. Sawston, U.K., 2019, pp. 519–538.
[348] M.-F. Chang, S.-S. Sheu, K.-F. Lin, C.-W. Wu, C.-C. Kuo, P.-F. Chiu, Y.-S. Yang, Y.-S. Chen, H.-Y. Lee, C.-H. Lien, F. T. Chen, K.-L. Su, T.-K. Ku, M.-J. Kao, and M.-J. Tsai, "A high-speed 7.2-ns read-write random access 4-Mb embedded resistive RAM (RRAM) macro using process-variation-tolerant current-mode read schemes," *IEEE J. Solid-State Circuits*, vol. 48, no. 3, pp. 878–891, Mar. 2012.
[349] S. Kim, H. Moon, D. Gupta, S. Yoo, and Y.-K. Choi, "Resistive switching characteristics of sol–gel zinc oxide films for flexible memory applications," *IEEE Trans. Electron Devices*, vol. 56, no. 4, pp. 696–699, Apr. 2009.
[350] M. Lanza *et al.*, "Recommended methods to study resistive switching devices," *Adv. Electron. Mater.*, vol. 5, no. 1, 2019, Art. no. 1800143.

USMAN BATURE ISYAKU (Student Member, IEEE) received the B.Eng. degree in computer engineering from Bayero University Kano (BUK), Kano, Nigeria, in 2010, and the M.Eng. degree (electrical—computer and microelectronic system) from the Universiti Teknologi Malaysia (UTM), Skudai, Johor Bahru, Malaysia, in 2015. He is currently pursuing the Ph.D. degree with the Department of Electrical Engineering, Universiti Teknologi PETRONAS (UTP), Malaysia, under the guidance of Dr. Mohd Haris Bin Md Khir. He has published some research papers in the international journals and conferences. His research interests include resistive random access memory (ReRAM), nano-material design, and embedded systems.

MOHD HARIS BIN MD KHIR (Member, IEEE) received the B.Eng. degree in electrical and electronic engineering from the Universiti Teknologi MARA, Selangor, Malaysia, in 1999, the M.Sc. degree in computer and systems engineering from the Rensselaer Polytechnic Institute, NY, USA, in 2001, and the Ph.D. degree in systems engineering from Oakland University, MI, USA, in 2010. He joined the Universiti Teknologi PETRONAS (UTP), in 1999, where he is currently an Associate Professor with the Department of Electrical and Electronic Engineering. He held several positions at UTP, such as the deputy head of the department and the director of mission-oriented research on nanotechnology. He has published three book chapters and more than 37 journals and 70 conference papers in the area of sensor, actuator, energy harvester, and sensor's application in the IoT. His research interests include micro/nano–electromechanical systems, and sensors and actuator development.

I. MD NAWI (Member, IEEE) was born in Petaling Jaya, Malaysia, in 1979. She received the B.Eng. degree (Hons.) from the University of Technology PETRONAS, Seri Iskandar, Perak, in 2002, and the M.Sc. degree in microelectronics systems design and the Ph.D. degree in electrical and electronic engineering from the University of Southampton, Southampton, U.K., in 2004 and 2018, respectively. At the end of 2003, she pursued the M.Sc. degree under the University of Technology PETRONAS's learning grants at the University of Southampton. In 2003, she has joined the teaching team of the Department of Electrical and Engineering, University of Technology PETRONAS, as a Tutor. She went on to serve the University of Technology PETRONAS, from 2004 to 2010. In 2010, she became the Research Officer with Tohoku University, Sendai. Returning from Sendai, she worked with SEGi University, Damansara, Malaysia, before pursuing the Ph.D. degree with the University of Southampton. Upon completion, she returned to her alma mater, University of Technology PETRONAS, where she is serving for the Department of Electrical and Electronic Engineering, as a Lecturer. She has authored a book section in *Advances in Electrical and Electronics Engineering*-IAENG Special Edition of the World Congress on Engineering and Computer Science 2008 and authored a number of technical articles, since 2004, based on the M.Sc. and Ph.D. theses, and also from the final year students' work. Her research interests ranges from microelectronics systems design, robotics and automations, automotive-mems, bio-mems, and reliability in IC design. Her current research interests include safety of automotive vehicles, and the reliability of chips and using electronics devices in aiding the agricultural-related problems. She has been a Registered Member of IEEE, since 2012. She has also been granted MIET Membership upon completion of the Ph.D. degree, in 2018. Apart from that, she has been a member of the Board of Engineers Malaysia, since 2002.

M. A. ZAKARIYA (Member, IEEE) born in Pahang, Malaysia, in 1972. He received the B.Eng. degree in electrical and electronic engineering from the Universiti Teknologi Malaysia, Malaysia, in 1999, the M.Sc. degree in communication and signal processing from the University of Newcastle Upon Tyne, in 2001, and the Ph.D. degree in RF and microwave from the Universiti Sains Malaysia, in 2015. He joined the Universiti Teknologi PETRONAS, in 1999. He is currently holding a position as a Senior Lecturer with the Department of Electrical and Electronic Engineering. He is also assigned as the Head of Research Group of Agriculture IoT (AIoT), under the Institute of Transportation and Infrastructure (ITI). He had published three book chapters and more than ten journals and 50 conference papers in the area of dielectric resonator antennas, RF microwave filter, RF energy harvester circuits, and the IoT application. His research interests include RF and microwave circuit design, antenna and wireless systems, and the IoT systems.

FURQAN ZAHOOR (Student Member, IEEE) received the B.Tech. degree in electronics and communication engineering from the University of Kashmir, Srinagar, in 2014, and the M.Tech. degree in electronics and communication engineering from Shri Mata Vaishno Devi University, Katra, in 2016. He is currently pursuing the Ph.D. degree in electrical and electronics engineering with the Universiti Teknologi PETRONAS, Malaysia. From May 2017 to September 2018, he was an Assistant Professor on contractual basis with the Department of Electronics and Instrumentation Technology, University of Kashmir. He has published several research papers in the international journals and conferences. His research interest includes resistive random access memory (RRAM) devices.